0^{th} and 1^{st} Generation Organometallic Nanostars

from

Ferrocenylamine and Ferrocenylaniline

by

Cynthia L. Perrine

Submitted in Partial Fulfillment of the Requirements

for the Degree of

Master of Science

in the

Chemistry

Program

YOUNGSTOWN STATE UNIVERSITY

August, 2004

0^{th} and 1^{st} Generation Organometallic Nanostars

from

Ferrocenylamine and Ferrocenylaniline

by

Cynthia L. Perrine

I hereby release this thesis to the public. I understand this thesis will be made available from the Ohio Link ETD Center and the Maag Library Circulation Desk for public access. I also authorize the University or other individuals to make copies of this thesis as needed for scholarly research.

Signature:

Cynthia L. Perrine, Student — Date: 7/12/04

Approvals:

Dr. Allen D. Hunter, Thesis Advisor — Date: 7/26/04

Dr. Larry S. Curtin, Committee Member — Date: 7/26/04

Dr. Timothy R. Wagner, Committee Member — Date: 7/26/04

Peter J. Kavinsky, Dean of Graduate Studies — Date: 7/22/04

Abstract

Covalently bonded organometallic oligomers and polymers have been designed to have rigid and thermally and chemically stable organometallic repeating units such as [trans-$Mo(Ph_2PCH_2CH_2Ph_2)_2$(μ-CN-1,4-C_6H_4-NC)]. In the first step towards such materials, the chemical and electronic properties of model compounds with only one or a few metal centers will be investigated. Putting electrochemical "sensors" (*e.g.*, ferrocenyl isocyanide or *para*-isocyanoferrocenylbenzene) at one or more ends of the oligomers, will give information pertaining to the electronic communication via the metal centers. Ferrocenylamine is the essential starting material for the synthesis of ferrocenyl isocyanide. The main drawback for the synthesis of ferrocenylamine is its multistage preparation. It has been found that the conventional methods of electrophilic substitution, which were appropriate for benzene analogues, resulted in the oxidation of the ferrocene to the ferricenium cation. A procedure using ferrocenylphthalimide as the precursor proved to be most successful. Bromo- or iodoferrocene were prepared as a precursor of N-ferrocenylphthalimide; the amine is then liberated using the Gabriel method. The electronic properties of the CN-R function can be altered by the nature of the various alkyl and aryl substituents. Using cyclic voltammetry, the oxidation potentials of the molybdenum or nickel centers having ferrocenylisonitrile ends will be determined depending on other substituents on the molecules. These substituents, in addition to chelating phosphines, include other isonitriles such as *p*-isocyanotetramethylbenzene, *p*-anisole, *p*-nitrobenzene, *p*–ferrocenylbenzene, and ferrocene.

Acknowledgements

I would like to thank Dr. Allen D. Hunter for his guidance, leadership and friendship throughout my studies.

I would like to thank Matthiaz Zeller for his knowledge, guidance and expertise in lab technique.

I would like to also thank the members of my group, whose friendships I will never forget.

I would like to especially thank Jim Updegraff for his everlasting support and camaraderie throughout our studies.

I would like to extend a special thanks to my family and friends for their continued support in my thirst for knowledge.

Table of Contents

List of Equations

List of Figures

List of Tables

List of Abbreviations

a	Length of unit cell axis (as in X-ray diffraction)
Å	Angstrom
Ar	Substituted aryl group
b	Length of a unit cell axis (as in X-ray diffraction)
β	Beta angle (as in X-ray diffraction) between *a* and *c* axis
n-Bu	*n*-Butyl
t-Bu	*tert*-Butyl
c	Length of a unit cell axis (as in X-ray diffraction)
$CDCl_3$	Deuterochloroform
CH_2Cl_2	Dichloromethane
cm^{-1}	Reciprocal centimeters, wave numbers
CO	Carbonyl ligand
"CN"	Coordination number
CN-R	Substituted isocyanide ligand
Cp	Cyclopentadienyl (η^5- C_5H_5)
CV	Cyclic voltammogram
d	Doublet (as in NMR spectroscopy)
δ	Chemical shift (as in NMR spectroscopy)
Δ	Heat (thermal reaction)
dd	Doublet of doublet (as in NMR spectroscopy)
dppe	1,2-Bis(diphenylphosphino)ethane
Dx	Density (as in X-ray diffraction)
Eq	Equivalents
Et	Ethyl
EtOH	Ethanol
F	Structure factor refinement (as in X-ray diffraction)
Fc	Ferrocene
Fc	Calculated structure factor (as in X-ray diffraction)
Fo	Observed structure factor (as in X-ray diffraction)

FTIR	Fourier transform infrared
g	Grams
h	Hour, Miller indices (as in X-ray diffraction)
Hz	Hertz
HOMO	Highest occupied molecular orbital
IR	Infrared (as in spectroscopy)
J	Coupling constant (as in NMR spectroscopy)
k	Miller indices (as in X-ray diffraction)
l	Miller indices (as in X-ray diffraction)
L	Ligand
LUMO	Lowest unoccupied molecular orbital
μ	Mu
m	multiplet (as in NMR)
Me	Methyl
MHz	Mega hertz
mL	Milliliters
Mo Kα	Molybdenum K alpha (as in X-ray diffraction)
mol	Mole
mmol	Millimole
mm	Millimeter
MO	Molecular Orbital
Mr	Molecular weight (as in X-ray diffraction)
M_w	Molecular weight
η	Eta
NLO	Non-linear optical
NMR	Nuclear Magnetic Resonance
o	*Ortho*
OMe	Methoxy
π	Bonding pi orbital
π^*	Anti-bonding pi orbital
p	*Para*

ph-	Phenyl
ppm	Parts per million (as in NMR)
PR_3	Phosphine or Phosphite
R	Alkyl or aryl group
R	Discrepancy index (as in X-ray diffraction)
σ	Bonding sigma orbital
S	Goodness of fit (as in X-ray diffraction)
s	Singlet (as in NMR spectroscopy)
T	Temperature
T*min*	Minimum transmission (as in X-ray diffraction)
T*max*	Maximum transmission (as in X-ray diffraction)
ω	Omega (*e.g*, measurement angle used in X-ray diffraction)
θ	Theta (*e.g.*, Angle between the incident and the diffracted beams in X-ray diffraction)
θ_{max}	Theta (*e.g.*, maximum Bragg angle as in X-ray diffraction)
t	Triplet (as in NMR spectroscopy)
THF	Tetrahydrofuran
UV vis	Ultraviolet-visible (as in spectroscopy)
V	Cell volume (as in X-ray diffraction)
ν	Stretching frequency (as in IR spectroscopy)
ν_{as}	Asymmetric stretching frequency (as in IR spectroscopy)
ν_{sy}	Symmetric stretching frequency (as in IR spectroscopy)
in vacuo	Under high vacuum
wR	Weighted discrepancy index (as in X-ray diffraction)
X	Cl, Br, or I ligand
Z	Number of molecules in unit cell (as in X-ray diffraction)

Chapter One - Introduction

Section One

Organometallic Structure and Bonding

Organometallic chemistry combines features of inorganic and organic chemistry. Approximately fifty years ago, research in this area went through a renaissance driven by breakthroughs in both synthetic methods and bonding theories leading to its current growth phase. Much of the interest in organometallic compounds has been due to their efficiency as catalysts for organic and polymer syntheses.[1] In turn, this efficacy stems from the seemingly infinite number of derivatives which can be obtained by varying the ligands and metals of organometallic complexes. A transition metal organometallic compound is composed of one or more metal centers surrounded by a set of ligands. In the most basic terms, the ligands may be thought of as Lewis bases that donate pairs of electrons to the central metal atom(s), which acts as a Lewis acid(s).

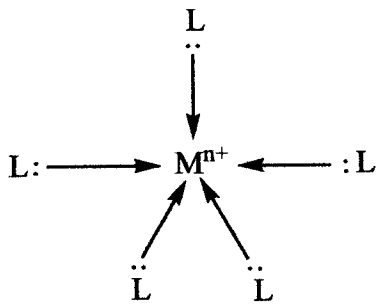

Figure 1.1.1 Metal "acting" as a Lewis acid.

The relative stability of each complex is related to the valence electron count of the metal. Thus, the 18-electron rule predicts that a complex will be relatively stable if it has eighteen valence electrons associated with each metal center (*i.e.*, in the non-bonding orbitals of the metal and in the metal-ligand bonds). There are some exceptions to the rule, but metals in the middle of the transition series in low formal oxidation states

generally obey the rule (*e.g.*, the complexes that will be discussed in this thesis which contain chromium and molybdenum).[1,2]

Organometallic ligands may vary in the manner in which their valence electrons interact with the metal. For π-complexes in which unsaturated organic ligands are bonded "side on" to the metal (*e.g.*, olefins and aromatics), one or more π-bonds on the ligand may donate electrons to one or more metal atoms. The hapticity of the ligand (*i.e.*, its η^n number) is defined as the number of atoms that are within bonding distance of the metal atom. The total number and the nature of the ligands that are coordinated to a metal center determine its coordination number, CN. The number of coordination positions that a ligand occupies typically is equal to the number of electron pairs donated to the metal. While metal oxidation states and formal charges assigned to ligands do not accurately reflect the net electron charges in the complexes, they are useful bookkeeping tools and so are still widely used. Different ligands may vary in formal charge, the number of electrons that may be donated to the metal atom, and the number of coordination positions around the metal as shown in Table 1.1.[2]

Table 1.1.1 Structure and bonding properties of some commonly encountered ligands

Ligand	**Formal Charge(s)**	**Electrons Donated**	**Coordination Positions**
Acyl	-1	2	1
η^2-alkene	0	2	1
Alkyl	-1	2	1
Alkylidene	-2	4	1
Alkylidyne	-3	6	1
η^1-allyl	-1	2	1

η^3-allyl	-1	4	2
η^2-alkyne	0	2 to 4	1
Amine	0	2	1
η^2-arene	0	2	1
η^6-arene	0	6	3
Carbene	0	2	1
Carbine	0	3	1
Carbonyl	0	2	1
η^1-cyclopentadienyl	-1	2	1
η^3-cyclopentadienyl	-1	4	2
η^5-cyclopentadienyl	-1	6	3
Dinitrogen	0	2	1
Halide (*e.g.*, Cl^-)	-1	2	1
Hydride	-1	2	1
Isocyanide (isonitrile)	0	2	1
Nitrile	0	2	1
Nitrosyl (linear)	+1	2	1
Nitrosyl (bent)	-1	2	1

Ligand	Formal Charge(s)	Electrons Donated	Coordination Positions
Phosphate	0	2	1
Phosphine	0	2	1
Pyridine	0	2	1

The carbonyl ligand is perhaps the most common ligand in transition metal organometallic chemistry. Its bonding in the linear terminal geometry is typical of other linear π-acidic ligands such as N_2, NO^+, and CN-R. In linear carbonyl complexes, the carbonyl is attached to the metal via the carbon atom, and the metal-carbon-oxygen angle is approximately 180°. According to the Dewar-Chatt-Duncanson model,[2] σ-bonding occurs when a lone pair of electrons is donated from a filled σ-symmetry orbital on carbon (*i.e.*, the approximately sp hybrid orbital) to an empty σ-symmetry orbital on the metal (*i.e.*, the approximately d^2sp^3 hybrid orbital in an octahedral complex). There are also two π-backbonding interactions, which are perpendicular to one another. In each of the two back bonds, there is a filled π-symmetry orbital on the metal (*e.g.*, the approximately d_{xy}, d_{xz}, or d_{yz} in an octahedral complex), which donates a pair of electrons into an empty π-symmetry orbital on carbon monoxide (*i.e.*, the approximately CO π*-antibonding orbital). These σ-bonding and π-backbonding components are synergic and the overall metal-carbonyl bond is thus stronger than the linear sum of the two components.

The electron transfer back to the ligand via the π-backbonding effectively neutralizes the

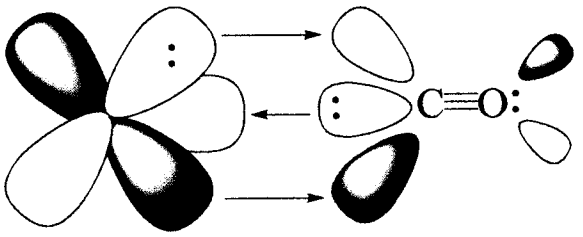

Figure 1.1.2 A "Dewar-Chatt-Duncanson" representation of the bonding of a carbonyl ligand to a transition metal.[3]

electron transfer of the σ-bonding interaction to the metal. Thus, the overall metal-carbonyl bond is not polarized very much and there is only a small net electron transfer to the carbonyl ligand.

An alternate and complementary explanation for the bonding of metal carbonyls

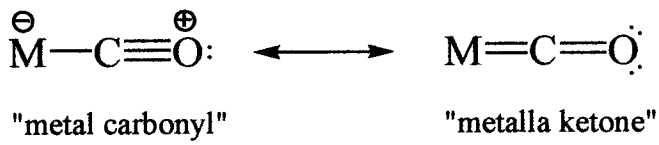

Figure 1.1.3 Valence Bond Theory representation of the bonding of a carbonyl ligand.

is provided by Valence Bond Theory.[2] Valence Bond Theory represents the bonding as contributions from two resonance forms. The first resonance form has metal-carbon single and carbon-oxygen triple bonds, with a formal charge of +1 on an sp hybridized oxygen. The second resonance form has both metal-carbon and carbon-oxygen interactions as double bonds, has no formal charges on carbon monoxide, and has oxygen

sp^2 hybridized. In this interpretation, increased backbonding to the carbonyl is reflected in an increased contribution from the second "metallo-ketone" resonance form.

Spectroscopy and X-ray diffraction may be used to provide experimental evidence of the nature and extent of the metal-carbonyl interaction. Infrared spectroscopy may be used to measure the amount of backbonding of the metal to the ligand. The IR stretching frequencies of carbonyls decrease from $2120cm^{-1}$ to below $1850cm^{-1}$ as the metal becomes more electron rich and, consequently, as the amount of backbonding increases. In turn, as the amount of backbonding increases, the CO bond order decreases and the carbon-metal bond order increases. Various studies have shown that carbonyl ligands are poor σ-donors and strong π-acceptors. Thus, carbonyls act as net electron withdrawing ligands. Nuclear magnetic resonance spectroscopy may also be used to examine the electron richness of the complex. As the amount of backbonding increases, the chemical shift of the carbonyl carbon correlates with the electron richness of the complex (*i.e.*, shifting either downfield or up-field for a series of related complexes). X-ray diffraction may also be used to examine metal-ligand interactions. Thus, as the bond order of the carbon-metal bond increases the corresponding bond length decreases and as the carbon-oxygen bond order decreases its bond length increases.[4]

Isonitrile ligands are isoelectronic with carbonyl ligands and their bonding is therefore closely related. However, isonitriles are less electronegative than carbon monoxide and the lobes of the π*-antibonding orbitals on CN are less polarized towards carbon. Thus, isonitriles are generally better net electron donors than carbonyls. In terms of the Dewar-Chatt-Duncanson model, there is σ-donation from the lone pair of electrons on the carbon (*i.e.*, the approximately sp hybrid orbital) to an empty σ-symmetry orbital of the metal (*i.e.*, approximately d^2sp^3 in octahedral complexes). There is also π-back donation from a pair of filled orbitals of π-symmetry on the metal (*i.e.*, the approximately d_{xy}, d_{xz}, or d_{yz} orbitals in octahedral metals) to a pair of empty π-symmetry orbitals on the isocyanide ligand (*i.e.*, the approximately π*-orbitals localized on CN).[3,4]

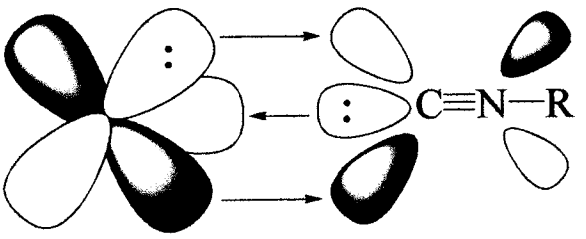

Figure 1.1.4 A Dewar-Chatt-Duncanson model representation of the bonding of an isocyanide ligand to a transition metal.

Valence Bond Theory provides an alternative and complementary explanations of the bonding that occurs during the coordination of an isonitrile to a transition metal. In Valence Bond terms, the coordination is explained via resonance. Thus, greater backbonding results in an increased contribution from the second resonance form and

Figure 1.1.5 Valence Bond Theory model for an isocyanide ligand.

hence a decreased CN-R bond angle due to the sp^2 hybridization of the nitrogen atom on the latter.[5]

Both the Dewar-Chatt-Duncanson and Valence Bond Theory explanation can be used to rationalize the same experimental observations. The electron richness of the metal center affects the bond orders for the metal-carbon and carbon-nitrogen bonds as well as the CN-R bond angles. If the electron richness of the metal is increased, there is more backbonding and the second resonance form is favored. The metal-carbon bond

order therefore increases and the carbon-nitrogen bond order decreases while the CN-R angle decreases. As with carbonyls, the electron richness of isonitrile complexes may be measured through infrared spectroscopy. The CN stretching frequency for isonitrile complexes is 250-350 wavenumbers lower than the stretching frequency for the free isonitrile reflecting both the weakening of the net CN σ- and π-bonds upon coordination.[3,4]

Olefins and related unsaturated organics are also common ligands. In the Dewar-Chatt-Duncanson model, the bonding of olefins involves a forward donation of π-electron density from the occupied π-bonding orbitals of the alkene (*i.e.*, σ-symmetry with respect to the metal) to empty σ-symmetry valence orbitals on the metal atom (*e.g.*, approximately d^2sp^3 on an octahedral complex). Back donation occurs from filled π-symmetry orbitals on the metal (*e.g.*, approximately d_{xz}, d_{yz}, and d_{xy} on an octahedral metal center) into an empty π* molecular orbital on the ligand, (*i.e.*, which have π-symmetry with respect to the metal).

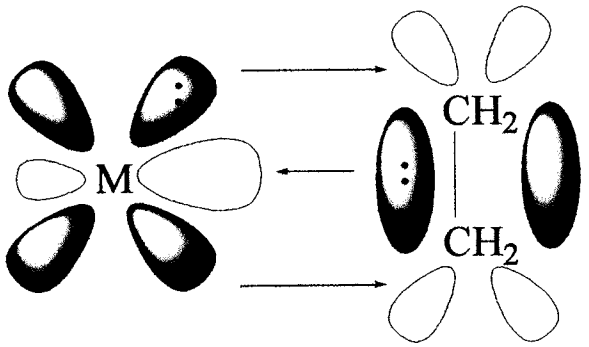

Figure 1.1.6 A Dewar-Chatt-Duncanson model representation for the bonding of an alkene ligand to a transition metal.

In Valence Bond terms, the two resonance forms of olefins are referred to as the metal-olefin and metallo-cyclopropane forms, which differ in both their metal-carbon and carbon-carbon bond orders and in the hybridizations of the carbon atoms. Thus, increased

backbonding increases the contribution of the second resonance form which increases the metal-carbon bond order, decreases the carbon-carbon bond order, and changes the carbon hybridization from sp^2 towards sp^3.

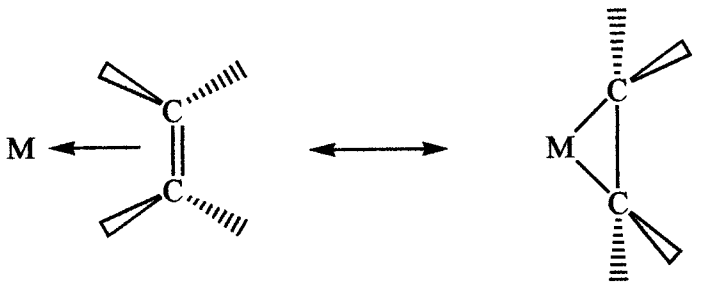

Figure 1.1.7 Valence Bond Theory representation of the bonding of a metal-olefin and metallocyclopropane.

As with carbon monoxide and CN-R, the electron richness of the metal containing olefin and related complexes may be measured through spectroscopy and X-ray diffraction. Increasing the electron richness on the metal produces increased backbonding and, therefore, the net bond order of the carbon-carbon bond decreases. X-ray diffraction has shown that increased electron richness on the metal and the subsequent backbonding, decreases the metal to ligand bond distance, increases the carbon-carbon bond length, and decreases the H-C-H bond angles from 120° towards 109°. The π-bonded hydrocarbons such as olefins and η^6-arenes generally increase the net electron density on the metal in contrast to π-acidic ligands such as carbonyls and isocyanates, which typically decrease the net electron density on the metal.

The PR_3 ligand is widely used in metal coordination chemistry because it is a soft ligand and can be incorporated into metal complexes having central atoms in low oxidation states. The stability of complexes with PR_3 ligands results from the soft acceptor nature of the metal in low oxidation states and the stability of soft-donor/soft-acceptor combinations.[6] It is generally accepted that the bonding of phosphines to metals is almost entirely σ-donor in nature for alkyl phosphines. However, for aryl phosphines, phosphites, and fluorinated phosphines π-backbonding into phosphorus orbitals that have

phosphorus-carbon σ* orbital character become increasingly important in the order given. The 1,2-bis-diphenylphosphinoethane ligand (dppe) is typically a bidentate ligand in most complexes, meaning that both phosphorus atoms coordinate to the metal. Each phosphorus atom has a lone pair of electrons from an sp^3 hybrid orbital that is donated to an empty σ-symmetry orbital on the metal (*e.g.*, approximately d^2sp^3 orbital on an octahedral metal center). For the phosphine ligands used in this research, backbonding plays little or no role because the aryl substituents are relatively electron rich.[7]

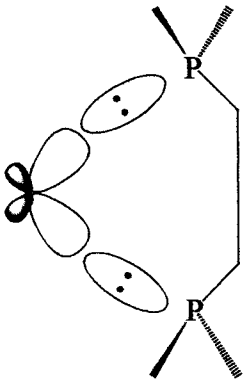

Figure 1.1.8 A Dewar-Chatt-Duncanson representation for the bonding of the bidentate dppe ligand to a transition metal.

The dinitrogen ligand is usually a linear monodentate ligand because only one pair of electrons from the dinitrogen molecule coordinates to the metal. As with carbon monoxide and CN-R, [2,7] one can describe M-N_2 bonding in both Dewar-Chatt-Duncanson (*i.e.*, σ-donation and π-back donation) and Valence Bond (*i.e.*, two resonance contributions) terms. Free dinitrogen is IR inactive due to its lack of a dipole moment, but it is Raman active. The polarization that results from its synergic bonding to metal atoms leads to the observation of a N-N stretching vibration between 1920-2150cm^{-1} and to chemical activation of the dinitrogen ligand.

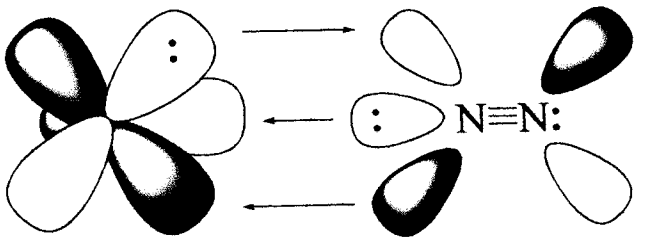

Figure 1.1.9 A Dewar-Chatt-Duncanson model representation for the bonding of a dinitrogen ligand to a transition metal.

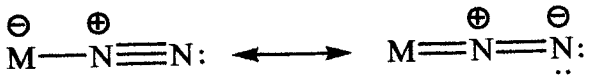

Figure 1.1.10 Valence Bond Theory representation of the bonding of a dinitrogen ligand to a transition metal.

However, for a terminal N_2 ligand net σ and π interactions are weaker than for other π-acid ligands such as carbonyls and isocyanides. Therefore, dinitrogen ligands often may be readily displaced from the complex by them, *e.g.*, as in equation 1.1.1[8]

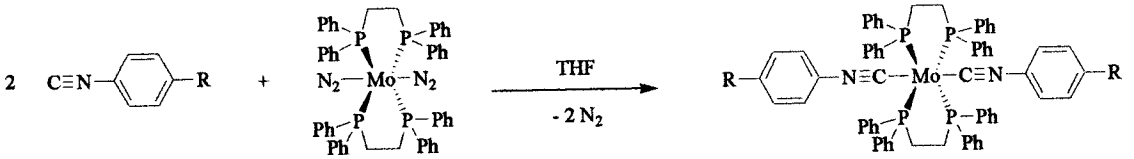

Equation 1.1.1 Displacement of dinitrogen ligands.

Section Two

Organometallic Polymers and Dendrimers

Metal-ligand complexes may be incorporated into polymers to produce new classes of organometallic polymers that are at least formally related to conventional organic and/or inorganic polymers. Most transition elements have a higher coordination number than carbon. This allows inorganic atoms incorporated into polymers to have more side groups. In addition, metal-ligand bonds are typically longer than conventional organic bonds (*e.g.*, carbon-carbon, carbon-nitrogen, and carbon-oxygen bonds). These differences in bonding and valences between carbon and metals produce different bond angles, internuclear distances, and backbone rigidities.[7] Because of their variable bonding characteristics, organometallic polymers may also possess intriguing electrical, conductivity, magnetic, optical, liquid crystalline, and redox properties. Polymers with inorganic fragments in their repeating unit have many actual and/or potential advantages compared to conventional organic polymers. In particular, inorganic elements are expected to induce properties in polymers that cannot easily be induced using conventional organic fragments.[9,10] Organometallic polymers of most relevance to this research are polymers having transition elements that possess M-C σ or π bonds in the backbone. Polyphosphazenes, polysiloxanes, and polysilanes are some inorganic polymers that have been produced commercially because of their novel properties.[7]

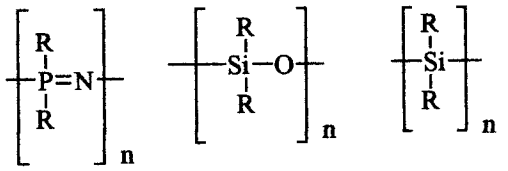

Figure 1.2.1 Structures of a polyphosphazene, polysiloxane, and polysilane.

To facilitate practical applications, a main goal of organometallic polymer researchers is to synthesize organometallic polymers with favorable materials processing characteristics (*e*.g., melting point, solubility, and high or controllable molecular weights (Mn > 10,000)). Since the early 1950s, many organometallic polymers have been synthesized; however, these polymers typically had low molecular weights. They were also often insoluble or could not be melted without decomposing. In order to overcome these obstacles, researchers have attempted various synthetic approaches. Step growth polycondensation reactions involving the reaction of bifunctional monomers were used because addition polymerization reactions could not usually be employed for main-chain organometallic polymers.[11] There are two approaches for preparing polymers using step growth polymerization.[12]

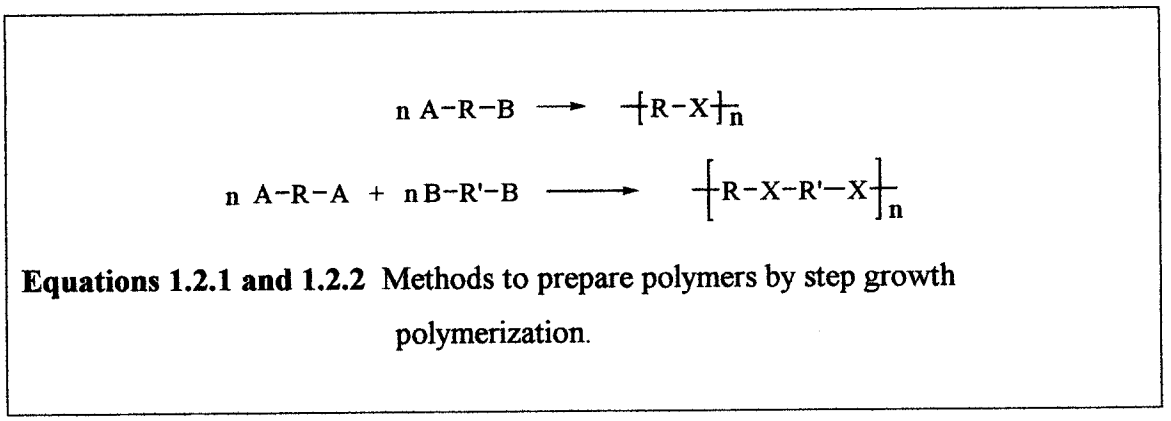

Equations 1.2.1 and 1.2.2 Methods to prepare polymers by step growth polymerization.

The first method uses a molecule that has two functional groups and the second method uses two different difunctional monomers.

The first soluble, well-characterized transition metal based polymers of appreciable molecular weight were ferrocene-containing materials with organosiloxane spacers, which were reported in 1974 by Pittman and co-workers.[13]

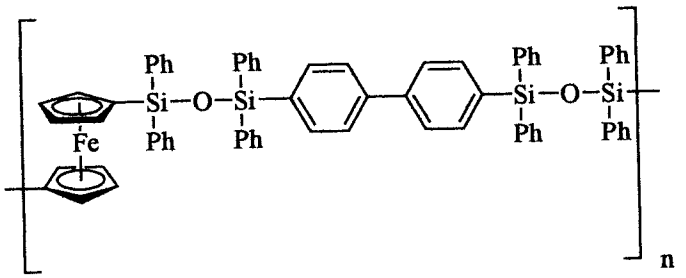

Figure 1.2.2 Transition metal based polymers containing ferrocene with organosiloxane spacers.

In 1977, the first high molecular weight rigid-rod metal polyyne materials were described by Hagihara et al.[14]

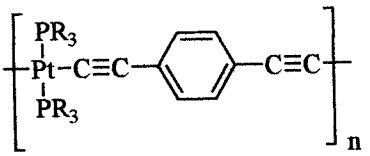

Figure 1.2.3 An example of a rigid-rod metal polyyne.

These are prototypical examples of main chain organometallic polymers: Poly(metallocenes) and rigid-rod acetylide polymers.

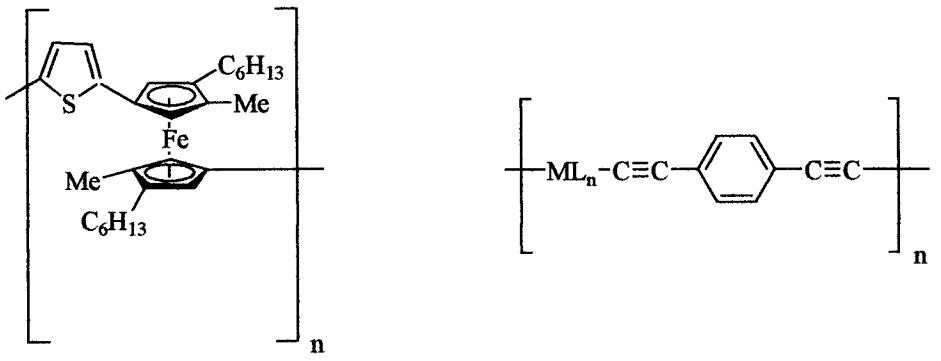

Figure 1.2.4 Some examples of main-chain organometallic polymers.

Many of the polymers shown in Figure 2.4 are soluble in common organic solvents such as benzene, toluene, tetrahydrofuran, and dichloromethane. They also have good electrical, optical, and nonlinear optical properties.[9]

Another type of organometallic compounds of interest are dendrimers (Greek: *dendron* = tree). Dendrimers are hyper-branched nanoscale materials that have potential applications as sequestration agents, micro-catalyst chambers, viscosity modifiers, analogues of proteins and enzymes, etc. Dendrimers are also being used in analytical and NLO applications. The generation number of a dendrimer is essentially the number of branching points along each arm.

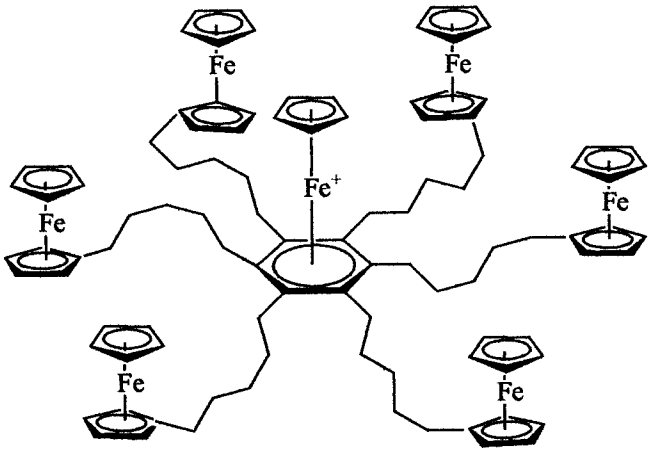

Figure 1.2.5 A first-generation organometallic dendrimer.

As the size of a dendrimer increases, steric crowding increases in the outermost layers. Thus, a typical high generation number dendrimer is sterically crowded on its surface layers, but has significant free space near its central core. This crowding gradient sets the maximum dendrimer generation number at about seven and is responsible for many of their useful properties.[15,16]

Many rigid-rod organometallic main chain oligomers and polymers are 0.5 to 1.0 nm in diameter and several hundreds of nanometers in length and are thus classified as nanomaterials. These materials may have potential uses for their electronic and nonlinear (NLO) properties.[17] Nonlinear optical properties arise from interactions of the electromagnetic fields of light with those of matter. Materials possessing nonlinear optical properties are able to change the nature of light as it propagates through them and also to charge their electronic and other properties as a function of the incident light. This allows different frequencies, amplitudes, polarization, or propagation characteristics to be produced and may also produce coupled changes in electrical and optical properties. Materials with NLO properties are of technological importance in areas that use optical devices such as optical data storage, optical communication, optical switching, image processing, and optical computing.[12,18]

Section Three

Organometallic Nanomaterials

1.3.1 Introduction

Aromatic isocyanides are of interest in the synthesis of organometallic nanomaterials because they are relatively stable, non-toxic, non-volatile and because they form strong complexes with rationally tunable bonding characteristics.

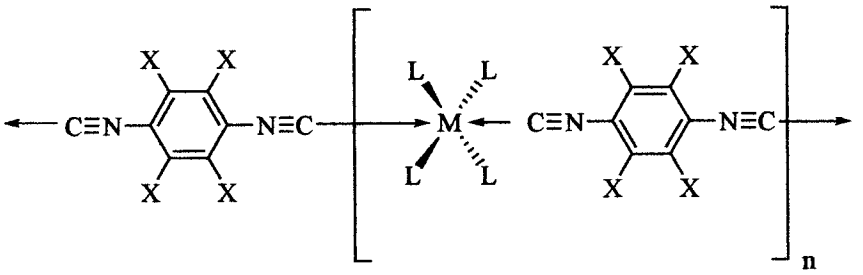

Figure 1.3.1 An example of an organometallic polymer containing aromatic isocyanides.

In addition, free aromatic diisocyanide ligands are also of interest because they are effective molecular-level conductors.[19] These ligands are capable of bridging transition metal centers while mediating communication between the centers through a conjugated dπ-pπ-dπ network.[20] Thus, aromatic diisocyanide ligands could be deposited on a gold surface (Figure 1.3.2) and thus enhance the surface's electrochemical properties.

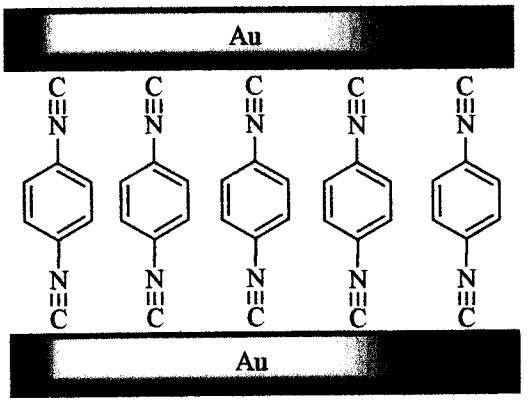

Figure 1.3.2 Free isonitriles bridging molecular wire junctions.[19]

If one uses metal phosphine centers, the steric and electronic properties of the resultant nanomaterials should also be tunable by varying the metal and PR_3 groups. There is a wide variety of structural data available from previous work on monometallic metal isonitriles and metal phosphines that should enable the prediction of the metal geometries of these complexes.

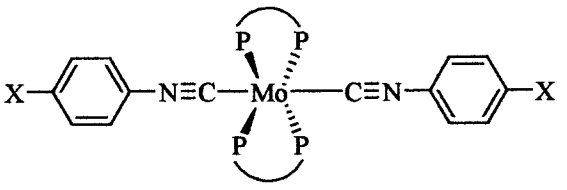

Figure 1.3.3 Metal phosphine center bridging aromatic isonitriles.

Inorganic materials having from three to seven ligands bound to a central metal atom or ion are expected to have star like shapes:

- Two coordinate: Au^{+}
- Three coordinate: Ag^{+}
- Four coordinate: Ni^{0}, Ag^{+}, Cu^{+}, Rh^{+}, Ni^{+2}, Pd^{+2}, Co^{+2}, etc.
- Five coordinate: Fe^{0}, Re^{0}, Co^{+}, Co^{+2}, etc.
- Six coordinate: Cr^{0}, Mo^{0}, W^{0}, Cr^{+}, Mn^{+}, Cr^{+2}, Fe^{+2}, etc.
- Seven coordinate: Mo^{+2}, W^{+2}, W^{+3}, etc.

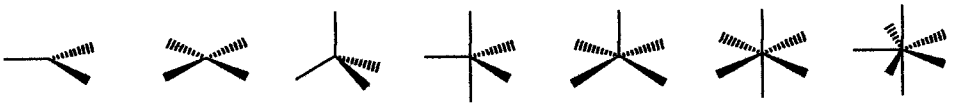

Figure 1.3.4 Possible geometries of homoleptic metal complexes.

Whether they are fluxional or rigid, many homoleptic complexes have such geometries about their metal centers. By using linear organometallic chains instead of simple ligands such as carbon monoxide with these centers, analogous organometallic nanostars having isocyanide-bridged arms should result.

1.3.2 Requisite Organic and Organometallic Reagents

The organometallic nanomaterials described in this thesis contain bifunctional isonitrile ligands of the type 1,4-$C_6H_4(NC)_2$ and 1,4-$C_6Me_4(NC)_2$, and monofunctional isonitriles such as MeO-C_6H_4-NC. The chelating phosphines, (1,4-$C_6H_4Y)_2PCH_2CH_2P$(1,4-$C_6H_4Y)_2$ and (1,4-$C_6H_4Y)_2PC_6H_4P$(1,4-$C_6H_4Y)_2$ (where Y = OMe, Me, and Et) have been chosen because it is thought that these phosphines will improve the solubilities of the complexes compared to the parent phenyl species. In turn, the phosphines will be used to synthesize the dinitrogen starting materials

$Mo(R_2PC_nH_mPR_2)_2(N_2)_2$. Based on molecular orbital arguments, it is expected that more electron rich metal centers (*e.g.*, Y = Me or Et) and electron poor bridges (*e.g.*, C≡N-C_6F_4-N≡C) will give increased electronic communication down the oligomer backbones.

Aromatic isonitriles have been prepared by a variety of methods. The two most common are treatment of aromatic amines with hydroxide in chloroform (A) and the dehydration of formamides with phosgene (B) or its precursors.[21]

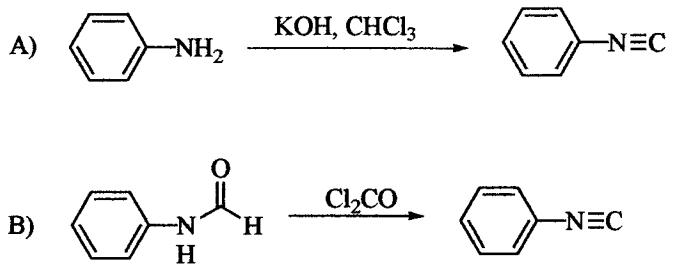

Equations 1.3.2a and 1.3.2b Common methods to synthesize isonitriles.

For the synthesis of diisocyanides, method A gives typically poor results so method B is used. As an alternative to hazardous phosgene gas, the safer "diphosgene" (trichloromethyl chloroformate) or "triphosgene" (bis(trichloromethyl)carbonate) liquid and solid may be used as the dehydrating agent.[22]

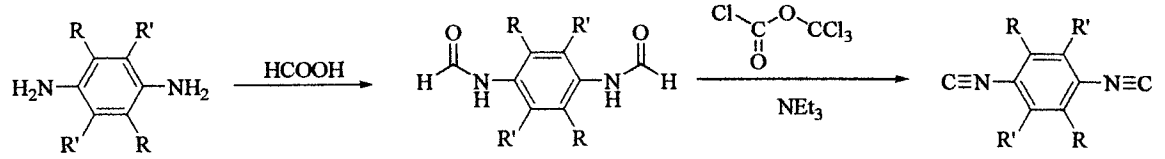

Equation 1.3.2c Synthesis of diisocyanides utilizing diphosgene.

Phosphines will be used as ancillary ligands because they will allow us to tune the solubilities and electron richness of the products. To improve the solubilities of these species over the relatively insoluble dppe complexes, substituted dppe derivatives (i.e., dppe' = $(1,4\text{-}C_6H_4Y)_2PCH_2CH_2P(1,4\text{-}C_6H_4Y)_2$ and $(1,2\text{-}C_6H_4Y)_2PC_6H_4P(1,4\text{-}C_6H_4Y)_2$ where Y = OMe, Me, Et, etc.) will be used to systematically change the electron richness at Mo and the materials' steric bulk.

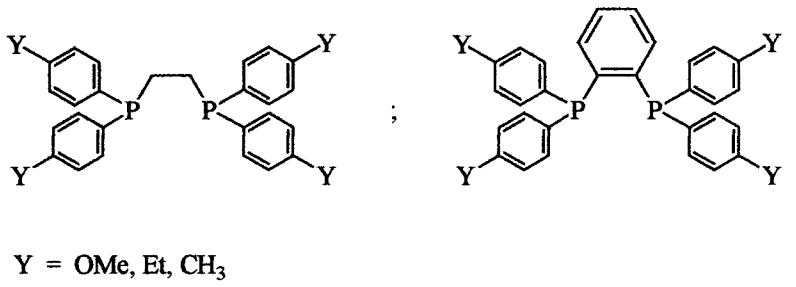

Figure 1.3.5 Examples of some chelating phosphines.

The typical synthetic route for preparing the phosphines is shown below.[23]

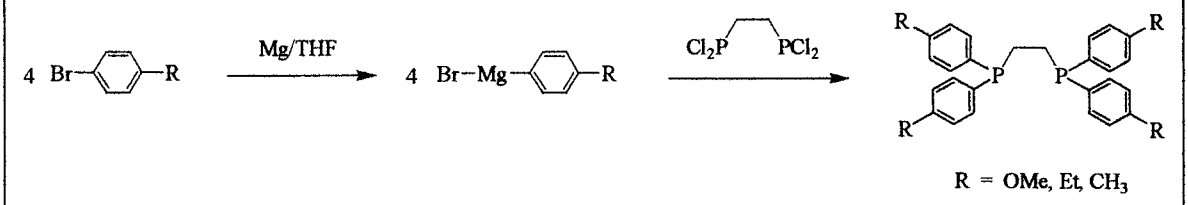

Equation 1.3.2d Synthesis of chelating phosphines.

In this reaction, commercially available bis(dichlorophosphino)ethane is used as the starting material. Reaction of this compound with a Grignard or organolithium reagent in THF generally produces the desired dppe derivatives.

The precursors used for the synthesis of our organometallic materials are molybdenum and tungsten dinitrogen complexes of the type $M(N_2)_2(PR_3)_4$. They are generally well known compounds for the phenyl derivatives and have been extensively investigated as possible catalysts for chemical low-pressure nitrogen fixation.[24] In our new chemistry, the dinitrogen ligands will be exchanged with diisonitrile molecules to get the first generation-metal-diisonitrile building blocks. Bis-isonitrile complexes of the molybdenum phosphine complex (*e.g.*, $Mo(PR_3)_4(C{\equiv}N\text{-}C_6H_5)_2$) have previously been prepared by displacement of a weak ligand such as N_2 from the phosphine center. These starting materials (*e.g.*, $Mo(PR_3)_4(N_2)_2$ and $Mo(PR_3)_4(N_2)(NCMe)$) can be made by several routes, most commonly by the reduction of a molybdenum halide under an atmosphere of dinitrogen using a variety of reducing agents, or by analogous multistep procedures involving the isolation of intermediate products of this process.[25]

Equation 1.3.2e Synthesis of molybdenum dinitrogen complex.

In the next step, the first new nanorod building blocks will be synthesized. To avoid the uncontrollable formation of polymers, an excess of the isonitrile ligand will be used:

Equation 1.3.2f Synthesis of nanorod building blocks.

Similar monometallic complexes with only one isonitrile ligand per molybdenum center have been reported using a slightly different approach starting with Shiff-bases instead of diisonitriles.[26]

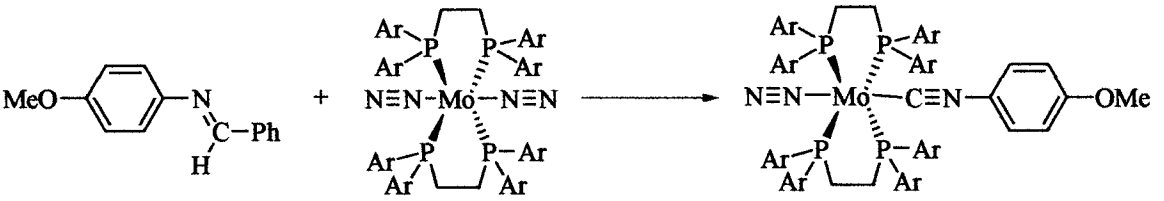

Equation 1.3.2g Synthesis of monometallic complexes.

Longer oligomers will then be synthesized by combining the dinitrogen terminated first generation nanorods, the isonitrile terminated first generation nanorods, the bifunctional isonitriles, and/or the bis-dinitrogen complexes in appropriate proportions. When oligomers of the final desired chain length are made, they will be capped with terminal organometallic groups, including: $M(CO)_5$ (M = Cr, Mo, W), $CpFe(CO)_2^+$, $CpMn(CO)_2$, $Mo(dppe')_2CO$, or $Mo(dppe')_2(CN\text{-}R)$. The organometallic 'caps' will be prepared via published routes (equation 1.3.2h).[27]

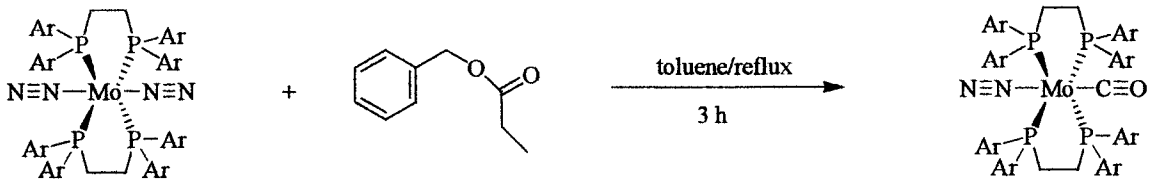

Equation 1.3.2h Synthesis of organometallic caps.

However, the syntheses will require careful exploration of the reaction conditions to optimize conditions and prevent mixtures of non-capped, mono-capped, and di-capped species from forming. When more electron poor caps such as $Mo(CO)_5$ are used, it is expected that they will tend to polarize the organometallic isocyanide backbone and will also influence the degree of conjugation between the backbones and the caps. The most electron rich caps are expected to display the best conjugation. These 'capped' complexes will then be used to form organometallic nanostars.

Many metal-isocyanide complexes of transition metals are known. They are typically prepared in excellent yields, either by reacting isocyanides with a metal salt or reducing the metal salt in the presence of isocyanides.[25]

$$MCl_x(solvent)_k + z\ CN\text{-}arene\text{-}X \longrightarrow M(CN\text{-}arene\text{-}X)_z^{x+}$$

$$MCl_x(solvent)_k + reducing\ agent + z\ CN\text{-}arene\text{-}X \longrightarrow M(CN\text{-}arene\text{-}X)_z$$

Equation 1.3.2i and 1.3.2j Synthesis of metal-isocyanide complexes.

Each nanostar will be prepared by using the specific reaction conditions used for the metal and conventional aryl isocyanides. It is expected that high yields will be obtained, but a major synthetic challenge will be the purification of the nanostars. Possible methods for purification are fractional crystallization and chromatography. Fractional crystallization works remarkably well if the synthesis is designed so that any byproducts are different from the desired material. Chromatography is very effective at removing byproducts that have different end-groups. However, column chromatography is quite tedious and often unsuccessful if there is a mixture of oligomers varying only in the number of repeating units.

The proposed organometallic nanostars are expected to have varying degrees of electronic conjugation down their arms and across their central vertices. They are likely to have fascinating electrical, conductive/semiconductive (i.e., when doped/partially oxidized, and NLO behavior when attached to surfaces. In molecular orbital terms, the maximum degree of electronic communication of the nanostars is expected when the metal fragment's highest occupied molecular orbitals, HOMOs (of predominately metal d character), are of relatively high energy and the isonitrile's lowest unoccupied molecular orbitals, LUMOs (of π^* character), are of relatively low energy. It is also expected that increasing the electron richness at the molybdenum centers and decreasing it at the isonitriles should result in increased HOMO-LUMO overlap and hence conjugation.

1.3.3 Characterization of the Organometallic Building Blocks

It is expected that the new organometallic materials will be relatively air and thermally stable. Elemental analysis, IR, and ^1H, ^{13}C, and ^{31}P NMR spectroscopy will be used to characterize the physical and spectroscopic properties and for information on

purity and identity. X-ray diffraction will be used to determine the solid-state crystal structures of these building blocks. This will provide detailed structural information including: the degree of linearity down their oligomer backbones, the three dimensional geometries at the central metal cores, and the extent of steric interactions. Intermetallic interactions can be quantitatively evaluated by cyclic voltammetric studies and qualitatively inferred from IR spectroscopy.

Section Four
Ferrocene Chemistry

1.4.1 Introduction

Ferrocene is one of the most important compounds in the fields of organometallic chemistry and electrochemistry. The accidental synthesis of ferrocene[28,29] in 1951 caused an explosion in the organometallic field that still continues. It is a prototypical metallocene that consists of two cyclopentadienyl rings bound on opposite sides of a central iron atom to form an organometallic "sandwich complex." Ferrocene's novel structure and chemistry are credited with the rapid acceleration of modern organotransition metal chemistry.

Because of ferrocene's unique properties, its derivatives are the most frequently used molecules for applications in molecular electronic devices. For example, when two ferrocenyl units are incorporated into a conjugated system, the intramolecular electronic interactions between them, so-called electrochemical communication, are readily observed. Thus, if one of the two ferrocenyl groups is oxidized to the monocation, the delocalization of the cationic charge between ferrocene and the ferrocenium ion may occur to give a mixed valence state.[30] Ferrocene is oxidized at a potential of approximately 0.35 with respect to SCE and the relative potential between free ferrocene and its complexes as measured by cyclic voltammetry acts as a sensitive probe of metal-ligand interactions.

A specific ferrocene derivative, isocyanoferrocene (η^5-C_5H_5)Fe(η^5-C_5H_4-N≡C:), is a redox-active ligand that was developed in the late 1980's.[31]

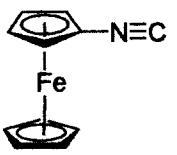

Figure 1.4.1 Isocyanoferrocene.

The chemical and physical properties of isocyanoferrocene promise to be very intriguing from both fundamental and practical points of view. It is a redox-active ligand that is compatible with highly electron rich fragments. Isocyanoferrocene also has remarkable thermal stability due to the partial delocalization of back-donated electron density into the rings' π^* system.[32] Finally, one of the most important aspects of its properties is that the iron atom ferrocenyl unit of isocyanoferrocene complexes should be in strong electron communication with the central metal unit in an oligomer or polymer[33] via the extended π system in the isonitrile bridge. The incorporation of isocyanoferrocene into our systems is not only because of ferrocenes unique properties, but also due to the distinctive properties of the isocyanide complex.

Continuous interest in isocyanide complexes of transition metals has been associated, in part, with their similarity to metal carbonyls. It has been found that certain CNR (R = aryl) ligands, *e.g.*, isocyanoferrocene, are far more versatile compared to CO not only sterically but also electronically. Isocyanides are commonly synthesized by the dehydration reaction of formamides. This method was first developed by Ugi et al.[34] in the early 1960's, which allows the synthesis of a wide range of substituted aryl and alkyl isocyanides. The Ugi dehydration method can also be used for the synthesis of organometallic isocyanides including isocyanoferrocene. The chemistry of isocyanoferrocene has remained practically undeveloped since its discovery in the late 1980's. This is undoubtedly, due to the tedious synthesis of the starting material aminoferrocene which involves one of several multiple step procedures.

In our research, isocyanoferrocene will be used as an electronic sensor. It will be placed at one or more sides of other metal centers to supply information pertaining to the electronic communication within and between the centers.

1.4.2 Synthesis of Aminoferrocene

The first successful methods for the synthesis of the aminoferocene were based on the reaction of the ferrocenyl anion with an amine reagent of reversed polarity.[35,31]

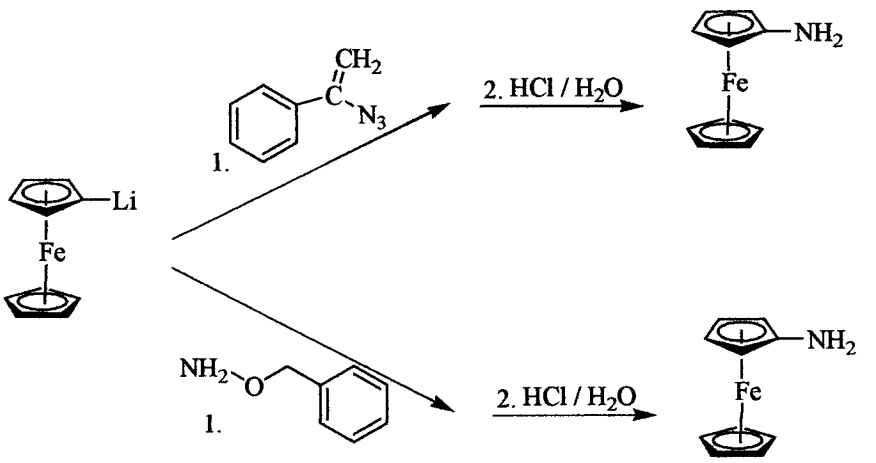

Equation 1.4.2a Synthesis of ferrocenylamine.

These methods utilizing either alpha-azido styrene[36] or benzylhydroxylamine[31] were not very reliable and the purity of the isolated amine was not acceptable. Among other problems, the *in situ* formation and reaction of the ferrocenyl anion seems to be critical. This anion is only moderately stable even at low temperatures and dilithiation is a common side reaction. The choice of solvent and the correct temperature were discovered to be important factors. For the selective monolithiation of ferrocene, THF below -20 °C was found to be the best solvent and ^{t}BuLi slowly added to the solution (over a period of 1 h) was found to be the preferable base. To overcome these problems, Bildstein et al.,[37] developed an alternative multi gram synthesis of ferrocenylamine based on using phthalimide as the protecting group for the synthesis.[38,39]

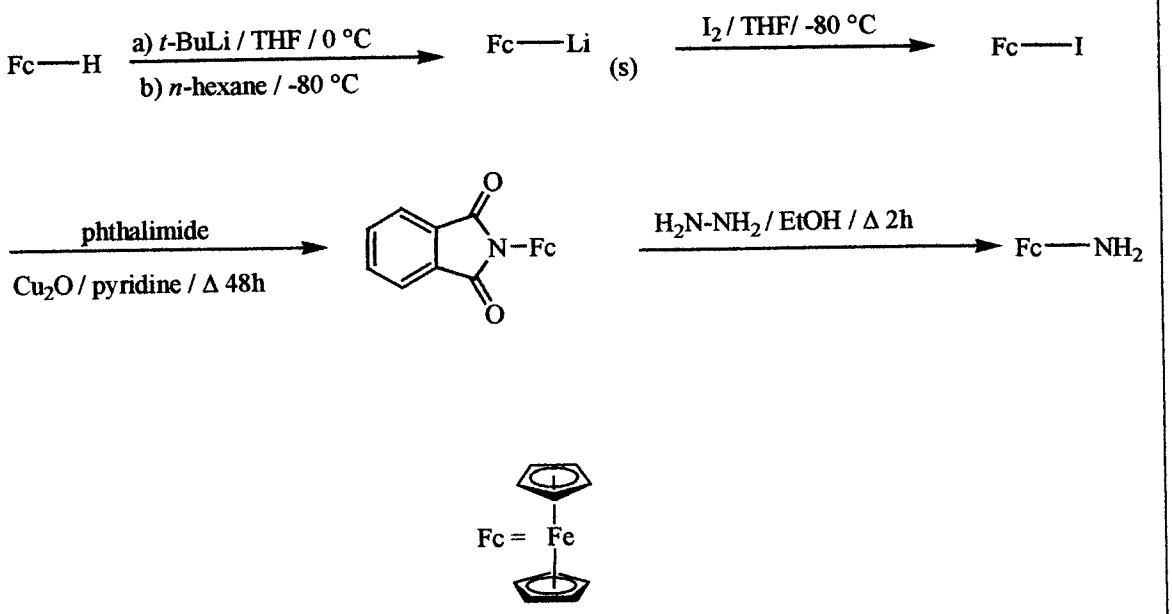

Equation 1.4.2b Synthesis of ferrocenylamine via the Gabriel synthesis.

In the first step, ferrocene is selectively monolithiated and isolated as a solid. In the next step, it is reacted with iodine to form iodoferrocene following which iodoferrocene is then converted via a copper catalyzed coupling reaction into the phthalimide. In the last step, deprotection with hydrazine using the Gabriel reaction gives high yields of analytically pure ferrocenylamine, the precursor of isocyanoferrocene.

1.4.3 Synthesis of monoisocyanoferrocene

As stated previously, isocyanoferrocene[40] is an attractive synthetic target due to its ability to act both as a cap for the organometallic oligomers as well as an electrochemical sensor for these compounds. It can be synthesized in a way similar to other aryl isocyanides and bisisocyanides by the dehydration of the corresponding formamide. The formamide is made from ferrocenyl amine by the reaction with a formylating agent such as ethyl formate.

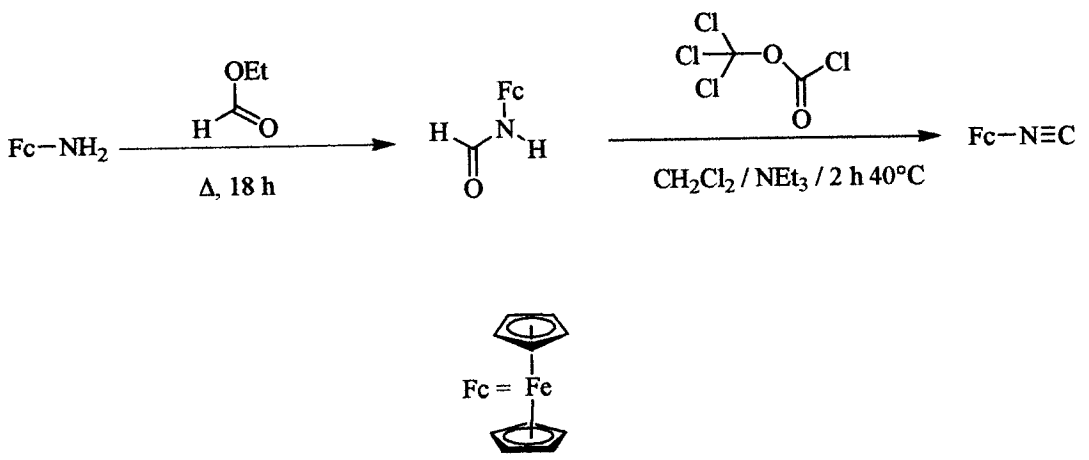

Equation 1.4.3a Synthetic route for the synthesis of isocyanoferrocene.

Ferrocenyl formamide is the first intermediate in this sequence and exists in solution as a mixture of several isomers as shown in Equation 1.4.3b. It was characterized by Knox et al.,[31] via analytical techniques such as mass spectrometry and ^{1}H and ^{13}C NMR and IR spectroscopies. The IR spectra are in agreement with the formamide structure and in the mass spectra only monomeric ferrocenyl formamide and its fragments were found. In contrast to this finding, the NMR spectra contain multiple sets of signals and thus in solution it appears to be an equilibrium of the *cis* and *trans* isomers of the monomer and at least one dimeric or oligomeric aggregate.

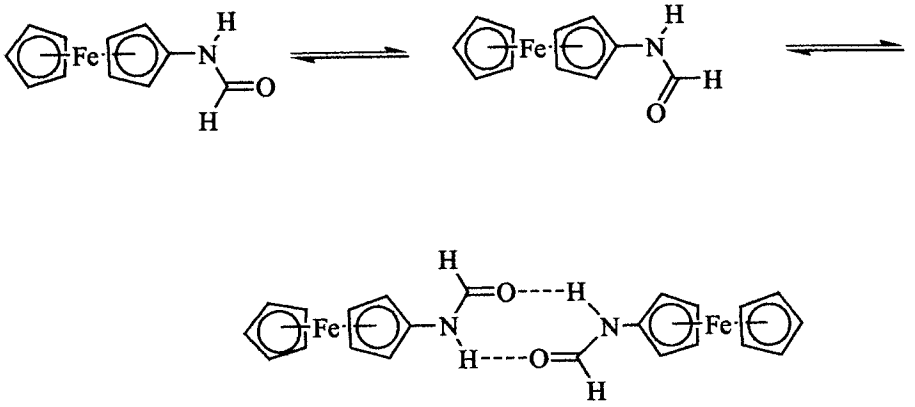

Equation 1.4.3b Equilibrium mixture of ferrocenyl formamide.

The formamide was found by Knox et al., to be a microcrystalline solid which could not be analyzed by single crystal X-ray diffraction. Knox also states that the resulting isocyanoferrocene compound was obtained in various non-reproducible yields (25-90%) and that the results may be effected by the numerous isomeric forms of the formamide.

1.4.4 Synthesis of 1,4-isocyanoferrocenylbenzene

A phenyl derivative of isocyanoferrocene (*e.g.*, 1,4-isocyanoferrocenylbenzene)[40] can also be prepared. *Para*-ferrocenylaniline is used as the starting point for the synthesis of isocyanoferrocenylbenzene. The starting material for this compound is *para*-nitrophenylferrocene. *Para*-nitrophenylferrocene is synthesized by the arylation of ferrocene with a diazonium salt under phase transfer conditions following which the nitro compound is then reduced with tin under acidic conditions to produce the ferrocenylaniline.[41]

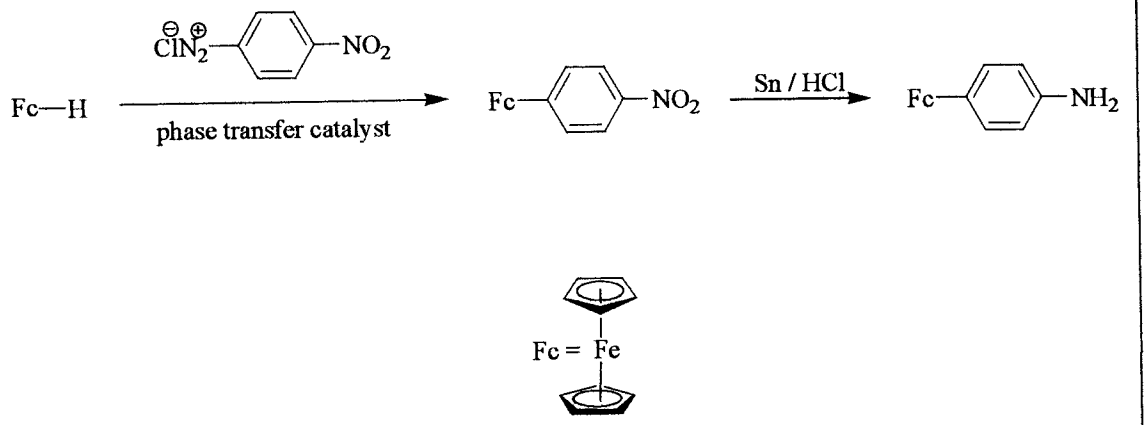

Equation 1.4.4a Synthesis of *para*-ferrocenylaniline.

Ferrocenylaniline will then be converted into isocyanoferrocenylbenzene by the same method as described in the previous literature as shown in Equation 1.4.4b.

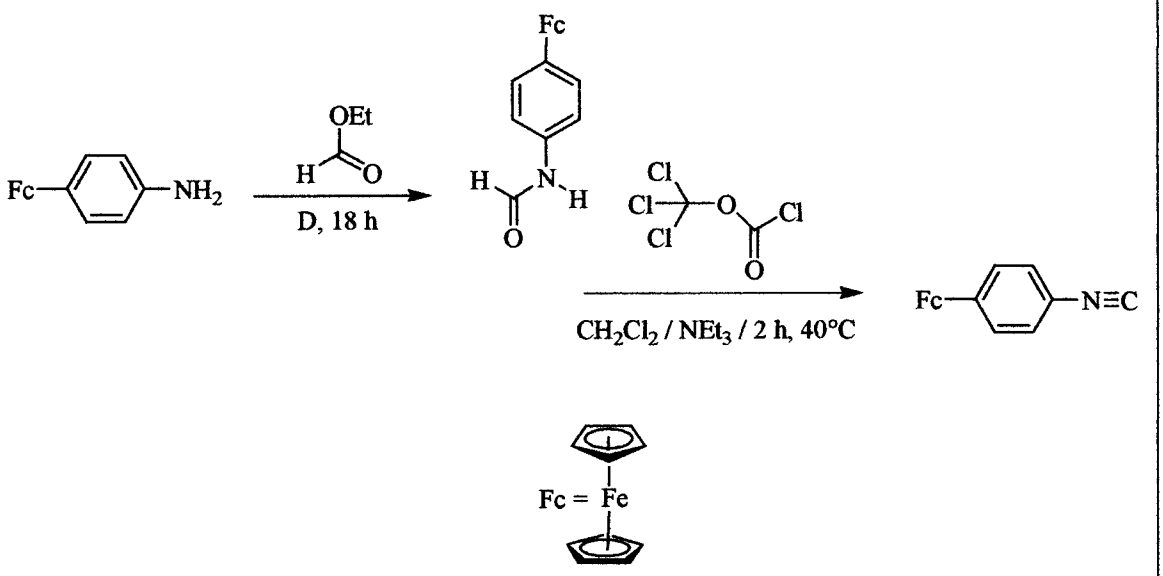

Equation 1.4.4b Synthesis of isocyanoferrocenylbenzene.

The solubility and electronic properties of the aniline derivative will be compared to the parent isocyanoferrocene. The electronic properties of the two complexes are expected to be similar. When comparing their solubility properties, the insertion of the aromatic ring between the ferrocene unit and the isocyanide should allow for an increased solubility in organic solvents. In the next phase of our research, the ferrocene derivatives will be integrated as ligands in our metal complexes to produce the first nanorod building blocks with a ferrocene moiety.

Based on the literature, it appears that the syntheses of the parent ferrocenylamine will be substantially more challenging than that of the 1,4-ferrocenylphenylanaline. However, the subsequent formylations and then dehydrations of these species are expected to be of similar difficulties and to be generally less challenging than the amine preparations.

1.4.5 Nanorod building blocks

The ferrocene units (*e.g.*, isocyanoferrocene and isocyanoferrocenylbenzene) on an oligomer will serve as electrochemical "sensors." Thus they will give information reguarding the electronic communication between the metal center and the ferrocene

components and between sets of intermediary metal-ligand-metal chains. A route for the synthesis of the molybdenum-monoisocyanide oligomers will start with Mo('dppe')$_2$ (dinitrogen)$_2$ complexes. The dinitrogen molecules of these complexes are only loosely bonded to the metal center and can be easily exchanged by other ligands such as isocyanoferrocene.

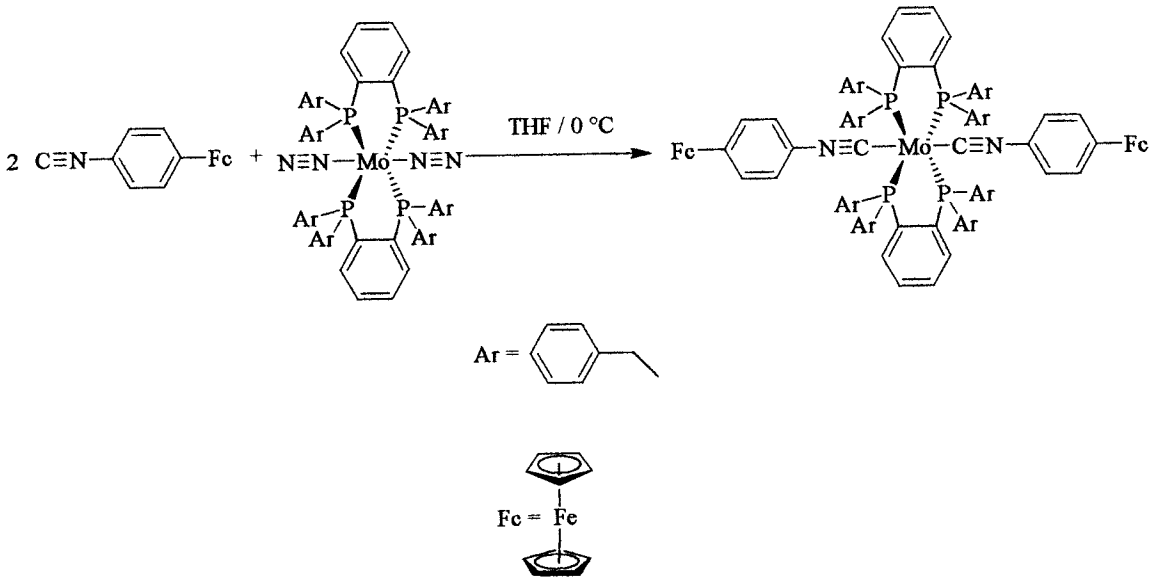

Equation 1.4.5a Synthesis of bis[bis{di(*p*-ethylbenzene)phosphino}benzene] bis (isocyanoferrocenylbenzene) molybdenum(0).

The isocyanide is able to displace the dinitrogen ligand due to the terminal N_2 ligands' net σ and π interactions being weaker than those for π-acid ligands such as isocyanides. With the ferrocenyl electrochemical sensors now incorporated into the metal chains and stars, the delocalization of charge between the two or more ferrocene units will be observed by electrochemistry.

1.4.6 Electrochemistry

With the importance of ferrocene in the field of material science, there has currently been great interest in the chemistry of ferrocene-based oligomers and ferrocenyl

containing conjugated compounds. The electrochemical properties of ferrocene and its derivatives have been extensively exploited in a large number of electronic applications including molecular switches, metal probes, molecular magnets, and non-linear optics. Complexes with ferrocene units can, upon oxidation, form mixed valence states and charge transfer complexes. The ferrocene / ferrocenium (Fe(II) / Fe(III)) couple is stable, is largely independent of solvent in terms of its redox behavior, and the redox processes are electrochemically generally totally reversible.[42]

It has been found that a combination of factors influence the electrochemical interactions between connected ferrocene moieties including the type of connection, the length of connector, and the orientation of the ferrocene units.[43] A few examples will be presented here to illustrate the different types of interactions between ferrocene units with various connectors (e.g alkyl groups or π-conjugated units) in their main or side chain.

The first example, in Figure 1.4.2, shows two ferrocene units that are connected by the covalent bonds of a pair of bridging alkynes. The compound displays an interesting redox activity which can be accounted for by the very fast electron exchange between the ferrocene centers.[44]

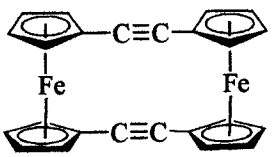

Figure 1.4.2 Example of a bridging ferrocene.

In the next example, Figure 1.4.3, it has been discovered that polymers with an undetermined number of ferrocene units give only "one" sharp redox couple in their cyclic voltammograms. This result indicated that each ferrocene unit is oxidized at the same potential.[45]

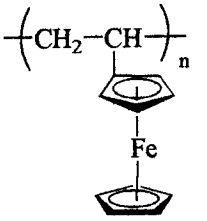

Figure 1.4.3 An example of a ferrocenic polymer (PVFc).

Finally, conjugated bridging ligands are advantageous as they allow the metal atoms to interact through the adjoining π segment, thus influencing the metal-metal electronic interaction between the 1,1'-ferrocenylene units.[46]

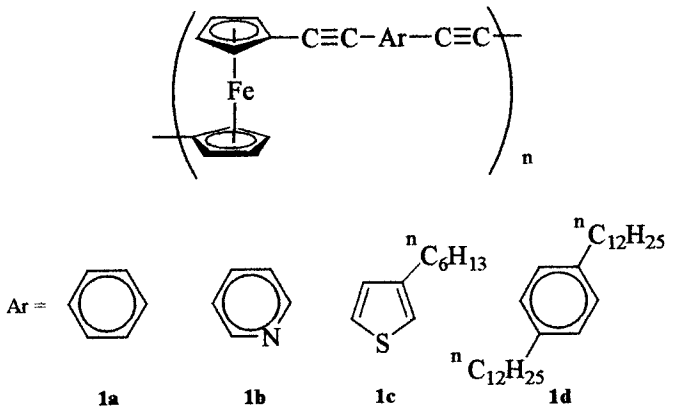

Figure 1.4.4 Ferrocene units with a π-conjugated system.

Cyclic voltammetry was performed on these π-conjugated systems in a 1:1 mixture of CH_3CN and CH_2Cl_2 containing 0.1 M [*n*-Bu_4N]BF_4 under nitrogen and with the concentration of the ferrocene unit being 1.0×10^{-3} M. A Ag+/Ag quasi-reference electrode was used in the determination of the redox potentials. The polymers were

shown to be redox active and showed a higher oxidation potential than that of ferrocene presumably due to the electron withdrawing nature of the ethynylene units attached to the ferrocenes. In the cyclic voltamograms, a broadened peak is observed indicating an electron exchange between the ferrocene units. Furthermore, the delocalization and intermolecular exchange of electrons were considered to be the origin of the bulk electrical conductivity in partially oxidized polymers.[46] The type of compounds in Figure 1.4.4 have been found to exhibit unique redox behavior and have the potential to lead to the development of new redox systems.[47] Yamamoto et al.[48] proposed that sequential super exchanges between the neighboring redox sites in these compounds would occur. The cyclic votamograms of these compounds have demonstrated one couple of Fe(II)/Fe(III) redox peaks and the CV's showed excellent reversibility.[46]

In addition to the investigation of these specific conjugated systems, attention has recently been given to new highly branched systems (metallodendrimers) containing a regular three-dimensional monodisperse macromolecule which has branches occurring from each monomer unit. Examples of various ferrocene dendrimers are shown in Figure 1.4.5.[49]

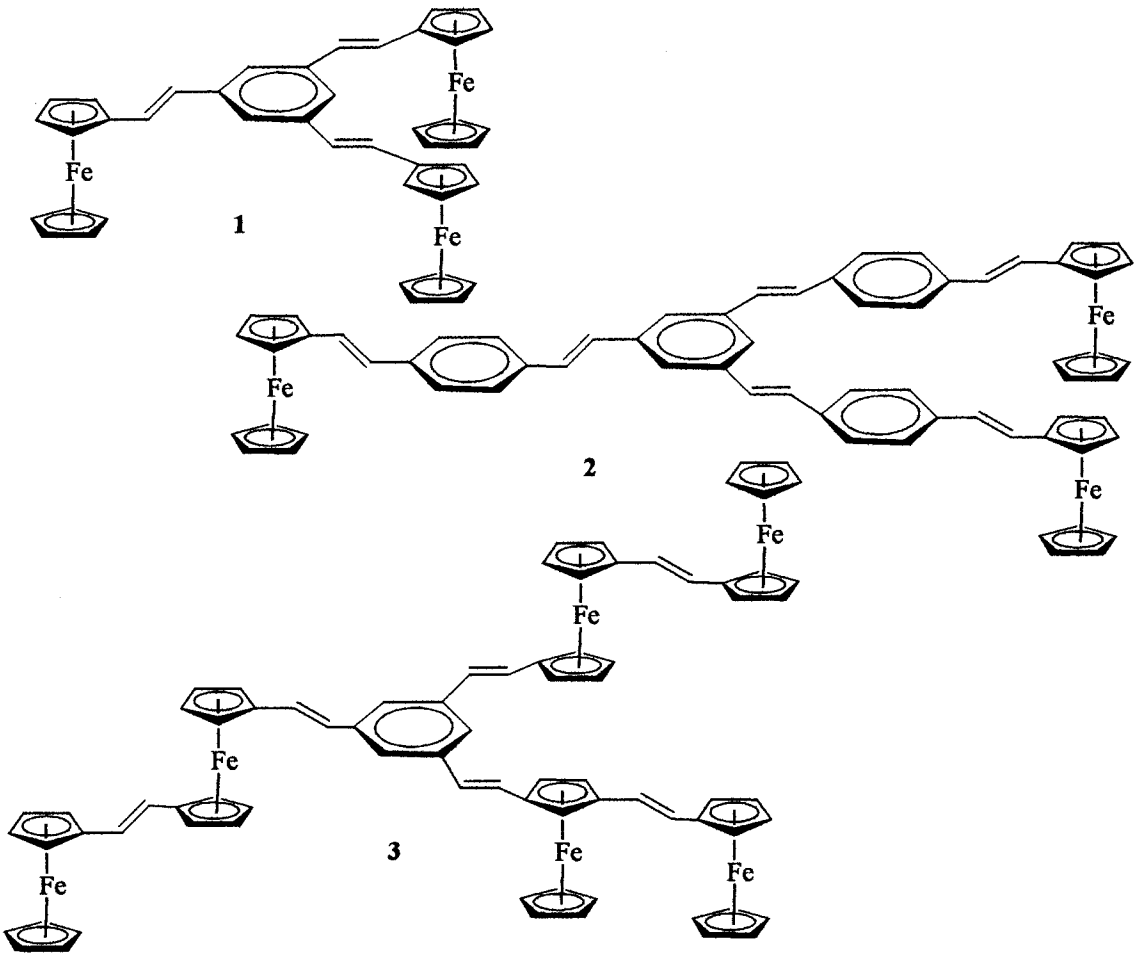

Figure 1.4.5 Ferrocene-containing dendrimers.

CV in CH_2Cl_2 revealed a chemically reversible ferrocene/ferrocenium couple indicating electron delocalization along the conjugated systems. It was also discovered that systems which contained a greater degree of delocalization were oxidized at lower potentials. Interestingly, a single reversible wave (i.e. having the same peak to peak separation of ferrocene but three times as intense) was found to occur for **1** and **2** which indicated that the iron centers are not interacting. Two reversible, three-electron oxidations were observed for **3** which probably arise from substituent effects. In an interesting note, investigation into the redox behavior of compounds **1-3** has yielded a correlation in the

nature of the redox behavior with solubility and the oxidation states of the compounds.[50] It was also found that the intensity of the cathodic peak is to some extent higher and sharper than the anodic one, which is due to precipitation onto the electrode surface.[49] The investigation into the electrochemistry of these complexes has generated interest into specific canidates that would be eligible for size tunable complexes.

It has been discovered that compound **3** is a size tunable complex in which the radius can be electrochemically switched as observed in Figure 1.4.6.[49]

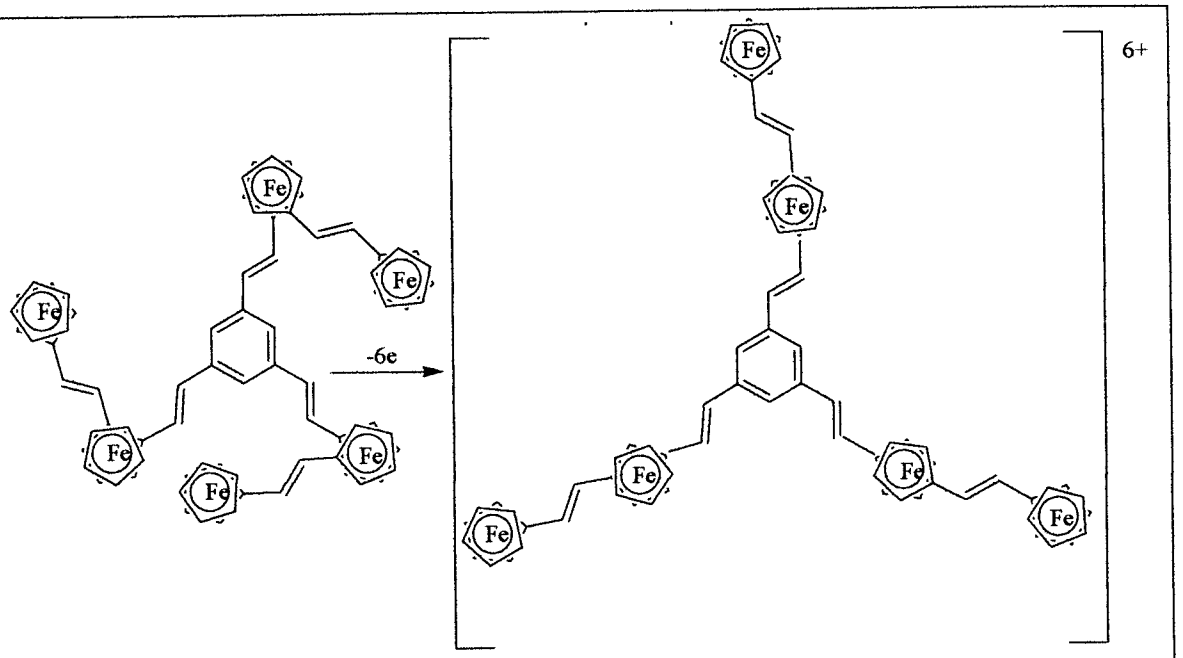

Figure 1.4.6 An example of a tunable complex.

When compound **3** is fully oxidized it shows a structural rearrangement to give a fully expanded form. This effect occurs to minimize the electrostatic repulsion between the six iron centers. The rearrangement could also be partially due to the stabilization produced by an intramolecular π-stacking of the ancillary ligands.[49]

The complexes in Figure 1.4.6 possess redox centers which have been incorporated into the molecule to give the supramolecular species interesting electrochemical properties. The electrochemical studies do not demonstrate any significant through bond interactions between the iron centers of different branches of the complexes.

1.4.7 Conclusion

Because of ferrocene's unique properties, its derivatives will be integrated into our metal complexes to produce the first nanorod building blocks with ferrocene caps. In the first step of our research, the chemical and electrochemical properties of model compounds with only one or two metal centers will be investigated. Putting electrochemical "sensors" such as isocyanoferrocene at one or two sides of the complexes will give information about the electronic communication via the metal centers. Using cyclic voltammetry, the oxidation potentials of the iron and molybdenum centers will be determined as functions of the other substituents of the molecule.

Section Five
Nickel Chemistry

1.5.1 Introduction

With a steadily growing interest in organometallic complexes, newly developed compounds continue to broaden the scope of possible chemical and electrochemical applications from the research to the industrial level. Tetrakis nickel(0) complexes have been recently investigated due to their chemical and electrochemical properties. One of the most important properties of the complexes is their tetrahedral star shape which are expected to have degrees of conjugation down its arms and across its central vertices with appropriate arms. These complexes are also expected to display electrical conductivity and semiconductivity when they are doped or partially oxidized. Last and foremost, the association of electronically delocalized stars with surfaces is expected to influence the electrochemical properties of the surfaces.

1.5.2 Nickel (0) complexes

Nickel(0) complexes have been chosen for this specific research because they can induce oxidative addition[51] and are also catalytically active.[52] Numerous complexes of nickel exist which contain a variety of ligands. As an example, unsaturated molecules (*e.g.*, alkenes and alkynes) are frequently used as substituents on nickel complexes along with group V donors (*e.g.*, As, P, and Sb). Bis(1,5-cyclooctadiene)nickel(0) is a common starting material for the NiL_4, NiL_2, and $NiL_2(UN)$ class of compounds (*e.g.*, L = phosphine, arsine, stibine, nitrogen base, or isocyanide, and UN = olefin, acetylene, or azide complex).[53] Bis(1,5-cyclooctadiene)nickel(0) has been found to be an exceptionally good starting material for the less π-accepting homoleptic isocyanide nickel(0) complexes. The complex $[Ni(Me_3Si\text{-}NC)_4]$ was the first homoleptic isocyanosilane complex reported and was prepared from bis(1,5-cyclooctadiene)nickel(0) and trimethylcyanosilane.[54] This reaction represents a successful isomerization of a nitrile to

an isocyanide. The homoleptic isocyanide complexes can also be prepared in reasonable yields by the reaction of nickelocene with an excess of an alkyl or aryl isocyanide.

$$[Ni(C_5H_5)_2] + CNR\ (excess) \longrightarrow [Ni(CNR)_4] + 2\ C_5H_5$$

Equation 1.5.2a Nickelocene reaction.

Otsuka et al.[55] investigated the synthesis of nickel isocyanide complexes. They discovered that treatment of the aliphatic isocyanide ligands (*e.g.*, *t*-BuNC) with bis(1,5-cyclooctadiene)nickel(0) gave the tetrakis nickel isocyanide complexes $Ni(RNC)_4$ (R = t-butyl or cyclohexyl).

$$[Ni(C_8H_{12})_2] + CNR\ (excess) \longrightarrow [Ni(CNR)_4] + 2\ C_8H_{12}$$

Equation 1.5.2b 1,5-cyclooctadiene reaction.

1.5.3 Peroxo complexes

Nearly all Ni^0 complexes are moderately to very air sensitive and give intractable oxidation products in the presents of oxygen.[56] Tetrakis nickel isocyanide complexes have been found to be air sensitive in organic solvents. In aromatic hydrocarbons, ether, or THF solutions below -20° C, a peroxo complex results when the nickel isocyanide compound is exposed to pure gaseous oxygen or air. In a preliminary study, a pale green peroxo complex (*e.g.*, $Ni(O_2)(RNC)_2$, R = *t*-butyl or cyclohexyl) resulted when oxygen was introduced into solutions of the nickel isocyanide complex $Ni(RNC)_4$. It has also been observed that an oxygen molecule introduced into an etheral solution of a *t*-butyl isocyanide nickel complex results in the quantitative formation of the equivalent peroxo complex.[55]

The peroxo complexes discussed above are sensitive towards air in the solid state and in solution. It has been discovered that a dried sample of the peroxo complex on exposure to air, even without shock, can explode. In a $CHCl_3$ solution at 0 °C, the peroxo complexes have also been found to slowly decompose.[55]

1.5.4 Transition-metal alkynyl complexes

Transition-metal alkynyl complexes are isoelectronic with CN^-, CO, CNAr, and N_2. The color, magnetic properties, and stoichiometry of the transition-metal alkynyl complexes are also very similar to the isocyanide complexes. Based on these findings, Hagihara[57] developed a method to synthesize σ-alkynyl derivatives of transition metals. It involved the direct dehydrohalogenation reaction between the Group 10 metal halides and terminal alkynes with electron withdrawing substituents. A few years later, a copper (I)–catalyzed reaction was developed for the dehydrohalogenation of a wider range of metal halides (Ni, Pt, and Pd) in an amine solvents.[58] In this reaction, the use of specific amines (*e.g.*, diethylamine, diisopropylamine, or piperidine) resulted in mono- or dialkynyl compounds which have square planar metal centers with a *trans-* orientation of the ligands.[59,60] After extensive research, the *cis* isomer was prepared using *N,N,N',N'*-tetramethylethylenediamine.[61]

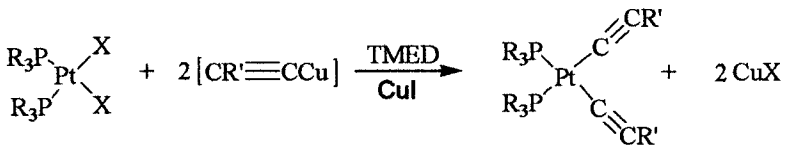

Equation 1.5.4a *Cis* and *trans* dialkynylplatinum complexes.

To prevent further reactions in compounds with a second terminal alkynyl group, a large excess of the alkyne needs to be used. This prevents the formation of oligomers or polymers. Slow isomerization was observed between the *cis* and *trans* forms in amine solutions under reflux. In addition, the addition of the cuprous halide was found to accelerate the isomerization process.[58]

Following the work of Hagihara,[57] three general copper catalyzed reactions can be employed to synthesize various rigid-rod σ-bonded alkynyl polymers with molecular weights (M_w) greater than 10^6. In the first reaction, diterminal alkynes and transition-metal halides react with an amine to induce dehydrohalogenation. Equation 1.5.4b shows the result of the dehydrohalogenation reaction.

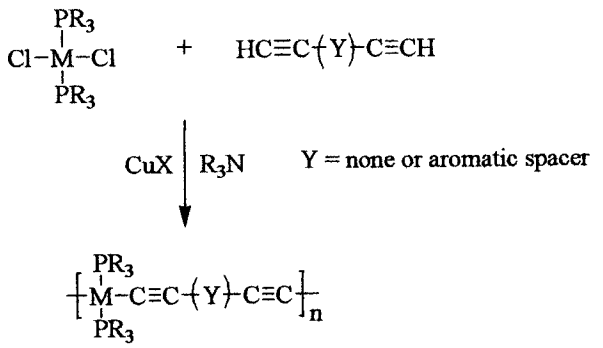

Equation 1.5.4b Dehydrohalogenation reaction.

Hence the amine acts as both an acid acceptor and as the solvent for this reaction. Polymerization was found to occur both at room temperature and under reflux.[62,63]

In the second copper catalyzed oxidative coupling reaction, transition-metal species with two terminal alkynyl groups are coupled by oxygen.

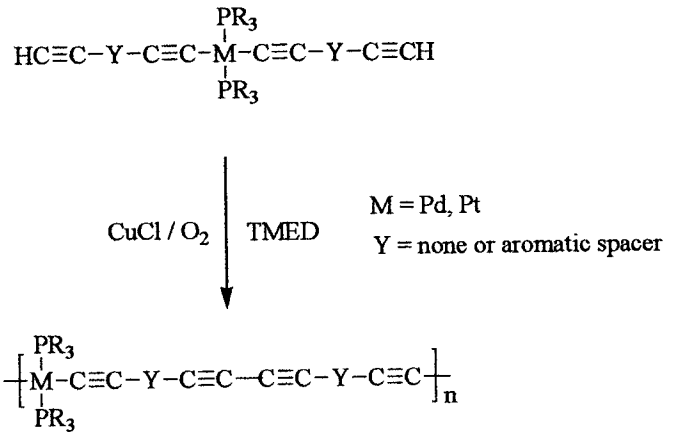

Equation 1.5.4c Hay's coupling reaction.

The degree of polymerization is usually very high in the reaction and there is no stoichiometric restrictions on a reactant bearing different functional groups. The dehydrohalogenation and the oxidative coupling reactions work well for Platinum (M_w of approximately 100,000 units) and fairly well for palladium (M_w of approximately 20,000) but neither of these methods work for Nickel.

Nickel complexes are not well suited for the dehydrohalogenation or oxidative methods due to reactions of the nickel centers with the oxidative-coupling reagents and the decomposition of the nickel complexes in amine solvents. To solve this problem, a third copper catalyzed route involving an alkynyl-ligand exchange process in amine solvents is used. Equation1.5.4d represents the result of the alkynyl-ligand exchange process.[64]

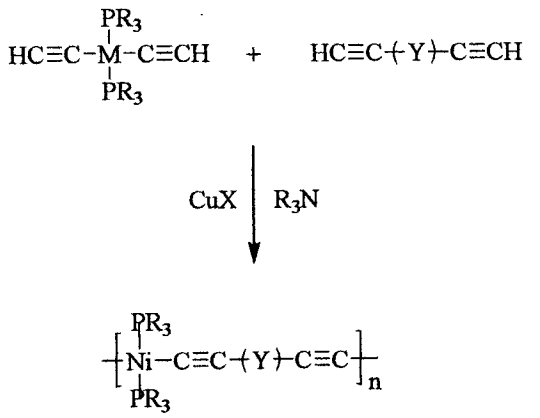

Equation 1.5.4d Result of copper-catalyzed alkynyl ligand exchange.

To prevent decomposition of the polymer, a small amount of free PR_3 is added to the reaction. The PR_3 presumably works by suppression of phosphine dissociation from the metal center. These three methods have been developed to add various end groups on the polymers and to vary their electronic properties. In addition, the degree of polymerization can be easily controlled by the amount of the alkynyl group added to the reaction. Along with the rigid-rod σ-bonded alkynyl polymers, polythiophenes are considered an important class of compounds in material science.

1.5.5 Related analogues

Polythiophenes have been found to exhibit excellent electronic conducting properties and are used in the construction of opto-electronic devices.[65] Figure 1.5.1 shows an example of four ferrocene units that are attached by triple bond to a thiophene core.

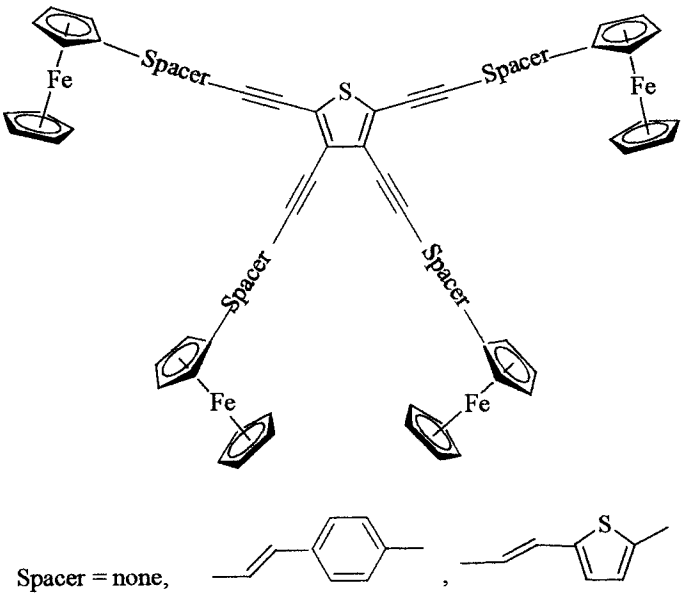

Figure 1.5.1 Star shaped tetraferrocene.

The tetra-ferrocenyl thiophene complex was synthesized by the palladium-catalyzed cross coupling reaction of ferrocenyl alkynes and 2,3,4,5-tetrabromothiophene. An excess of the terminal alkyne was used in the synthesis to ensure complete conversion. It was discovered that the air-stable compounds were soluble in common chlorinated solvents. It was also found that the solubility of the complexes decreased with increasing chain lengths. The UV-vis data of the complex exhibited a π-π^* absorption band with a high absorption coefficient. A d-d transition was responsible for the weak, low energy band from the ferrocene complex. Subsequently, cyclic voltammetry demonstrated the electronic properties of the complexes.

A lack of interactions between the ferrocene units was observed in the cyclic voltammetry (CV) data.[66] As noted above, the communication between the ferrocene units depends upon the chain length and the specific components in the chain. Along

with thiophene complexes, the electronic properties of other transition metal complexes are currently being investigated.

1.5.6 Tetrakis nickel (0) complexes

Ittel et al.[53] describes the synthesis of nickel (0) complexes such as tetrakis (*tert*–butyl isocyanide)nickel(0), tetrakis(triphenylphosphine)nickel(0), and tetrakis (triethyllphosphite)nickel(0) via bis(1,5-cyclooctadiene)nickel(0). A similar method to that of Ittel will be used to synthesize nickel complexes of isocyanides containing various substituents, including: *para*-methoxyisocyanobenzene, *para*-nitro-isocyanobenzene, isocyanoferrocene, and *para*-isocyanoferrocenylbenzene.

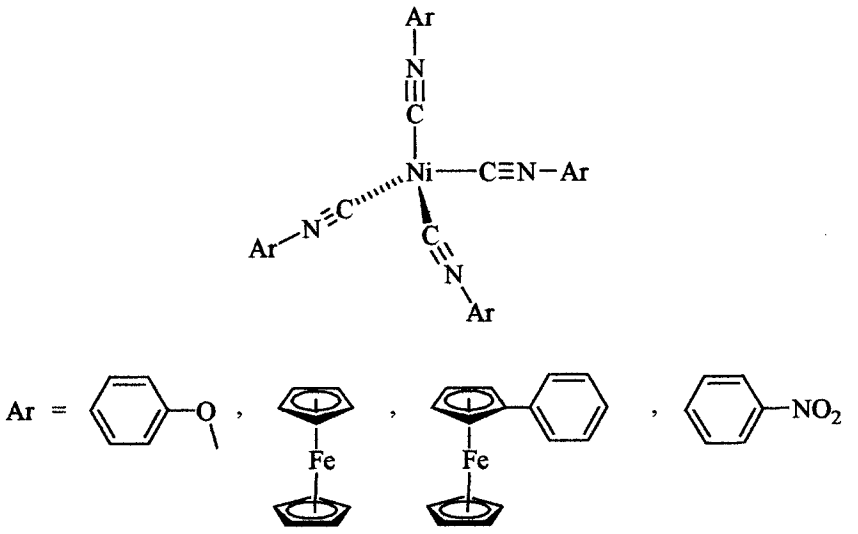

Figure 1.5.2 Examples of tetrakis isocyanide nickel(0) complexes.

The materials properties of these complexes will also be explored and contrasted to the properties of conventional organic and organometallic rigid rod analogues. As discussed in the introduction, the nickel complexes are expected to have measurable amounts of conjugation down their arms and across their central vertices due to metal d-ligand π^*-overlap. The incorporation of a ferrocene moiety into a nickel complex will allow the electrical conjugation down the arms to be investigated. The interaction between the

terminal subunits will be of great interest and will allow the modulation of the electronic properties of the material.

1.5.7 Conclusion

Cyclic voltammetry will be used to investigate the red/ox properties of ferrocene containing nanostars. The redox potentials of the complexes will be determined to assess their prospective use as electron reservoir complexes for stoichiometric redox reactions. The electronic properties of the tetrahedral nickel(0) complexes will be compared to the properties of conventional organic and organometallic analogues. The successful synthesis of these complexes will further our understanding of their potential in chemical and electrochemical applications.

References

1. P. R. Jenkins, *Organometallic Reagents in Synthesis*; Oxford University Press: NewYork, **1992**.
2. (a) B. Douglas, D. McDaniel, J. Alexander, *Concepts and Models of Inorganic Chemistry*; John Wiley and Sons Inc.: New York, **1994**. (b) J. J. Eisch, *The Chemistry of Organometallic Compounds: The Main Group Elements*; The Macmillan Company: New York, **1967**. (c) J. E. Huheey, *Inorganic Chemistry: Principles of structure and reactivity*; Harper Collins Publishers Inc.: New York, **1983**.
3. R. F. Heck, Organotransition Metal Chemistry: A Mechanistic Approach, Academic Press: New York, **1974**.
4. C. M. Lukehart, *Fundamental Transition Metal Organometallic Chemistry*; Brooks/Cole: Monterey, **1985**.
5. (a) H. K. Hall Jr., *J. Amer. Chem. Soc.*, **1956**, *78*, 2717. (b) E. L. Wittbecker, P. W. Morgan, *J. Polymer Sci.*, **1959**, *40*, 289. (c) H. F. Mark, S. M. Atlas, N. Ogata, *J. Polymer Sci.* **1962**, *61*, S49.
6. D. F. Shriver, Atkins, P. W. *Inorganic Chemistry*; 3rd ed, Oxford University Press: Oxford, **1999**, p 278.
7. J. E. Mark, H. E. Allcock, R. West, *Inorganic Polymers*, Prentice-Hall Inc.; Englewood Cliffs, New Jersey, **1992**.
8. T. A. George, C. D. Seibold, *Inorg. Chem.* **1973,** *12*, 2544-2547.
9. P. Nguyen, P. Gomez-Elipe, I. Manners, *Chem. Rev.* **1999,** *99*, 1515-1548.
10. J. E. Keaton, *Organic Semiconducting Polymers*, Marcel Dekker: New York, **1968,** p 240.
11. I. Manners, Angew. Chem., Int. Ed. Engl. **1996,** 35, 1602.
12. M. P. Stevens, *Polymer Chemistry: An Introduction*; 3rd ed.; Oxford University Press: New York, **1999**; Vol. 120, p 12.

13. C. U. Pittman Jr., O. E. Ayers, B. Suryanarayanan, S. P. McManus, J. E. Sheats, *Makromol. Chem.* **1974,** *175*, 1427.

14. (a) Y. Fujikura, K. Sonogashira, N. Hagihara, *Chem. Lett.* **1975**, 1067. (b) K. Sonogashira, S. Takahashi, N. Hagihara, *Macromolecules* **1977,** *10*, 879.

15. A. W. Bosman, H. M. Janssen, E. W. Meijer, *Chem. Rev.*, **1999,** *99*, 1665-1668.

16. C. E. Carraher Jr., *Polymer Chemistry*; 5th ed.; Marcel Dekker, Inc.: New York, 2000; p 380.

17. A. M. McDonagh, N. T. Lucas, M. P. Cifuentes, M. G. Humphrey, S. Houbrechts, A. Persoons, *J. Organomet. Chem.* **2000,** *605*, 184-192.

18. I. R. Whittall, A. M. McDonagh, M. G. Humphrey, *Adv. Organomet. Chem.* **1998,** *42*, 291-362.

19. J. Chen, L. C. Clavet, M. A. Reed, D. W. Carr, D. S. Grubisha, D. W. Bennett, *Chem. Phys. Lett.* **1999,** *313*, 741-748.

20. N. L. Wagner, F. E. Laib, D. W. Bennett, *Inorg. Chem. Comm.* **2000,** *3*, 87-90.

21. I. Ugi, U. Fetzner, U. Ebholzer, H. Knupfer, K. Offermann, *Angew. Chem., Int. Ed. Engl.* **1965,** *4*, 472.

22. A. Efraty, I. Feinstein, L. Wackerle, A. Goldman, *J. Org. Chem.* **1980,** *45*, 4059-4061.

23. J. Chatt, W. Hussain, G. J. Leigh, H. M. Ali, C. J. Pickett, K. A. Rankin, *J. Chem. Soc. Dalton. Trans* **1985**, 1131-1136.

24. M. Hidai, K. Tominari, Y. Uchida, A. Misono, *Chem. Commun.* **1969,** 1392.

25. J. Chatt, J. R. Dilworth, R. L. Richards, *Chem. Rev.* **1978,** *78*, 589.

26. G. Nakamura, Y. Harada, C. Arita, H. Seino, Y. Mizobe, M. Hidai, *Organometallics* **1998,** *17*, 1010-1012.

27. M. Sato, T. Tatsumi, T. Dodama, M. Hidai, T. Uchida, Y. Uchida, *J. Am. Chem. Soc.* **1978,** *100*, 4447-52.

28. T. J. Kealy, P. L. Pauson, *Nature*: London, 1951; p 1039, 168.

29. S. A. Miller, J. A. Tebboth, J. F. Tremaine, *J. Chem, Soc.* **1952,** 632.

30. S. Barlow, D. O'Hare, Chem. Rev. **1997**, 97, 637.

31. G. R. Knox, P. L. Pauson, D. Willison, *Organometallics* **1990**, *9*, 301-306.

32. M. Barybin, T. C. Holovics, S. F. Deplazes, G. H. Lushington, D. R. Powell, M. Toriyama, *J. Am. Chem. Soc.* **2002**, *124*, 13668-13669.

33. L. Malatesta, F. Bonati, *Isocyanide Complexes of Metals*; Wiley: London, 1969.

34. (a) I. Ugi, R. Meyer, *Chem Ber.* **1960**, *93*, 239. (b) I. Ugi, U. Fetzer, E. Eholzer, H. Knupfer, K. Offerman, *Angew Chem. Int. Ed. Engl.* **1965**, *4*, 472. (c) R. Obrecht, R. Herrmann, I. Ugi, *Synthesis* **1985**, 400.

35. G. Smolinsky, *J. Am. Chem. Soc.* **1962**, *27*, 3557-3559.

36. D. Van Leusen, B. Hessen, *Organometallics* **2001**, *20*, 224-226.

37. B. Bildstein, M. Malaun, H. Kopacka, K. Wurst, M. Mitterbock, K. H. Ongania, G. Opromolla, P. Zanello, *Organometallics* **1999**, *18*, 4323-4336.

38. A. N. Nesmeyanov, W. A. Ssazonowa, V. N. Drosd, *Chem. Ber.* **1960**, *93*, 2717.

39. M. Herberhold, B. Distler, H. Maisel, W. Milius, B. Wrackermeyer, P. Zanello, *Z. Anorg. Allg. Chem.***1996**, 622, 1515.

40. M. Hanack, S. Kamenzin, C. Kamenzin, L. R. Subramonian, *Synthetic Metals* **2000**, *110*, 93-103.

41. P. Hu, K. Quing Zhao, H. Bo Xu, *Molecules* **2001**, *6*, M249.

42. G. Grizner, J. Kuta, *Pure Appl. Chem.* **1984**, *56*, 461.

43. P. J. Kim, H. Masai, K. Sonogashira, N. Hagihara, *Inorg. Nucl. Chem.* Lett. **1970**, *6*, 181.

44. J. A. Karmmer, D. N. Hendrickson, *Inorg. Chem.* **1980**, *19*, 3330.

45. C. Iwakura, T. Kawai, M. Nojima, H. Yoneyama, *J. Electrochem. Soc.* **1987**, 134, 791.

46. T. Morikita, T. Yamamoto, *J. Org. Chem.* **2001**, *637-639*, 809-812.

47. T. Morikita, T. Maruyama, T. Yamamoto, K. Kubota, M. Katada, *Inorg. Chim. Acta,* **1998**, *269*, 310-312.

48. (a) T. Yamamoto, T. Maruyama, Z. H. Zhou, T. Ito, T. Fukuda, Y. Yoneda, F. Begum, T. Ikeda, S. Sasaki, H. Takezoe, A. Fukuda, K. Kubota, *J. Am. Chem. Soc.* **1994**, *116*, 4832. (b) T. Maruyama, T. Yamamoto, *Inorg. Chim. Acta,* **1995**, *9*, 238.

49. A. Peruga, J. A. Mata, D. Sainz, E. Peris, *J. Org. Chem.* **2001**, *637-639*, 191-107.

H. Fink, N. J. Long, A. J. Martin, G. Opromolla, A. J. P. White, D. J. Williams, P. Zanello, *Organometallics* **1997**, *16*, 2646.

51. D.H. Fahey, *J. Am. Chem. Soc.*, **1970**, *92*, 402.
52. S. Otsuka, T. Yoshida, Y. Tatsuno, *Chem. Commun.*, **1967**, 836.
53. S.D. Ittel, "Complexes of Nickel (0)," in *Inorg. Synth.*, R.J. Angelici, Ed.; Wiley: New York, **1990**; Vol 28, pp 98-99.
54. D. Lentz, Chem. Ber., **1985**, *118*, 560.
55. S. Otsuka, A. Nakamura, Y. Tatsuno, *J. Am. Chem. Soc.*, **1969**, *91*, 6994-6999.
56. M. Matsumoto, K. Nakatsu, *Acta Crystallogr., Sect. B*, **1975**, *31*, 2711.
57. P. J. Kim, H. Masai, K. Sonogashira, N. Hagihara, *Inorg. Nucl. Chem.* Lett. **1970**, *6*, 181.
58. N. J. Long, C. K. Williams, *Agnew. Chem. Int. Ed.* **2003**, *42*, 2586-2617.
59. K. Sonogashira, T. Yatake, Y. Tohda, S. Takahashi, N. Hagihara, *J. Chem. Soc. Chem. Comm.*, **1977**, 291.
60. K. Sonogashira, N. Hagihara, S. Takahashi, *Macromolecules*, **1977**, *10*, 879.
61. K. Sonogashira, Y. Fujikura, T. Yatake, N. Toyoshima, S. Takahashi, N. Hagihara, *Chem. Lett.* **1978**, *145*, 101.
62. K. Sonogashira, S. Kataoka, S. Takahashi, N. Hagahara, *J. Organomet. Chem.*, **1978**, *160*, 319.
63. S. Takahashi, H. Morimoto, E. Murata, S. Kataoka, K. Sonogashira, N. Hagihara, *J. Polym. Sci. Polym. Chem. Ed.* **1982**, *20*, 565.
64. K. Sonogashira, K. Ohga, S. Takahashi, N. Hagahara, *J. Organomet. Chem.*, **1980**, *188*, 237.
65. K. J. Thomas, J. T. Lin, *J. Organomet. Chem.*, **2001**, *637-639*, 139-144.
66. H. Fink, N. J. Long, A. J. Martin, G. Opromolla, A. J. P. White, D. J. Williams, P. Zanello, *Organometallics*, **1997**, *16*, 2646. (b) T. Nakashima, T. Kunitake, *Bull. Chem. Soc. Jpn.*, **1972**, *45*, 2892.

Chapter 2 - Experimental

The reactions were performed under an atmosphere of ultra high purity dinitrogen (Praxair 99.9999%) using standard Schlenk techniques for the manipulation of air-sensitive compounds unless stated otherwise.[1,2]

2.1 Reagents

Unless otherwise stated, the reagents used were purchased from commercial suppliers and were of reagent grade or comparable purity. They were not further purified before use. The solvents used were dried and deaerated by standard procedures[3] and stored under purified N_2. Thus, THF, diethylether, and toluene were distilled from benzophenone ketyl radical using Na-K alloy for THF and diethylether and using sodium for toluene. Methylene chloride was distilled from calcium hydride.

2.2 Instrumentation

Infrared spectra were recorded on a JASCO FT/IR-410 infrared spectrophotometer. ^{1}H (400 MHz), ^{13}C (100 MHz), and ^{31}P (161.88 MHz) NMR spectra were recorded on a 400 MHz Varian Gemini-2000 spectrometer. ^{1}H and ^{13}C NMR chemical shifts are reported in parts per million (ppm) downfield from external Me_4Si ($\delta = 0$). The ^{31}P NMR chemical shifts are reported in parts per million (ppm) downfield from external 85% H_3PO_4 ($\delta = 0$). Single Crystal X-ray analysis was completed via Bruker AXS Smart Apex CCD Diffractometer.

2.3 Syntheses

2.3.1 Para-methoxyisocyanobenzene[4]

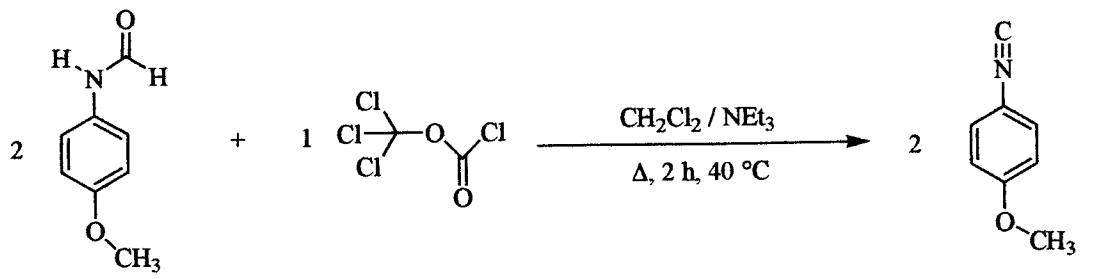

Equation 2.3.1 Synthesis of *para*-methoxyisocyanobenzene.

Para-formamidoanisole (10.0 g, 66.15 mmol), previously prepared by Matthias Zeller using the method as described by Hanack et al.[4], CH_2Cl_2 (200 mL), and triethylamine (45.85 mL, 33.29 g, 0.329 mol) were combined in a nitrogen purged 250 mL three-necked round bottom flask equipped with a nitrogen adapter, reflux condenser, dropping funnel, and magnetic stirring bar. Diphosgene (3.9 mL, 6.54 g, 33.0 mmol) was placed into a dropping funnel containing CH_2Cl_2 (46 mL). The diphosgene solution was added drop wise to the solution over a 15 minute period and then the solution was refluxed for an additional 2 h. The solution was allowed to cool to ambient temperature and washed under nitrogen with a 10% solution of Na_2CO_3 (3 × 100 mL) and with H_2O (1 × 100 mL). The organic layer was dried over anhydrous $MgSO_4$. The $MgSO_4$ was filtered off, washed with CH_2Cl_2 (3 × 20 mL), and all volatile materials were removed *in vacuo* from the combined filtrates (*e.g.*, high vacuum manifold at room temperature). Crystallization of the resulting light brown solid from pentane at 4 °C gave white-yellow needles. The crystals were dissolved in a 2:1 hexane / CH_2Cl_2 mixture (~ 40 mL). The solution was filtered through a neutral aluminum column (0.50 m) using a 2:1 hexane / CH_2Cl_2 mixture (~ 150 mL) and all volatile materials were removed from the filtrate *in vacuo*. The solid was again crystallized from pentane at 4°C to give a 21% yield (1.84, 13.8 mmol) of the product as white-yellow needles exhibiting a pronounced isonitrile

smell. The crystals start to melt at room temperature and have to be stored under nitrogen at -19 °C to avoid rapid decomposition.

No spectroscopic properties were recorded due to the thermal sensitivity of the compound. The identity of the compound was verified by its conversion into the Ni(0) tetraisocyanide complex, see below.

2.3.2 1,4-Bis(n-formylamino)-2,3,5,6-tetramethylbenzene [4]

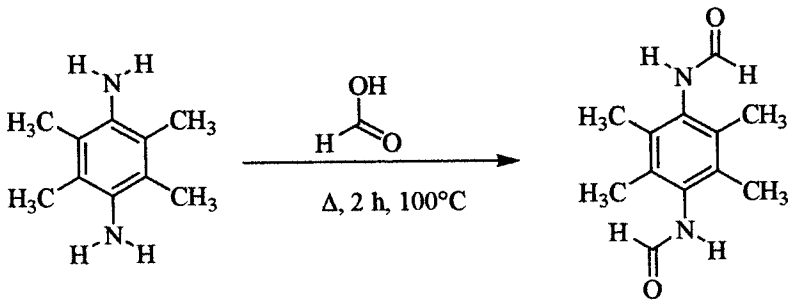

Equation 2.3.2 Synthesis of 1,4-bis(*n*-formylamino)-2,3,5,6-tetramethylbenzene.

The 2,3,5,6-tetramethylphenylene-1,4-diamine (10.09 g, 61.4 mmol) was combined with formic acid (150 mL) in a nitrogen purged 250 mL three-necked round bottom flask equipped with a nitrogen adapter, reflux condenser, dropping funnel, and magnetic stirring bar. The stirred solution was heated to reflux for 2 h. It was then cooled to room temperature, water (100 mL) was added, and the resulting suspension was stirred at ambient temperature for approximately 12 h. The beige solid was collected by filtration and was rinsed with H_2O until the filtrate was neutral (pH-paper). The solid was dried *in vacuo* to give an 80% yield (10.9g, 0.0493 mol) of the product as a white solid.

No spectroscopic properties were recorded due to the insolubility of the product in common organic solvents. The identity of the compound was verified by its dehydration to form 1,4-diisocyano-2,3,5,6-tetramethylbenzene.

MP: 350 °C.

2.3.3 1,4-Diisocyano-2,3,5,6-tetramethylbenzene [4]

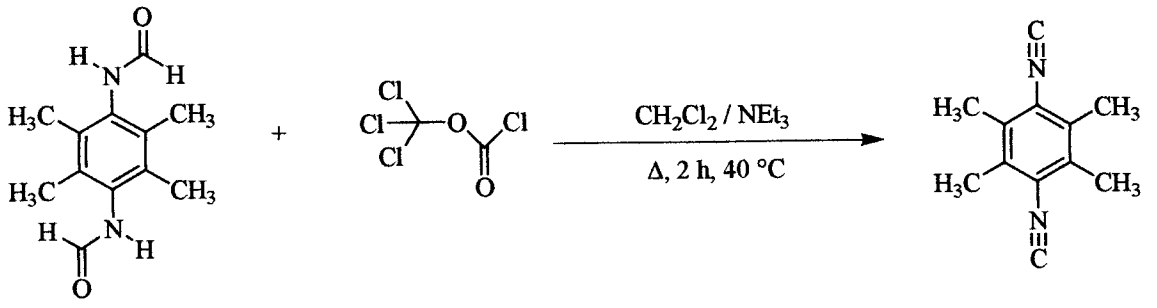

Equation 2.3.3 Synthesis of 1,4-diisocyano-2,3,5,6-tetramethylbenzene.

1,4-Bis(*n*-formylamino)-2,3,5,6-tetramethylbenzene (10.87 g, 49.32 mol) was combined with CH_2Cl_2 (150 mL) and triethylamine (34.2 mL, 24.83g, 0.245mol) in a nitrogen purged 250 mL three-necked round bottom flask equipped with a nitrogen adapter, reflux condenser, dropping funnel, and magnetic stirring bar. Diphosgene (6.1 mL, 10.0 g, 50.6 mmol) was placed into a dropping funnel containing CH_2Cl_2 (34 mL). The diphosgene solution was added drop wise to the refluxing suspension over a 15 minute period and then the solution was refluxed for an additional 3 h. The solution was cooled to ambient temperature and washed under nitrogen with a 10% solution of Na_2CO_3 (3 × 100 mL) and with H_2O (1 × 100 mL). The organic layer was dried over anhydrous $MgSO_4$ for 1 h. The $MgSO_4$ was filtered off, washed with CH_2Cl_2 (3 × 20 mL), and all volatile materials were removed from the combined filtrates *in vacuo*. The brownish solid that resulted was sublimed at 75 °C under oil pump vacuum to give a 34% yield (2.19 g, 17.0 mmol) of the product as a white crystalline solid. It is stable in air for a short time and can be stored at 4 °C under nitrogen for extended periods without signs of decomposition.

Spectroscopic Properties:

^{13}C {^{1}H} NMR ($CDCl_3$): δ = 168.870 (s, C≡N), 131.550 (s, C-CH_3), 126.724 (t, $^{1}J(^{13}C,^{14}N)$ = 11.4 Hz, C-N), 16.366 (s, CH_3).

^{1}H NMR (399.905 MHZ, $CDCl_3$): δ = 2.357 (s, 12 H, CH_3).

IR (emulsion in paraffin oil, NaCl plates): 2115 cm^{-1} (s, ν C≡N).

MP: 112 °C.

X-Ray structure analysis: see Results and Discussion and Appendix 1.

2.3.4 Para-nitro-isocyanobenzene [4]

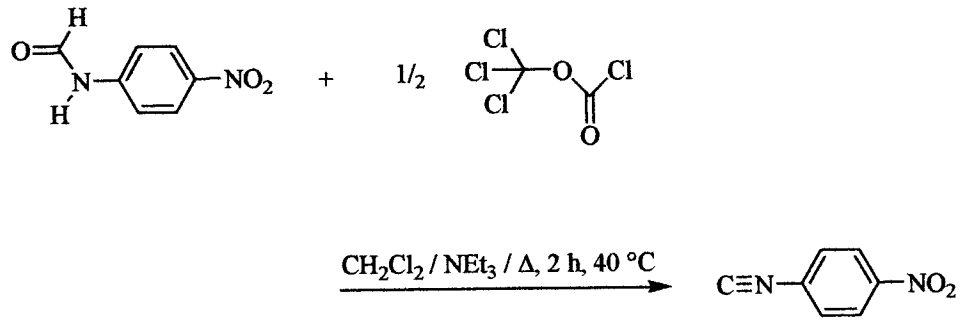

Equation 2.3.4 Synthesis of *para*-nitroisocyanobenzene.

Para-nitro-formamide (4.050 g, 0.02438 mol), previously prepared by Matthias Zeller using the method as described by Hanack et al.[4], was combined with CH_2Cl_2 (50 mL) and triethylamine (50 mL, 36.3 g, 0.359 mol) in a nitrogen purged 250 mL three-necked round bottom flask equipped with a nitrogen adapter, reflux condenser, dropping funnel, and magnetic stirring bar. Diphosgene (2.1 mL, 3.36 g, 17.0 mmol) was placed into a dropping funnel containing CH_2Cl_2 (10.0 mL). The diphosgene solution was added drop wise to the refluxing suspension over a 15 minute period and then the solution was refluxed for an additional 3 h. The solution was cooled to ambient temperature and washed under nitrogen with a 10% solution of Na_2CO_3 (3 × 100 mL) and with H_2O (1 × 100 mL). The CH_2Cl_2 solution was dried over anhydrous $MgSO_4$ for 1 h. The $MgSO_4$ was filtered off, washed with CH_2Cl_2 (3 × 20 mL), and all volatile materials were removed from the combined filtrates *in vacuo*. The brownish solid was sublimed at 75

°C under oil pump vacuum to give a 21% yield (0.750 g, 50.6 mmol) of the product as a white solid.

Spectroscopic Properties:

^{13}C $\{^1H\}$ NMR ($CDCl_3$): δ = 169.3 (s, C≡N), 147.3 (s, C-NO_2), 131.0 (t, $^1J(^{13}C^{14}N)$ = 16.0 Hz, C=NC), 127.4 (s, C Ph-C), 124.9 (s,C Ph-C).

^1H NMR (399.905 MHZ, $CDCl_3$): δ = 8.230 (d, $^3J(^1H^1H)$ = 9.00 Hz, 2H), 7.508 (d, $^3J(^1H^1H)$ = 9.00 Hz, 2H, Ph-H).

IR (toluene, CaF_2): 2121 cm^{-1} (s, ν C≡N), 1520 cm^{-1} (s, ν_{as} NO_2), 1345 cm^{-1} (s, ν_{sy} NO_2). IR (KBr): 2130 cm^{-1} (br, ν C≡N), 1541 cm^{-1} (br, ν_{as} NO_2), 1349 cm^{-1} (br, ν_{sy} NO_2).

MP: 81 °C.

2.3.5 Tris(p-anisyl)phosphine[5]

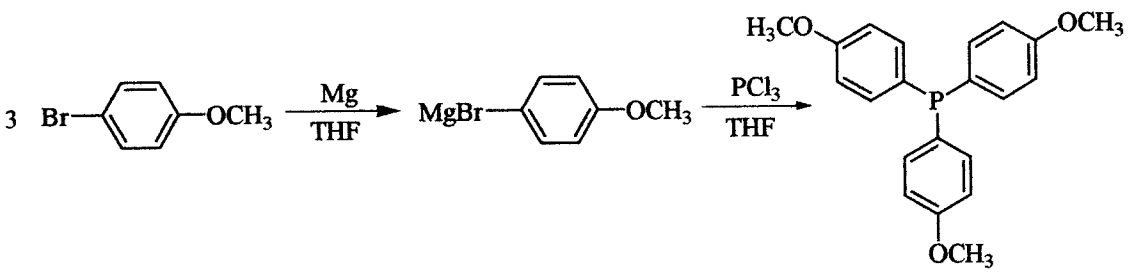

Equation 2.3.5 Synthesis of tris(*p*-anisyl)phosphine.

Magnesium turnings (9.707 g, 0.399 mol) were combined with a few crystals of iodine and THF (50.0 mL) in a nitrogen purged 250 mL three-necked round bottom flask equipped with a nitrogen adapter, reflux condenser, dropping funnel, and magnetic stirring bar. The mixture was warmed with a heat gun until the color of the iodine disappeared. The 4-Bromoanisole (14.94 g, 0.0798 mol, 99% Aldrich) in THF (50 mL) was added drop wise to this solution and a heat gun was used to initiate the reaction. After the addition was complete the solution was stirred an additional 0.5 h at 40 °C,

filtered under nitrogen to remove the excess magnesium and then the solid was washed with THF (3 × 20 mL).

A second round bottom flask (500 mL) was equipped with a nitrogen adapter, Schlenk filter, and a magnetic stirring bar. The Grignard suspension was transferred into the Schenk filter via transfer tube. Phosphorus trichloride (3.54 g, 25.8 mmol, 2.25 mL) dissolved in THF (30.0 mL) was placed into the 500 mL flask and the mixture was cooled to 0 °C. The Grignard suspension was then filtered into the phosphoros trichloride solution over a period of 0.5 h, the solid washed with THF (3 × 20 mL), and the solution was stirred for approximately 12 h at ambient temperature. The resulting suspension was hydrolyzed with a degassed 10% aqueous NH_4Cl solution and extracted with diethylether (3 × 100 mL). The organic extracts were dried over anhydrous $MgSO_4$ for 1 h. The $MgSO_4$ was filtered off under nitrogen, washed with diethylether (3 × 20 mL), and all volatile materials were removed from the filtrate *in vacuo*. The resulting solid was crystallized from diethylether to give a 39% yield (3.50 g, 99.4 mmol) of the product as white needles.

Spectroscopic Properties:

^{13}C $\{^1H\}$ NMR ($CDCl_3$): δ = 159.780 (s, C-OCH_3), 134.740 (d, $J(^{13}C,^{31}P)$ = 20.51 Hz, Ph-C), 114.009 (d, $J(^{13}C,^{31}P)$ = 7.64 Hz, Ph-C), 113.895 (d, $J(^{13}C,^{31}P)$ = 7.64 Hz, Ph-C), 55.196 (s, CH_3).

^1H NMR ($CDCl_3$): δ = 7.220 (dd, $^3J(^1H,^1H)$ = 8.70 Hz, $J(^1H,^{31}P)$ = 7.40 Hz, 6H, Ph-H), 6.870 (d, $^3J(^1H,^1H)$ = 8.70 Hz, 6H, Ph-H), 3.795 (s, 9H, CH_3).

^{31}P NMR (161.884 MHZ, $CDCl_3$, 25 °C): δ = -10.83 (s).

2.3.6 1,2-Bis[di(p-anisyl)phosphino]ethane [5]

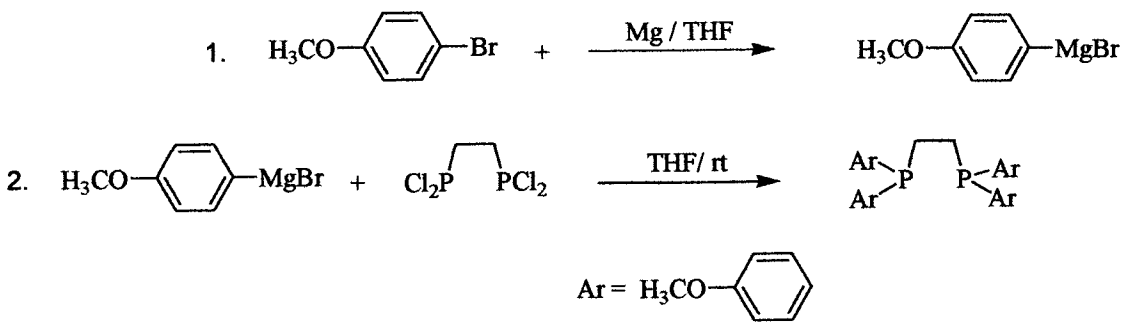

Equation 2.3.6 Synthesis of 1,2-bis[di(*p*-anisyl)phosphino]ethane.

Magnesium turnings (7.32 g, 0.301 mol) were combined with a few crystals of iodine and THF (50.0 mL) in a nitrogen purged 500 mL three-necked round bottom flask equipped with a nitrogen adapter, reflux condenser, dropping funnel, and magnetic stirring bar. The mixture was warmed with a heat gun until the color of the iodine disappeared. *p*-Bromoanisole (0.043 mol, 8.04 g, 31.0 mL, 99% Aldrich) in THF (50 mL) was added drop wise to this solution and a heat gun was used to initiate the reaction. After the addition was complete the solution was stirred an additional 12 h at ambient temperature, filtered under nitrogen to remove the excess magnesium, and the solid was then washed with THF (3 × 20 mL). Bis(dichlorophosphino)ethane (6.5 mL, 9.97 g, 0.043 mol) dissolved in THF (35.0 mL) was placed into a dropping funnel and added to the Grignard suspension over a 15 minute period at 0 °C. The solution was then allowed to stir for approximately 12 h at ambient temperature. The resulting solution was hydrolyzed with a degassed 10% aqueous NH_4Cl solution (120 mL) and the organic layer removed via cannula. The organic extracts were dried over anhydrous $MgSO_4$ for 1 h and then the $MgSO_4$ was filtered off under nitrogen, washed with toluene (3 × 20 mL), and all volatile materials were removed from the filtrate *in vacuo*. The resulting solid was crystallized from toluene (~ 30 mL) at -19 °C to give a 40% yield (8.33 g, 17.0 mmol) of the product as a white crystalline powder.

Spectroscopic Properties:

^{1}H NMR ($CDCl_3$): δ = 7.280-7.241 (m, Ph-H), 6.84 (d, $^3J(^1H,^1H)$ = 8.80 Hz, 8H, Ph-H), 2.000 (pt, $J(^1H,^{31}P)$ = 4.00 Hz, 4H, CH_2), 3.788 (s, 12H, CH_3).

^{31}P NMR (161.884 MHZ, $CDCl_3$): δ = -16.621 (s).

2.3.7 1,2-Bis[bis(p-ethylphenyl)phosphino]ethane [5]

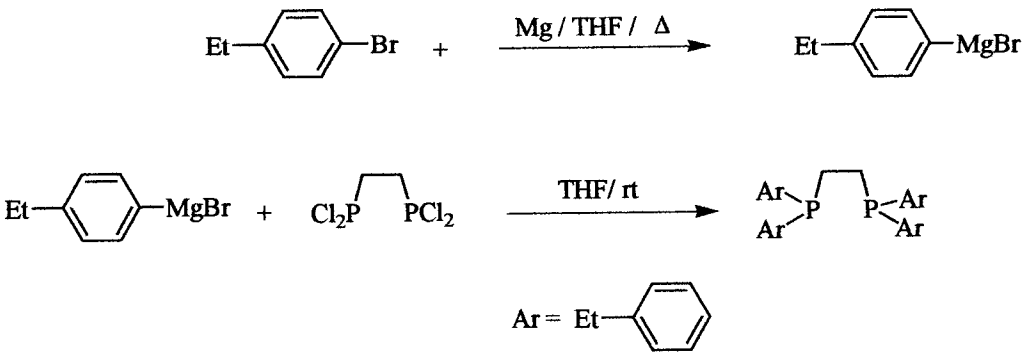

Equation 2.3.7 Synthesis of 1,2-bis[bis(*p*-ethylphenyl)phosphino]ethane.

Magnesium turnings (7.86 g, 0.323 mol) were combined with THF (60.0 mL) in a nitrogen purged 250 mL three-necked round bottom flask equipped with a nitrogen adapter, reflux condenser, dropping funnel, and magnetic stirring bar. 1-Bromo-4-ethyl benzene (0.290 mol, 53.72 g, 40.0 mL) in THF (70 mL) was added drop wise to this suspension and a heat gun was used to initiate the reaction. After the addition was complete the solution was stirred an additional 2 h at ambient temperature, filtered under nitrogen to remove the excess magnesium, and the solid was then washed with THF (3 × 20 mL). Bis(dichlorophosphino)ethane (9.8 mL, 14.99 g, 0.065 mol) dissolved in THF (40.0 mL) was placed into a dropping funnel and added to the Grignard suspension over a 15 minute period at 0 °C following which the solution was allowed to stir for approximately 12 h at ambient temperature. The resulting solution was then hydrolyzed with a degassed 10% aqueous NH_4Cl solution (120 mL) and the THF removed via cannula. The organic extract was dried over anhydrous $MgSO_4$ for 1 h and then the

$MgSO_4$ was filtered off under nitrogen, washed with toluene (3 × 20 mL), and all volatile materials were removed from the filtrate *in vacuo*. The resulting solid was crystallized from toluene (~ 40 mL) at -19 °C to give an 82% yield (18.6 g, 0.163 mmol) of the product as a white crystalline solid.

Spectroscopic Properties:

^1H NMR ($CDCl_3$): δ = 7.271-7.233 (m, Ph-H), 7.146 (d, $^3J(^1H,^1H)$ = 8.80 Hz, 8H, Ph-H), 2.623 (q, $^3J(^1H,^1H)$ = 7.60 Hz, $^3J(^1H,^1H)$ = 15.20 Hz, 8H, CH_2), 2.062 (pt, $J(^1H,^{31}P)$ = 4.00 Hz, 4H, CH_2), 1.218 (t, $^3J(^1H,^1H)$ = 8.00, 12H, CH_3).

^{31}P NMR (161.884 MHZ, $CDCl_3$, 25 °C): δ = -14.774 (s).

2.3.8 Attempted synthesis of trans- bis[bis{di(p-anisyl)phosphino}ethane] bis(dinitrogen)molybdenum(0)[5]

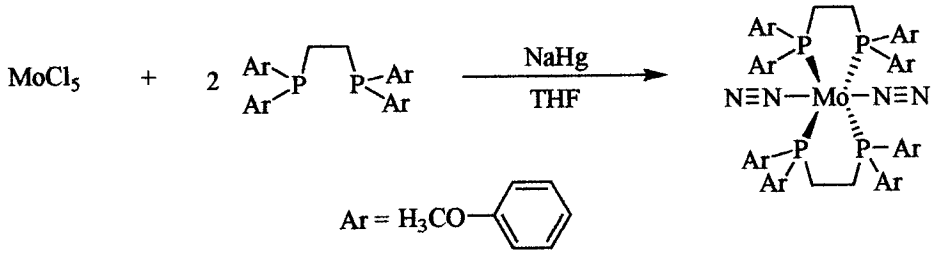

Equation 2.3.8 Attempted synthesis of *trans*- bis[bis{di(*p*-anisyl)phosphino}ethane] bis(dinitrogen)molybdenum(0).

The 1,2-Bis(di(*p*-anisyl)phosphino)ethane (8.33g, 0.0170 mol) was combined with THF (20.0 mL) and added to liquid NaHg (2% by weight Na, 3.811g Na, 0.00829 mol Na; 15.6 g Hg, 0.0778 mol Hg, 12.0 mL Hg)[6] in a nitrogen purged 500 mL Schlenk flask equipped with a magnetic stirring bar. THF (80 mL) and $MoCl_5$ (2.26g, 0.00829 mol) were then added to the solution and the mixture was stirred vigorously with a large stirring bar for 60 h at ambient temperature with a constant pressure of nitrogen. The suspension was filtered through celite under nitrogen, the celite rinsed with toluene (3 × 20 mL), and all volatile materials were removed from the combined filtrates *in vacuo*.

The resulting solid was dissolved in toluene (100 mL) and anhydrous methyl alcohol (150 mL) was then added to precipitate the product. The solution was removed by filtration and the solid rinsed with methyl alcohol (3 × 20 mL). All volatile materials were removed from the solid *in vacuo* to give a 39% yield (3.63 g, 3.20 mmol) of the product as an orange-yellow powder. This powder, as determined by NMR, contains approximately 20% tetrahydride (*e.g.*, $(C_{30}H_{16}O_4P_2)_2H_4Mo$) which formed as side product and was not successfully removed via crystallization.

Spectroscopic Properties:

^{13}C {^1H} NMR (Benzene): δ = 160.523 (s, Ph-C-O), 130.306 (d, $J(^{31}P,^{13}C)$ = 7.44 Hz, Ph-C), 134.513 (d, $J(^{13}C,^{31}P)$ = 11.46 Hz, Ph-C), 114.558 (d, $J(^{13}C,^{31}P)$ = 21.12 Hz, Ph-C), 54.787 (s, CH_3), 25.787 (s, CH_2).

^1H NMR (399.905 MHZ, $CDCl_3$): δ = 7.283-7.244 (m, Ph-H), 6.71 (d, $^3J(^1H,^1H)$ = 8.80 Hz, 16H, Ph-H), 3.234 (s, 24H, CH_3), 2.323 (pt, $J(^1H,^{31}P)$ = 4.00 Hz, 8H, CH_2).

^{31}P NMR (161.884 MHZ, $CDCl_3$, 25 °C): δ = 39.347 (s).

IR (toluene, CaF_2): 2359 cm^{-1} (s, ν_{as} N≡N), 2336 cm^{-1} (s, ν_{sy} N≡N).

MP: 74°C.

2.3.9 Attempted synthesis of trans-bis[bis{di(p-ethylphenyl)phosphino} ethane]bis(dinitrogen)molybdenum(0)[5]

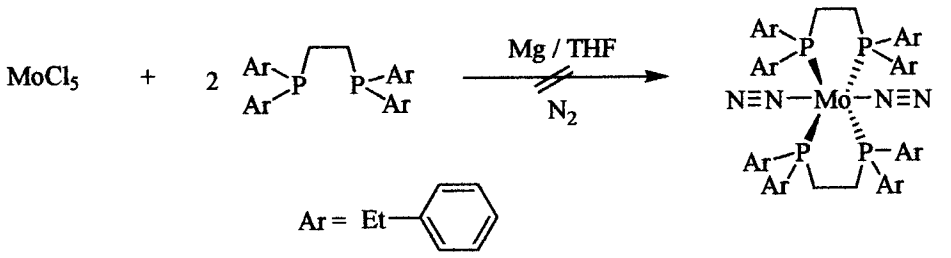

Equation 2.3.9 Attempted synthesis of *trans*-bis[bis{di(*p*-ethylphenyl) phosphino}ethane]bis(dinitrogen)molybdenum(0).

Mg turnings (7.42 g, 0.305 mol, Aldrich 99.9%) and 1,2-bis(di(*p*-ethylphenyl) phosphino)ethane (2 eq, 10.0 g, 20.7 mmol) were placed into a nitrogen purged 500 mL Schlenk flask equipped with a stirring bar. THF (500 mL) and $MoCl_5$ (1 eq, 2.841 g, 0.0104 mol, Aldrich 98%) were added to the mixture and the mixture was stirred vigorously at ambient temperature for 48 h. The solution was filtered over celite under nitrogen, the celite rinsed with THF (3 × 20 mL), and the combined filtrates reduced *in vacuo* to approximately 100 mL. Methyl alcohol (200 mL) was added at 0 °C to precipitate a yellow solid. The resulting solid was filtered off under nitrogen, washed with methyl alcohol (3 × 20 mL), and all volatile materials were removed from the solid *in vacuo*. The yellow solid was dissolved in toluene (~ 100 mL) and methyl alcohol (100 mL) was added to precipitate the product. Crystallization at 4 °C gave a yellow solid which was determined by NMR to be the starting material, 1,2-bis(di(*p*-ethylphenyl)phosphino)ethane.

Spectroscopic Properties:

^{1}H NMR (Benzene): δ = 7.370-7.332 (m, Ph-H), 7.113 (s, 8H, Ph-H), 2.318 (q, $^3J(^1H,^1H)$ = 7.60 Hz, $^3J(^1H,^1H)$ = 15.20 Hz, 8H, CH_2), 0.969 (t, $^3J(^1H,^1H)$ = 8.00, 12H, CH_3).

^{31}P NMR (161.884 MHZ, $CDCl_3$, 25 °C): δ = -14.774 (s).

2.3.10 O-Benzylhydroxylamine [7]

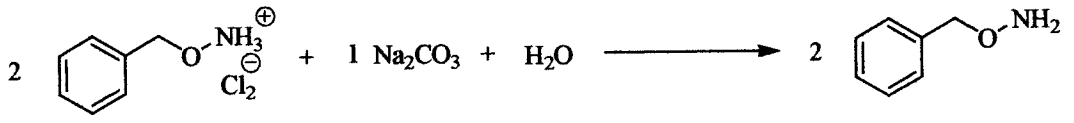

Equation 2.3.10 Synthesis of *o*-benzylhydroxylamine.

O-benzylhydroxylamine hydrochloride (25 g, 0.157 mol, Aldrich 99%) was combined with Na_2CO_3 (15.5 g, 0.157 mol) in 100 mL of H_2O in a nitrogen purged 250

mL three-necked round bottom flask equipped with a nitrogen adapter and magnetic stirring bar. The resulting aqueous suspension was stirred for approximately 15 minutes until it was converted into an oil. This biphasic liquid was saturated with NaCl and the resulting suspension was extracted with diethylether (5 × 100 mL). The etheral extracts were combined and all volatile materials were removed from them *in vacuo*. The light yellow oil produced was purified by distillation under oil pump vacuum to give an 83% yield (16.0 g, 0.130 mol) of the product as a light yellow oil.

Spectroscopic Properties:

^{13}C $\{^1H\}$ NMR ($CDCl_3$): δ = 136.941 (s, $\underline{C}$-CH_2), 127.700 (s, Ph-$\underline{C}$), 127.647 (s, Ph-$\underline{C}$), 127.146 (Ph-$\underline{C}$), 77.088 (s, $\underline{C}H_2$).

^1H NMR ($CDCl_3$): δ = 7.45-7.28 (m, 5H, Ph-$\underline{H}$), 5.390 (s, 2H, $N\underline{H}_2$), 4.676 (s, 2H, $C\underline{H}_2$).

2.3.11 α-Azidostyrene [8]

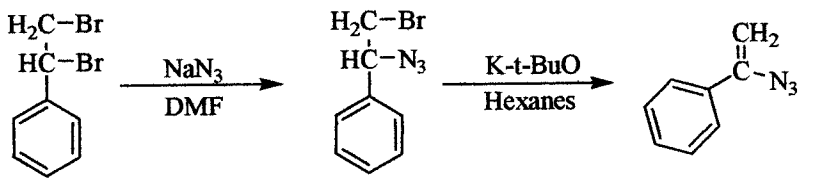

Equation 2.3.11 Synthesis of α-azidostyrene.

1,2-Dibromo-1-phenyl ethane (74.60 g, 0.283 mol, 99% Aldrich), sodium azide (18.37 g, 0.283 mol, 99% Aldrich), and dimethylformamide (404 g, 5.52 mol, 430 mL, 99.8% Aldrich) were combined in a 1,000 mL round bottom flask equipped with a stirring bar and the solution was stirred at ambient temperature for approximately 12 h. Water (400 mL) and hexanes (200 mL) were then added to the solution, the organic layer was separated, and the aqueous layer was extracted with hexanes (3 × 100 mL). The combined organic extracts were dried over anhydrous Na_2SO_4 for 1 h. The Na_2SO_4 was

filtered off under nitrogen, washed with hexanes (3 × 20 mL), and all volatile materials were removed from the combined organic solutions *in vacuo*. The resulting solid was dissolved in toluene (~ 200 mL). Potassium tert-butoxide (45.21 g, 0.403 mol, 95% Aldrich) was added to the solution and the solution was stirred for approximately 12 h. The solution was diluted with hexanes (1,000 mL) and washed with H_2O (3 × 700 mL). The combined hexane solutions were dried over anhydrous Na_2SO_4 for 1 h. The Na_2SO_4 was filtered off under nitrogen, washed with hexanes (3 × 20 mL), and all volatile materials were removed *in vacuo*. The resulting solid was dissolved in hexanes (~ 50 mL), filtered through a neutral Al_2O_3 column (50 cm), and the column was then eluted with hexanes (~ 300 mL) until the filtrate became clear. All volatile materials were removed from the combined hexanes filtrate *in vacuo* to give a 74% yield (30.3 g, 0.208 mol) of the product as a yellow solid.

Spectroscopic Properties:

^{1}H NMR ($CDCl_3$): δ = 8.90 -7.20 (m, 5, Ph-H), 5.553 (s, 1H, =C$\underline{H}_2$), 5.076 (s, 1H, =C$\underline{H}_2$).

2.3.12 Ferrocenylamine[9]

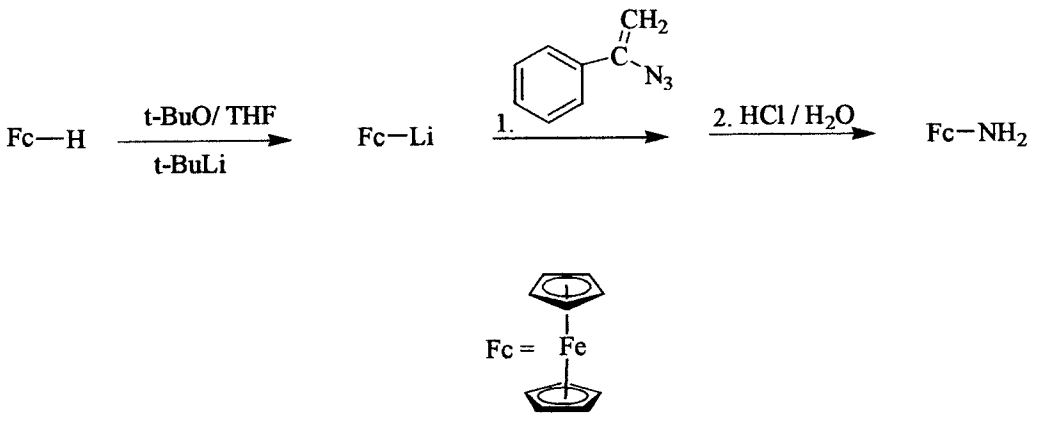

Equation 2.3.12 Synthesis of ferrocenylamine.

Ferrocene (8.0 g, 0.043 mol, Aldrich 98%) and potassium tert-butoxide (0.6 g, 5.35 mmol) were combined with THF (450 mL) in a nitrogen purged 1,000 mL three-necked round bottom flask equipped with a nitrogen adapter and magnetic stirring bar. Tert-butyllithium (1.7 M, 32.99 g, 0.515 mol, 50.6 mL) was added to the solution at -80 °C over a 15 minute period and the solution was stirred for 1h at -80 °C. The α-azidostyrene (6.200g, 0.0375 mol) was added to the solution following which the solution was slowly allowed to warm to -10 °C over 1 h and then was allowed to warm to ambient temperature. A solution of 3N HCl (~ 10.0 mL) was added drop wise over a 30 minute period to the solution. H_2O (50 mL) was then added to the solution and the resulting suspension was extracted with diethylether (3 × 100 mL). The combined organic extracts were dried over anhydrous $MgSO_4$ for 1 h and the $MgSO_4$ was then filtered off under nitrogen and washed with diethylether (3 × 20 mL). The ether extracts were combined and all volatile materials were removed *in vacuo*. The red oil which resulted was sublimed at 120 °C under oil pump vacuum to give a 9% yield (0.780 g, 0.386 mmol) of the product as a crude dark red oil.

Spectroscopic Properties:

^1H NMR ($CDCl_3$): mixture of *cis* and *trans*: δ = 4.150 (s, Cp-H), 3.983 (s, Cp-H), 3.915 (s, Cp-H), 3.831 (s, Cp-H), 3.740 (s, Cp-H), 2.612 (s, NH_2), 2.331 (s, NH_2).

2.3.13 Lithioferrocene[10]

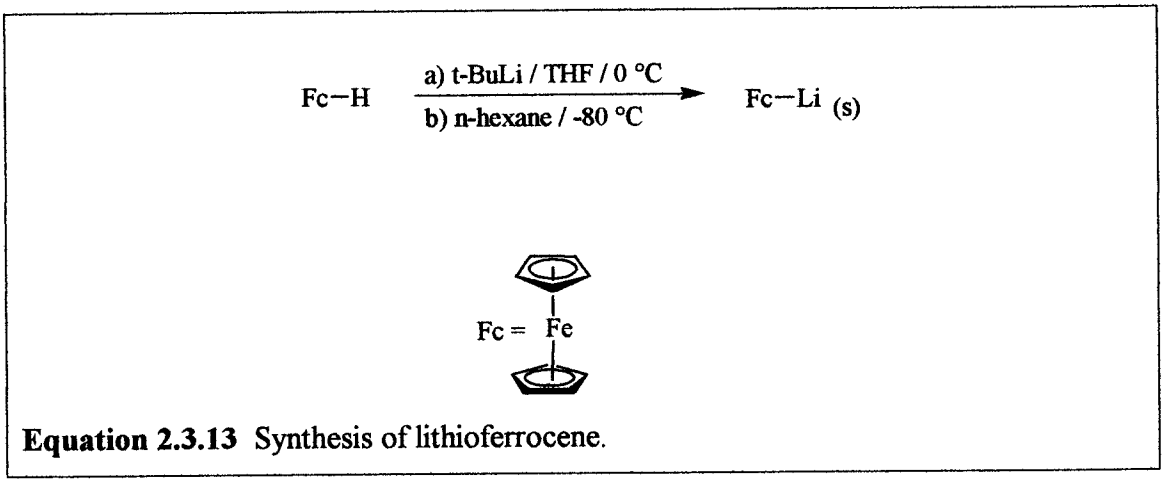

Equation 2.3.13 Synthesis of lithioferrocene.

Ferrocene (40.0 g, 0.215 mol, Aldrich 98%) was combined with dry / degassed THF (250.0 mL) in a nitrogen purged 1,000 mL three necked flask equipped with a magnetic stirring bar and a nitrogen adapter. *Tert*-butyl-lithium (146.0 mL, 95.15 g, 0.248 mol, Aldrich 1.7 M) was added to the solution via cannula over a 15 minute period at 0 °C. The solution was then cooled to −80 °C and *n*-hexanes (300 mL) were added to precipitate the product. The suspension was allowed to warm to ambient temperature, filtered off under nitrogen, and the solid was then washed with hexanes (5 × 20 mL). All volatile materials were removed from the combined organic solutions *in vacuo* to give a 92% yield (38.2 g, 0.198 mol) of the product as a yellowish pyrophoric powder.

No spectroscopic properties were collected due to the pyrophoric nature of the material.

2.3.14 Iodoferrocene[10]

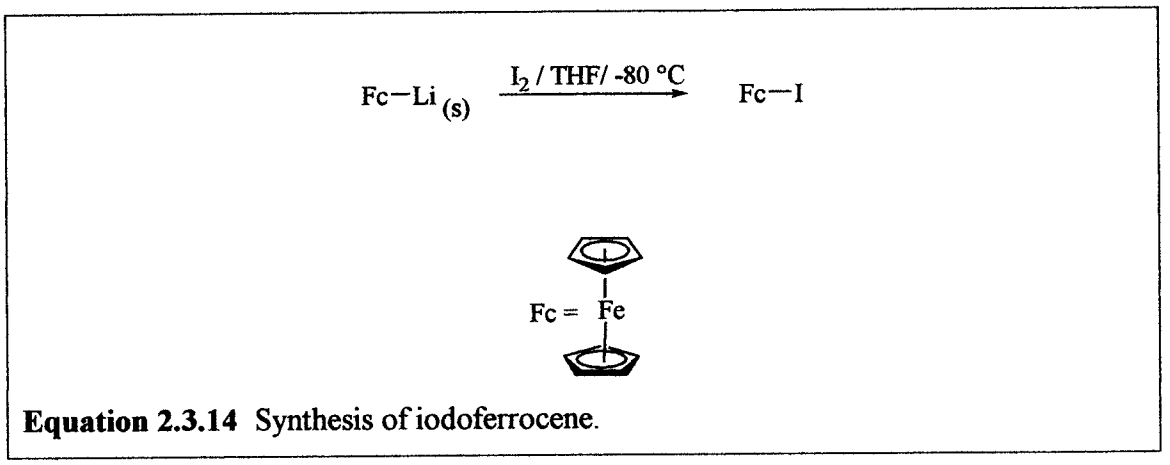

Equation 2.3.14 Synthesis of iodoferrocene.

THF (200 mL, Aldrich 99.9%) was combined with lithioferrocene (24.93 g , 0.130 mol) in a nitrogen purged 1,000 mL three necked flask equipped with a magnetic stirring bar and a nitrogen adapter. The solution was cooled to −80 °C following which iodine (33.06 g, 0.130 mol, Aldrich 98%) was added to the solution and the solution was then allowed to warm to ambient temperature and was stirred for a further 12 h. Diethylether (600 mL) was then added to the mixture and the solution was washed with a 10 % aqueous solution of $Na_2S_2O_3$ (3 × 100 mL) and H_2O (3 × 100 mL). The solution was dried over anhydrous Na_2SO_4 for 1 h and then the Na_2SO_4 was filtered off and

washed with diethylether (3 × 20 mL). All volatile materials were removed from the combined organic extracts *in vacuo*. A 70% yield (28.5 g, 91.0 mmol) of the product was produced as an orange-brown oil. The oil solidified upon standing at 4 °C.

Spectroscopic Properties:

^{1}H NMR ($CDCl_3$): δ = 4.412 (dd, $^3J(^1H,^1H)$ = 2.40 Hz, $^3J(^1H,^1H)$ = 2.40 Hz, 2H, Cp-H), 4.192 (s, 5H, Cp-H), 4.154 (dd, $^3J(^1H,^1H)$ = 1.60 Hz, $^3J(^1H,^1H)$ = 1.60 Hz, 2H, Cp-H).

2.3.15 N-ferrocenylphthalimide[10]

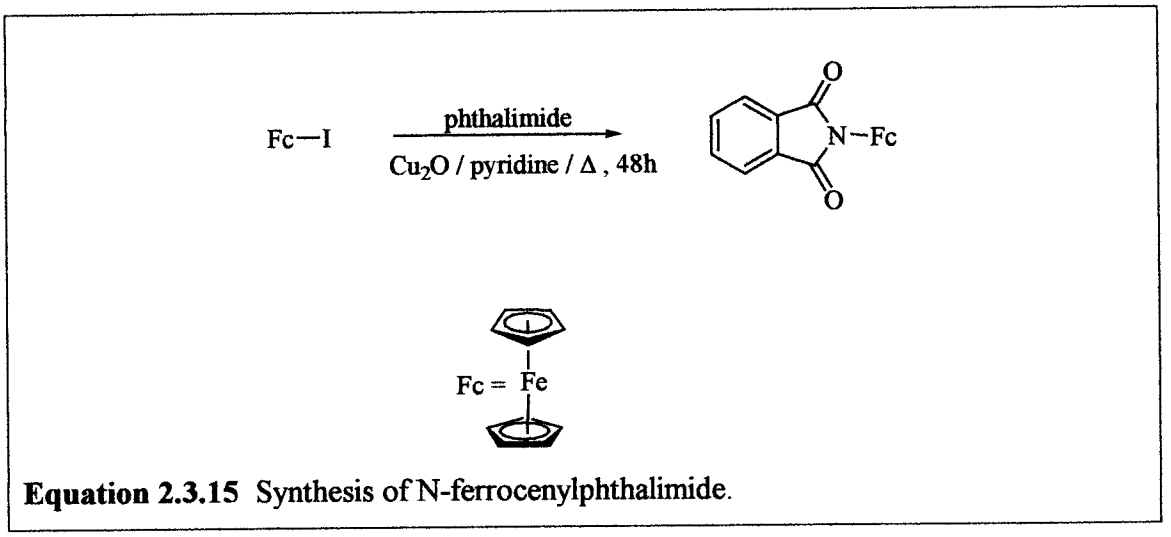

Equation 2.3.15 Synthesis of N-ferrocenylphthalimide.

Pyridine (80 mL, Aldrich 99.8%) was combined with iodoferrocene (13.32 g, 0.043 mol), phthalimide (6.91 g, 0.070 mol, Aldrich 99%), and Cu_2O (3.05 g, 0.021 mol, Strem 99.9%) in a nitrogen purged 250 mL Schlenk flask equipped with a stirring bar. The solution was allowed to reflux for 43 h and all volatile materials were then removed *in vacuo*. The solid was triturated with hexanes (~ 120 mL) and the suspension was filtered through a short (0.25 m) neutral Al_2O_3 column without protection from air. The column was then washed with hexanes (~ 500 mL) to remove the unreacted ferrocene until the filtrate was clear. The product was collected by elution of the column with diethylether (~ 300 mL). The ether extract was dried over anhydrous Na_2SO_4 for 1 h and then the Na_2SO_4 was filtered off and washed with diethylether (3 × 20 mL). All volatile

materials were removed from the combined organic extracts *in vacuo*. Crystallization of the resulting solid from ethanol at 4 °C produced a 28% yield (3.75 g, 11.3 mmol) of the product as dark red crystals.

Spectroscopic Properties:

^{13}C $\{^1H\}$ NMR ($CDCl_3$): δ = 166.806 (s, C=O), 134.016 (s, Ph-C), 123.079 (s, Ph-C), 88.570 (s, Cp-C), 69.508 (s, Cp-C), 65.537 (s, Cp-C), 62.935 (s, Cp-C).

^1H NMR ($CDCl_3$): δ = 7.897 (m, 2H, Ph-H), 7.760 (m, 2H, Ph-H), 5.009 (dd, $^3J(^1H,^1H)$ = 2.00 Hz, $^3J(^1H,^1H)$ = 2.00 Hz, 2H, Cp-H), 4.226 (s, 5H, Cp-H), 4.208 (dd, $^3J(^1H,^1H)$ = 2.00 Hz, $^3J(^1H,^1H)$ = 2.00 Hz , 2H, Cp-H).

2.3.16 Ferrocenylamine[10]

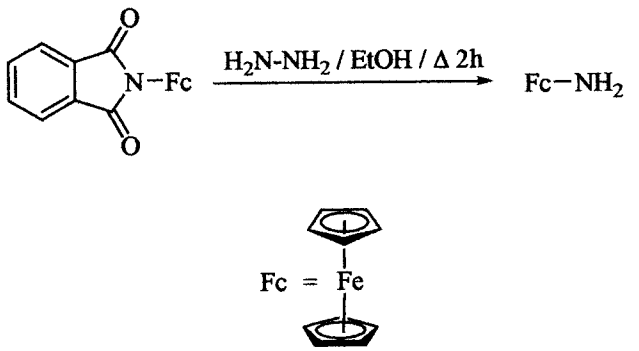

Equation 2.3.16 Synthesis of ferrocenylamine.

Ethanol (97 mL, Pharmco 95%) and hydrazine monohydrate (21.46 g, 0.412 mol, 20.0 mL, Aldrich) were combined with N-ferrocenylphthalimide (6.93 g, 0.0209 mol) in a nitrogen purged 250 mL three-necked round bottom flask equipped with a nitrogen adapter, reflux condenser, and a magnetic stirring bar. The solution was heated to reflux for 2 h, cooled to ambient temperature, and then 100 mL of H_2O were added. The aqueous layer was washed with diethylether (3 × 100 mL) and the combined organics were dried over anhydrous Na_2SO_4 for 1 h. The Na_2SO_4 was then filtered off, washed with diethylether (3 × 20 mL), and all volatile materials were removed from the combined filtrates *in vacuo*. A 97% yield (4.10 g, 0.203 mol) of the product was produced as a yellow solid.

Spectroscopic Properties:

^1H NMR ($CDCl_3$): δ = 4.099 (s, 5H, Cp-H), 3.994 (s, 2H, Cp-H), 3.842 (s, 2H, Cp-H), 2.588 (s, 2H, N-H).

X-Ray structure analysis: see Results and Discussion and Appendix 2.

2.3.17 N-formylferrocenylamine[7]

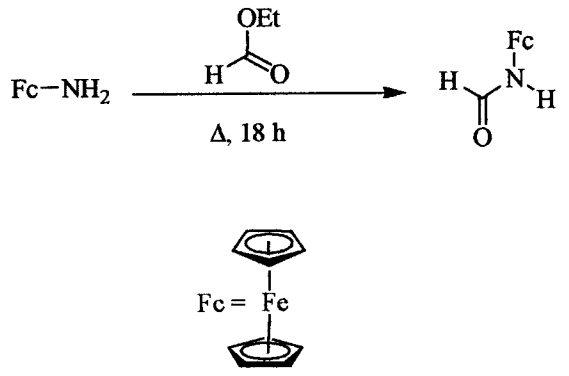

Equation 2.3.17 Synthesis of N-formylferrocenylamine.

Ethyl formate (15.0 mL, 13.95 g, 0.188 mol, Aldrich 97%) was combined with ferrocenylamine (0.80 g, 0.00396 mol) in a 250 mL three-necked round bottom flask equipped with a reflux condenser, and a magnetic stirring bar. The solution was heated

to reflux for 18 h and the solvent was then removed *in vacuo*. The resulting solid was filtered through a neutral Al_2O_3 column (50 cm) without protection from air following which the column was eluted with a 1:1solution of diethylether and hexanes (~ 200 mL). All volatile materials were removed from the combined organic solvents *in vacuo* to give a 76% yield (0.692 g, 3.01 mmol) of the product as a dark orange solid.

Spectroscopic Properties:

Downfield region:

^{1}H NMR ($CDCl_3$): δ = 8.309 (s, 1H, H-C=O or N-H), 7.817 s, 1H, H-C=O or N-H)

Upfield region:

First set (relative intensity 1): δ = 4.575 (dd, $^3J(^1H,^1H)$ = 4.00 Hz, $^3J(^1H,^1H)$ = 4.00 Hz, 2H, Cp-H), 4.061 (s, 2H, Cp-H), 3.789 (dd, $^3J(^1H,^1H)$ = 4.00 Hz, $^3J(^1H,^1H)$ = 4.00 Hz, 2H, Cp-H)

second set(relative intensity 0.09): δ = 4.002 (s, 5H, Cp-H), 3.906 (dd, $^3J(^1H,^1H)$ = 4.00 Hz, $^3J(^1H,^1H)$ = 4.00 Hz, 2H, Cp-H), 3.695 (dd, $^3J(^1H,^1H)$ = 4.00 Hz, $^3J(^1H,^1H)$ = 4.00 Hz, 2H, Cp-H)

third set (relative intensity 2): δ = 3.985 (s, 5H, Cp-H), 3.731 (dd, $^3J(^1H,^1H)$ = 3.60 Hz, $^3J(^1H,^1H)$ = 3.60 Hz, 2H, Cp-H), 3.712 (dd, $^3J(^1H,^1H)$ = 3.60 Hz, $^3J(^1H,^1H)$ = 3.60 Hz, 2H, Cp-H).

MP: 62 °C.

2.3.18 Isocyanoferrocene[4]

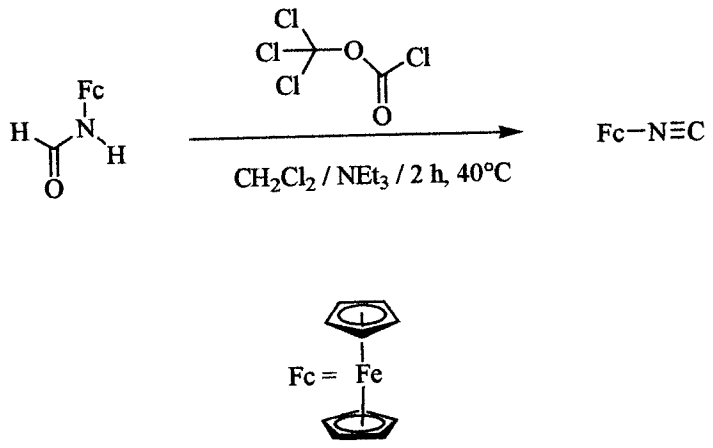

Equation 2.3.18 Synthesis of isocyanoferrocene.

CH_2Cl_2 (110 mL, Fisher 99.9%) and triethylamine (32 mL, 23.23 g, 0.230 mol) were combined with N-formylferrocenylamine (0.577 g, 2.51 mmol) in a a nitrogen purged 250 mL three-necked round bottom flask equipped with a nitrogen adapter, reflux condenser, dropping funnel, and a magnetic stirring bar. Diphosgene (0.22 mL, 0.356 g, 1.8 mmol) was placed into a dropping funnel containing CH_2Cl_2 (40 mL). The diphosgene solution was added drop wise to the refluxing suspension (over a 15 minute period) and then the solution was refluxed for an additional 3 h. The solution was allowed to cool to ambient temperature and extracted under nitrogen with a 10% solution of Na_2CO_3 (3 × 100 mL) and with H_2O (1 × 100 mL). The organic layer was dried over anhydrous $MgSO_4$ for 1 h and then the $MgSO_4$ was filtered off under nitrogen and washed with CH_2Cl_2 (3 × 20 mL). All volatile materials were removed from the combined organics *in vacuo* and the resulting brownish solid was sublimed at 75 °C to give a 77% yield (0.410 g, 1.93 mmol) of the product as a dark orange crystalline material.

Spectroscopic Properties:

^{13}C {^1H} NMR ($CDCl_3$): 167.040 (t, $J(^{13}C,^{14}N)$ = 5.23 Hz, C≡N), 79.416 (t, $J(^{13}C,^{14}N)$ = 15.29 Hz, 2C, C≡N-C), 70.938 (s, Cp-C), 70.764 (s, Cp-C), 66.860 (s, Cp-C).

^{1}H NMR ($CDCl_3$): 4.089 (dd, $^3J(^1H,^1H)$ = 2.00 Hz, $^3J(^1H,^1H)$ = 2.00 Hz, 2H, Cp-H), 3.900 (s, 5H, Cp-H), 3.545 (dd, $^3J(^1H,^1H)$ = 2.00 Hz, $^3J(^1H,^1H)$ = 2.00 Hz , 2H, Cp-H).

MP: 48 °C

IR (toluene, CaF_2): 2122 cm^{-1} (s, ν C≡N).

2.3.19 Para-nitrophenylferrocene[11]

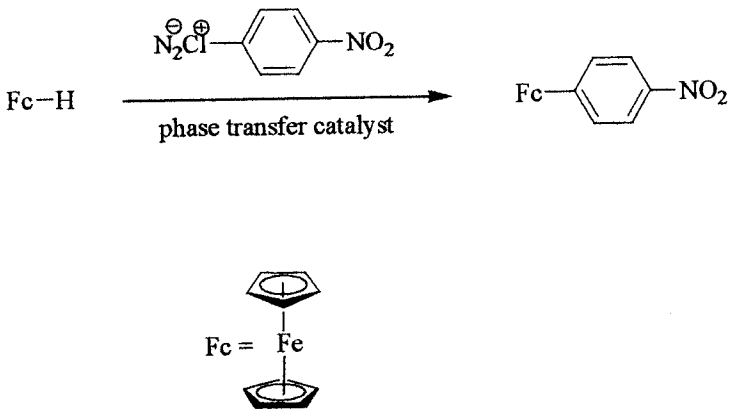

Equation 2.3.19 Synthesis of *para*-nitrophenylferrocene.

H_2O (30 mL), and concentrated hydrochloric acid (30 mL) were combined with *para*-nitroaniline (14 g, 0.1 mol, Aldrich 99+%) in a 250 mL three-necked round bottom flask equipped with a dropping funnel and magnetic stirring bar. The suspension was cooled to 5 °C and then a solution of sodium nitrite (7 g, 0.1 mol, Fisher A.C.S.) in H_2O (100 mL) was added drop wise to the suspension over a 15 minute period. After the addition was complete, the suspension was stirred for a further 30 minutes at 5 °C. A solution of ferrocene (9.5 g, 0.05 mol, Aldrich 98%), cetyltrimethylammonium bromide (1 g, 2.74 mmol, Acros 99+%), and diethylether (200 mL, Fisher A.C.S.) was cooled to 5 °C following which it was added drop wise to the aqueous suspension via syringe. After the addition was complete, the suspension was stirred at ambient temperature for 5 h and all volatile materials were then removed from the combined organics *in vacuo*. The resulting solid was washed with H_2O (10 × 20 mL), dissolved in THF (~ 50 mL), and

dried over anhydrous $MgSO_4$ for 1 h. The $MgSO_4$ was filtered off and all volatile materials were removed from the organic layer *in vacuo*. The resulting solid was dissolved in hexanes (~ 200 mL) at reflux and the hot solution was filtered. Cooling of this filtrate to 4 °C produced very dark purple crystals that were collected by filtration. Sublimation of these crystals at 100 °C produced a 55% yield (8.55 g, 27.7 mmol) of the product as dark purple crystals.

Spectroscopic Properties:

^{1}H NMR ($CDCl_3$): 8.153 (d, $^3J(^1H,^1H)$ = 8.80 Hz, 2H, Ph-H), 7.668 (d, $^3J(^1H,^1H)$ = 8.80 Hz, 2H, Ph-H), 4.742 (dd, $^3J(^1H,^1H)$ = 5.20 Hz, $^3J(^1H,^1H)$ = 5.20 Hz, 2H, Cp-H), 4.475 (dd, $^3J(^1H,^1H)$ = 4.40 Hz, $^3J(^1H,^1H)$ = 4.40 Hz, 2H, Cp-H), 4.068 (s, 5H, Cp-H).

2.3.20 Para-ferrocenylaniline[11]

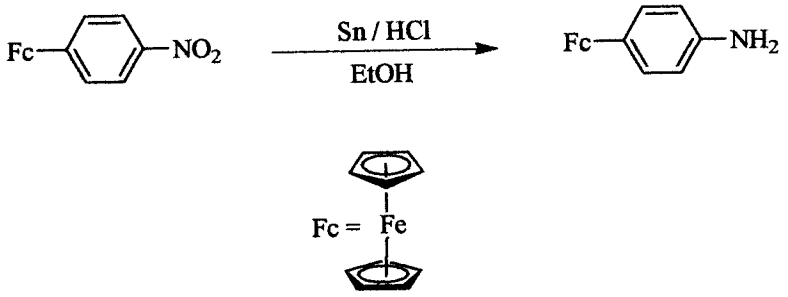

Equation 2.3.20 Synthesis of *para*-ferrocenylaniline.

Concentrated 12N hydrochloric acid (58 mL) and ethanol (92 mL) were combined with *para*-nitrophenylferrocene (4.96 g, 0.016 mol) and tin (10.9 g, 0.092 mol) in a 250 mL three-necked round bottom flask equipped with a reflux condenser and magnetic stirring bar. The suspension was heated to reflux for 4 h and then stirred at ambient temperature for 12 h. Water (500 mL) was then added to the suspension followed by a solution of NaOH sufficient to neutralize to a pH of 14. The suspension was filtered, extracted with CH_2Cl_2 (3 × 200 mL), and dried over anhydrous Na_2SO_4 for 1 h. The Na_2SO_4 was filtered off and all volatile materials were removed from the organic filtrates

in vacuo. A 93% yield (4.17 g, 0.150 mol) of the product was produced as a dark orange solid.

Spectroscopic Properties:

^{1}H NMR ($CDCl_3$):

7.303 (d, $^3J(^1H,^1H)$ = 8.40 Hz, 2H, Ph-H), 6.651 (d, $^3J(^1H,^1H)$ = 8.40 Hz, 2H, Ph-H), 4.552 (m, 2H, Cp-H), 4.249 (m, 2H, Cp-H), 4.045 (s, 5H, Cp-H), 3.620 (s, 2H, NH_2-H).

2.3.21 N-formylferrocenylaniline[7]

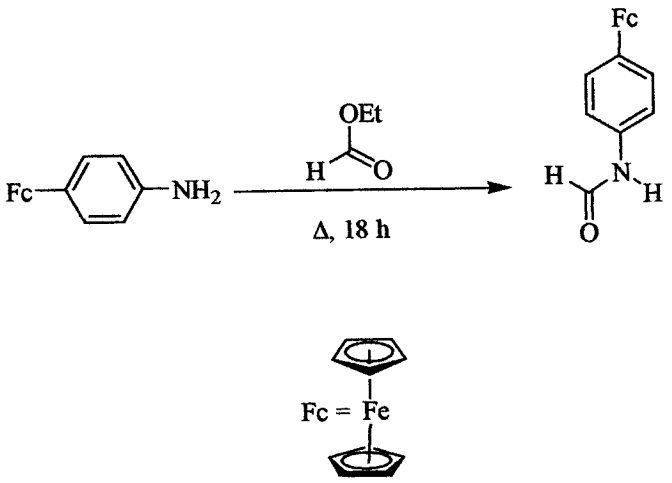

Equation 2.3.21 Synthesis of N-formylferrocenylaniline.

Ethyl formate (15.0 mL, 13.95 g, 0.188 mol, Aldrich 97%) was combined with *para*-ferrocenylaniline (1.345 g, 0.00484 mol) in a nitrogen purged 250 mL three-necked round bottom flask equipped with a reflux condenser, and a magnetic stirring bar. The suspension was heated to reflux for 18 h. The solvent was then removed *in vacuo* and the resulting solid was filtered through a neutral Al_2O_3 column (0.5 m) without protection from air. The column was eluted with a 1:1 solution of diethylether and hexanes (~ 500 mL). All volatile materials were removed from the filtrate *in vacuo* to give a 76% yield (0.692 g, 3.01 mol) of the product as a dark orange solid.

Spectroscopic Properties:

^{1}H NMR ($CDCl_3$): 8.685 (dd, $^3J(^1H,^1H)$ = 11.60 Hz, $^3J(^1H,^1H)$ = 11.60 Hz, 1H, HC=O), 8.406 (s, 1H, NH), 7.466 (d, $^3J(^1H,^1H)$ = 8.40 Hz, 2H, Ph-H), 7.013 (d, $^3J(^1H,^1H)$ = 8.40 Hz, 2H, Ph-H), 4.625 (dd, $^3J(^1H,^1H)$ = 6.00 Hz, $^3J(^1H,^1H)$ = 6.00 Hz, 2H, Cp-H), 4.327(dd, $^3J(^1H,^1H)$ = 8.00 Hz, $^3J(^1H,^1H)$ = 8.00 Hz, 2H, Cp-H), 4.049 (s, 1H, Cp-H).

2.3.22 Para-isocyanoferrocenylbenzene[4]

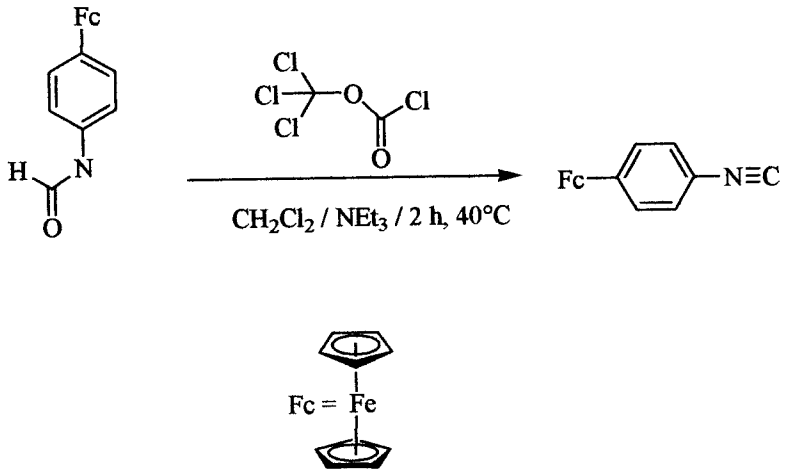

Equation 2.3.22 Synthesis of *para*-isocyanoferrocenylbenzene.

CH_2Cl_2 (200 mL) and triethylamine (32 mL, 23.2 g, 0.23 mol) were combined with N-formylferrocenylamine (2.147 g, 7.01 mmol) in a nitrogen purged 500 mL three-necked round bottom flask equipped with a nitrogen adapter, reflux condenser, dropping funnel, and a magnetic stirring bar. Diphosgene (0.507 mL, 0.832 g, 4.21 mmol) was placed into a dropping funnel containing CH_2Cl_2 (40 mL). The diphosgene solution was added drop wise to the refluxing suspension (over a 15 minute period) and then the solution was refluxed for an additional 3 h. The solution was cooled to ambient temperature and washed under nitrogen with a 10% solution of Na_2CO_3 (3 × 100 mL) and with H_2O (1 × 100 mL). The CH_2Cl_2 solution was dried over anhydrous $MgSO_4$ for 1 h, the $MgSO_4$ was filtered off, washed with CH_2Cl_2 (3 × 20 mL), and all volatile materials were removed from the combined filtrates *in vacuo*. The brownish solid which resulted

was sublimed *in vacuo* at 75 °C to give a 28 % yield (0.480 g, 0.00167 mol) of the product as a dark orange solid.

Spectroscopic Properties:

^{1}H NMR ($CDCl_3$): 6.939 (d, $^3J(^1H,^1H)$ = 8.40 Hz, 2H, Ph-H), 6.806 (d, $^3J(^1H,^1H)$ = 8.40 Hz, 2H, Ph-H), 4.282 (dd, $^3J(^1H,^1H)$ = 2.00 Hz, $^3J(^1H,^1H)$ = 2.00 Hz, 2H, Cp-H), 4.085 (dd, $^3J(^1H,^1H)$ = 1.60 Hz, $^3J(^1H,^1H)$ = 1.60 Hz, 2H, Cp-H), 3.801 (s, 5H, Cp-H).

IR (toluene, CaF_2): 2120 cm^{-1} (s, ν isonitrile).

MP: 84 °C.

2.3.23 Tetrakis(para-methoxyisocyanobenzene)nickel(0)[12]

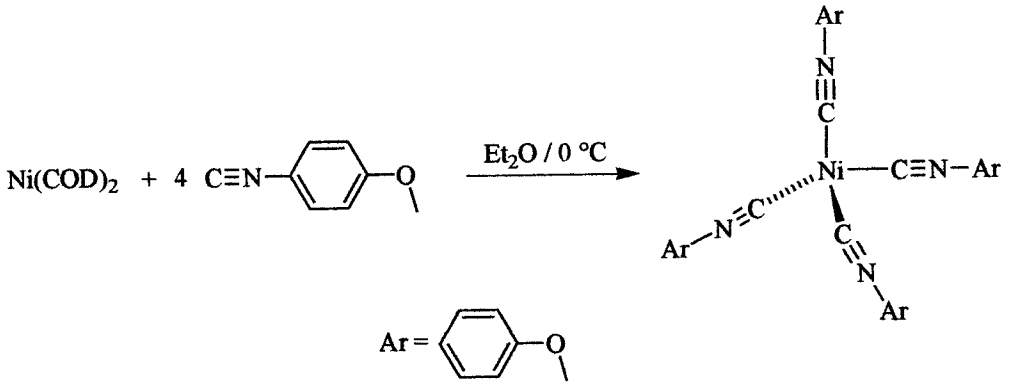

Equation 2.3.23 Synthesis of tetrakis(*para*-methoxyisocyanobenzene)nickel(0).

Diethylether (25.0 mL) was combined with bis(1,5-cyclooctadiene)nickel(0) (0.580 g, 2.12 mmol, Strem 98+%) in a nitrogen purged 250mL three-necked round bottom flask equipped with a nitrogen adapter, dropping funnel, and a magnetic stirring bar. *Para*-methoxyisocyanobenzene (1.41 g, 10.6 mmol) was then dissolved in diethylether (40 mL) and cooled to 0 °C following which it was added drop wise to the solution over a 15 minute period. The suspension was allowed to stir for 2 h at ambient temperature producing a yellow precipitate. This solid was removed by filtration and rinsed with hexanes (3 × 10 mL). All the volatile materials were removed from the solid

in vacuo to give an 87% crude yield (0.530 g, 0.896 mmol) of the crude product as a bright yellow solid. Crystallization from THF at -19 °C further purified the product.

Spectroscopic Properties:

^{13}C {^{1}H} NMR ($CDCl_3$): 165.373 (d, $^{1}J(^{13}C, ^{14}N)$ = 4.73 Hz, C≡N), 157.770 (s, Ph-C), 126.653 (s, Ph-C), 123.371 (s, Ph-C), 114.146 (s, Ph-C), 55.473 (s, CH_3).

^{1}H NMR ($CDCl_3$): 6.982 (d, $^{3}J(^{1}H,^{1}H)$ = 8.40 Hz, 8H, Ph-H), 6.337 (d, $^{3}J(^{1}H,^{1}H)$ = 8.40 Hz, 8H, Ph-H), 3.034 (s, 12H, CH_3).

IR (toluene, CaF_2): 2017 cm^{-1} (s, ν isonitrile).

MP: 98 °C.

X-Ray structure analysis: see Results and Discussion and Appendix 3.

2.3.24 Attempted synthesis of tetrakis(isocyanoferrocene)nickel(0)[12]

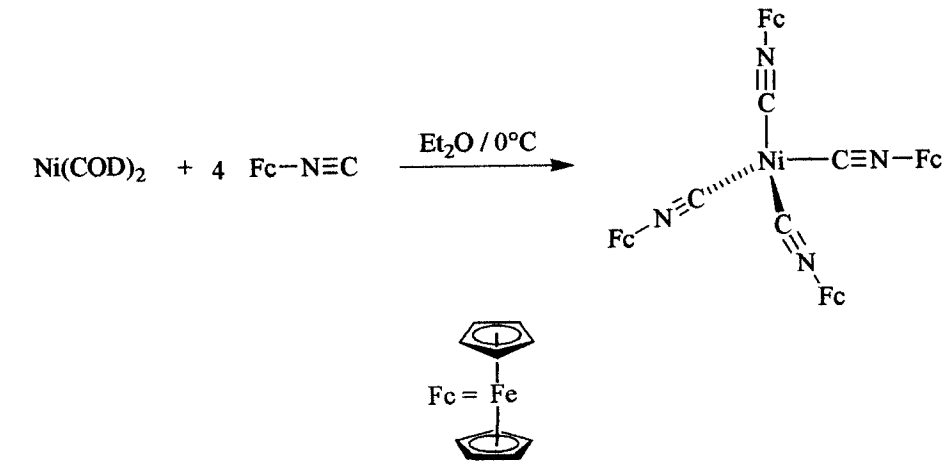

Equation 2.3.24 Synthesis of tetrakis(isocyanoferrocene)nickel(0).

Diethylether (10 mL) was combined with bis(1,5-cyclooctadiene)nickel (0) (0.106 g, 0.387 mmol, Strem 98+%) in a nitrogen purged 250mL three-necked round bottom flask equipped with a nitrogen adapter, dropping funnel, and a magnetic stirring bar. Isocyanoferrocene (0.41 g, 1.93 mmol) was then dissolved in diethylether (25 mL) and cooled to 0 °C following which it was added drop wise to the solution over a 15 minute

period. The suspension was allowed to stir for 2 h at ambient temperature producing an orange precipitate. This solid was removed by filtration and rinsed with hexanes (3 × 10 mL). All the volatile materials were removed from the solid *in vacuo* to give an 81% yield (0.284g, 0.387 mol) of the product as a crude dark orange powder. The crude product was then dissolved in CH_2Cl_2 and the solution was layered with hexanes. Attempts to crystallize the compound at -19 °C resulted in discoloration, which gave a dark blue solution. The product has not been isolated at this time.

Spectroscopic Properties:

Crude solid IR (KBr): 2122 cm^{-1} (s, ν isonitrile).

2.3.25 Tetrakis(para-isocyanoferrocenylbenzene)nickel(0)[12]

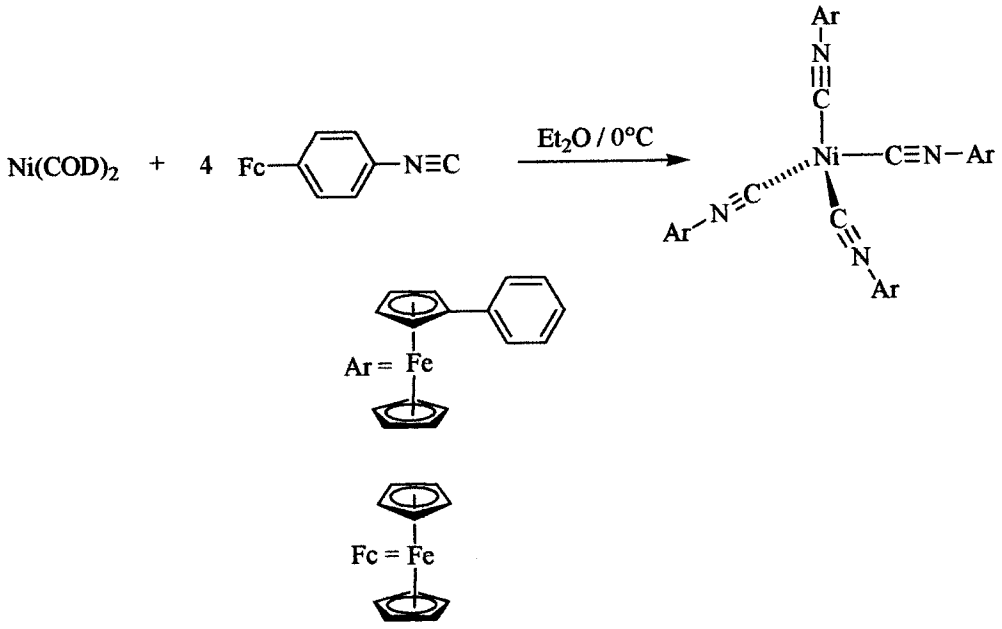

Equation 2.3.25 Synthesis of tetrakis(*para*-isocyanoferrocenylbenzene)nickel(0).

THF (15 mL) was combined with bis(1,5-cyclooctadiene)nickel(0) (0.386 g, 1.4 mmol, Strem 98+%) in a nitrogen purged 250mL three-necked round bottom flask equipped with a nitrogen adapter, dropping funnel, and a magnetic stirring bar. *Para-*

isocyanoferrocenylbenzene (0.160 g, 0.00701 mol) was then dissolved in dry / degassed THF (25.0 mL) and cooled to 0 °C following which it was added drop wise to the solution over a 15 minute period. The solution was allowed to stir for 3 h at ambient temperature, concentrated *in vacuo* to approximately 20 mL, and layered with hexanes (50 mL). Recrystallization attempts at -19 °C are still ongoing.

2.3.26 Tetrakis(para-nitro-isocyanobenzene)nickel(0)[12]

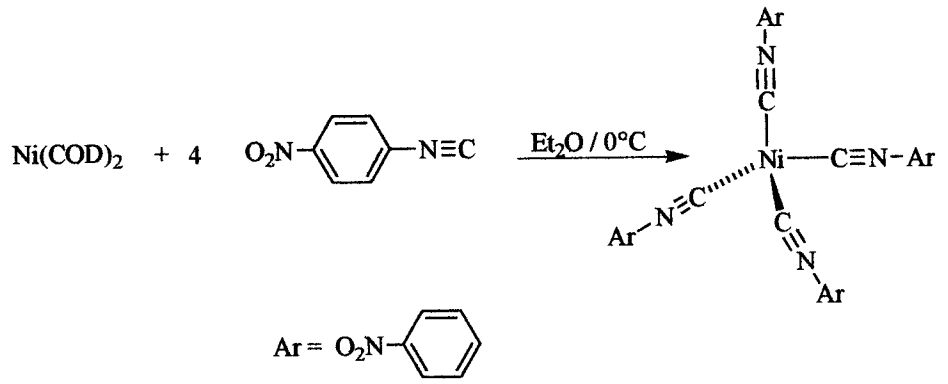

Equation 2.3.26 Synthesis of tetrakis(*para*-nitro-isocyanobenzene)nickel(0).

Diethylether (12 mL) was combined with bis(1,5-cyclooctadiene)nickel(0) (0.279 g, 1.01 mmol, Strem 98+%) in a nitrogen purged 250mL three-necked round bottom flask equipped with a nitrogen adapter, dropping funnel, and a magnetic stirring bar. *Para*-nitro-isocyanobenzene (0.75 g, 0.00506 mol) was then dissolved in diethylether (25 mL) and cooled to 0 °C following which it was added drop wise to the solution over a 15 minute period. The suspension was allowed to stir for 3 h at ambient temperature producing a dark red precipitate. This solid was removed by filtration, and rinsed with hexanes (3 × 10 mL). All the volatile materials were removed from the solid *in vacuo*. The crude dark red product was dissolved in dry / degassed THF (Aldrich 99.9%) and the solution layered with hexanes. Recrystallization attempts at -19 °C are still ongoing.

2.3.27 *Bis[bis{di(p-ethylphenyl)phosphino}benzene]bis(isocyanoferrocene) molybdenum(0)*

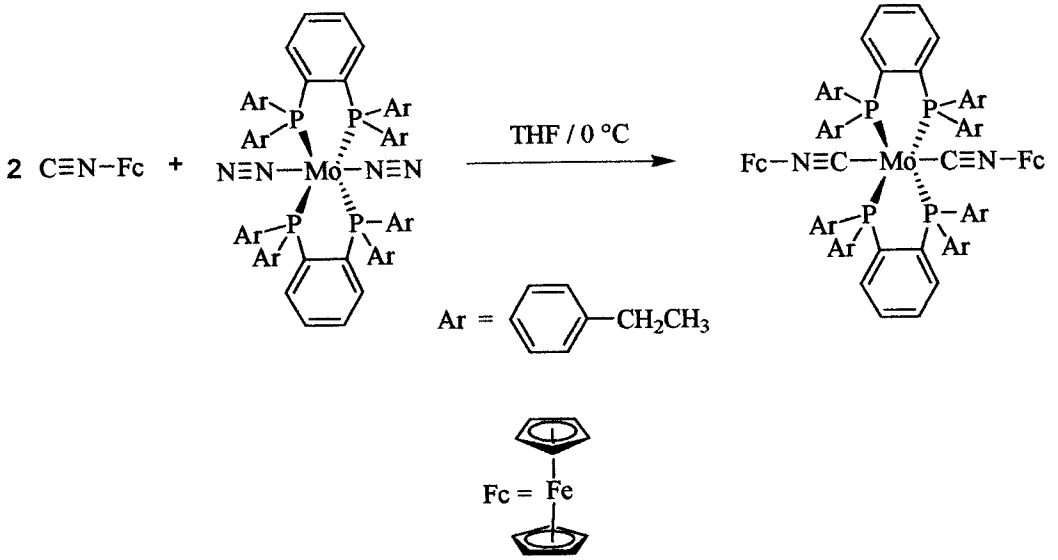

Equation 2.3.27 Synthesis of bis[bis{di(*p*-ethylphenyl)phosphino} benzene]bis(isocyanoferrocene)molybdenum(0).

THF (20 mL) was combined with isocyanoferrocene (0.10 g, 0.472 mmol) in a nitrogen purged 250 mL three-necked round bottom flask equipped with a nitrogen adapter, dropping funnel, and a magnetic stirring bar. The dinitrogen complex[13] (0.260 g, 0.214 mmol) was then dissolved in THF (75 mL) and added drop wise to the solution over a 15 minute period. After the addition of the dinitrogen complex, the solution was allowed to stir for 30 minutes and the precipitate was then collected by filtration and washed with hexanes (3 × 20 mL). The resulting solid was dissolved in THF (~ 20 mL) and the solution was layered with hexanes (~ 50 mL). Cooling to -19°C produced a 20% yield (0.150 g, 0.0949 mmol) of the product as dark orange fibrous crystals.

Spectroscopic Properties:

^{1}H NMR ($CDCl_3$): 7.799 (br, 8H, Ph-H), 7.304 (d, $^3J(^1H,^1H)$ = 7.20 Hz, 16H, Ph-H), 6.987 (d, $^3J(^1H,^1H)$ = 8.00 Hz, 16H, Ph-H), 4.065 (br, 4H, Cp-H), 3.921 (br, 10H, Cp-H), 3.774 (br, 4H, Cp-H), 2.500 (q, $^3J(^1H,^1H)$ = 7.60 Hz, $^3J(^1H,^1H)$ = 15.00 Hz, 16H, CH_2), 1.154 (t, $^3J(^1H,^1H)$ = 7.60 Hz, 24H, CH_3).

IR (benzene, CaF_2): 1883 cm^{-1} (s, ν isonitrile).

MP: 104 °C.

2.3.28 *Bis[bis{di(p-ethylphenyl)phosphino}benzene]bis(isocyanoferrocenylbenzene) molybdenum(0)*

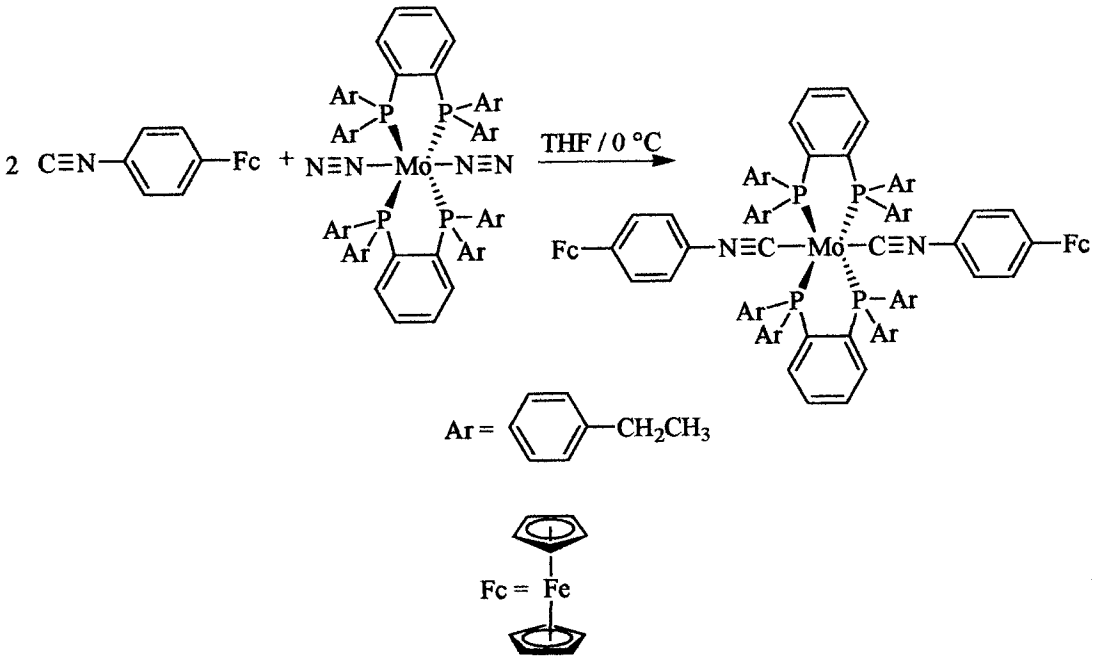

Equation 2.3.28 Synthesis of bis[bis{di(*p*-ethylphenyl)phosphino} benzene]bis(isocyanoferrocenylbenzene)molybdenum(0).

THF (20 mL) was combined with isocyanoferrocenylbenzene (0.100 g, 0.472 mmol) in a nitrogen purged 250 mL three-necked round bottom flask equipped with a nitrogen adapter, dropping funnel, and a magnetic stirring bar. The dinitrogen complex[13]

(0.260 g, 0.214 mmol) was then dissolved in THF (75 mL) and added drop wise to the to the solution over a 15 minute period. After the addition of the dinitrogen complex, the solution was allowed to stir for 30 minutes and the precipitate was collected by filtration and washed with hexanes (3 × 20 mL). The resulting solid was dissolved in THF (~ 20 mL) and the solution layered with hexanes (~ 50 mL). Crystallization at -19°C gave a dark purple solution. All the volatiles were then removed *in vacuo* and the remaining solid was dissolved in toluene, filtered under nitrogen, and layered with hexanes. Recrystallization at -19°C produced an 81% yield (0.300 g, 17.3 mmol) of the product as a dark purple crystalline material.

Spectroscopic Properties:

^{1}H NMR ($CDCl_3$): 7.802 (br, 8H, Ph-H), 7.371 (d, $^3J(^1H,^1H)$ = 7.60 Hz, 16H, Ph-H), 6.881(d, $^3J(^1H,^1H)$ = 8.00 Hz, 16H, Ph-H), 6.079 (br, 8H, Ph-H), 4.405(br, 4H, Cp-H), 4.078 (br, 10H, Cp-H), 3.3.905 (br, 4H, Cp-H), 2.446(q, $^3J(^1H,^1H)$ = 7.60 Hz, $^3J(^1H,^1H)$ = 15.20 Hz, 16H, CH_2), 1.093 (t, $^3J(^1H,^1H)$ = 7.20 Hz, 24H, CH_3).

IR (benzene, CaF_2): 1877 cm^{-1} (s, ν C≡N).

MP: 225 °C.

References

1. W. Chasar, *J. Org. Chem.* **1985**, *50*, 545.
2. D. F. Shriver, M.A. Drezdzon, *The Manipulation of Air Sensitive compounds*; 2nd ed.; Wiley & Sons: New York, **1986**.
3. W. L. F. Armarego, D.D. Perrin, *Purifiation of Laboratory Chemicals*; 4nd ed.; BH: NewYork, **1996.**
4. M. Hanack, S. Kamenzin, C. Kamenzin, L. R. Subramonian, *Synthetic Metals* **2000**, *110*, 93-103.
5. G. J. Kubas, C. J. Burns, J. Eckert, S. W. Johnson, A. C. Larson, P. J. Vergamini, C. J. Unkefer, G. R. K. Khalsa, S. A. Jackson, O. Eisenstein, *J. Am. Chem. Soc.* **1993**, *115*, 569-581.
6. ADH Chemistry Experiment Papers: Hunter, A. D.: "Solid Sodium Amalgam," in *Inorganic Experiments*, 2nd ed.; J. D. Woollins Ed.; VCH: New York, **2003**; pp 211.
7. G. R. Knox, P. L. Pauson, D. Willison, *Organometallics* **1990**, *9*, 301-306.
8. G. Smolinsky, *J. Am. Chem. Soc.* **1962**, *27*, 3557.
9. D. Van Leusen, B. Hessen, *Organometallics* **2001**, *20*, 224-226.
10. B. Bildstein, M. Malaun, H. Kopacka, K. Wurst, M. Mitterbock, K. H. Ongania, G. Opromolla, P. Zanello, *Organometallics* **1999**, *18*, 4323-4336.
11. P. Hu, K. Quing Zhao, H. Bo Xu, *Molecules* **2001**, *6*, M249.
12. S. D. Ittel, "Complexes of Nickel (0)," in *Inorg. Synth.*, R.. J. Angelici, Ed.; Wiley: New York, **1990**; Vol. 28, pp 98-99.
13. J. B. Updegraff III, The Synthesis of Organometallic Nanorods from Molybdenum and Tungsten diisonitrile complexes and a New Method to Synthesize Air Stable Sodium Cyclopentadienide, Master of Science, Youngstown State University, August 2004.

Chapter Three - Results and Discussion

3.1 Isonitriles

3.1.1 Synthesis of para-methoxyisocyanobenzene

In the isonitriles, the nature of the various alkyl and aryl substituents can be used to alter the electronic properties of the CN-R function. The *p*-anisyl group was used as a substituent on NC to enhance the solubility of the complexes and make it a more electronic rich NC. The synthesis of *para*-methoxyisocyanobenzene was done using a procedure similar to the literature method described by Hanack et al.[1]

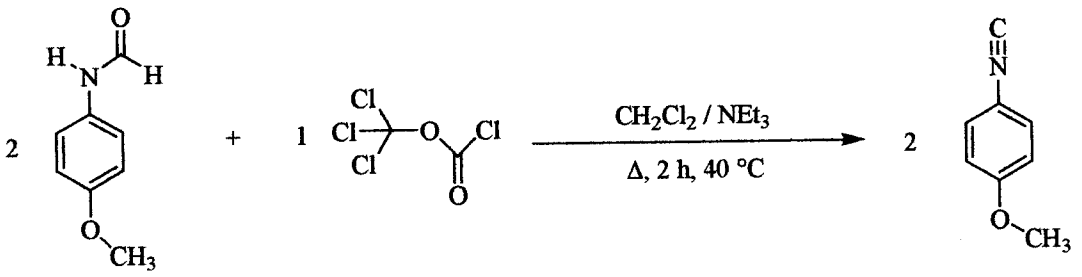

Equation 3.1.1 Synthesis of *para*-methoxyisocyanobenzene.

Under reflux conditions, *para*-formamidoanisole was reacted with diphosgene in the presence of triethylamine, which was used as the base, in a methylene chloride solution. Diphosgene was used as the dehydrating reagent to avoid the use of phosgene which is a highly toxic gas that has to be synthesized each time before the reaction. With diphosgene, the reaction conditions are not as mild as with phosgene itself. Thus, slightly lower yields or more forcing conditions have to be expected. Crystallization from pentane produced a 21% yield of the product as white-yellow needles exhibiting a pronounced isonitrile smell. The crystals start to melt at room temperature and have to be stored under nitrogen at -19 °C to avoid rapid decomposition. Even under N_2, it decomposes at room temperature within less than an hour to leave a brown tar.

Recrystallization could have probably removed small amounts of impurities in the isolated product. Due to the loss of valuable material in recrystallization, however, it was decided to use the compound as is. No spectroscopic properties were recorded due to thermal sensitivity of the compound and the identity of the compound was verified by its conversion into the tetraisocyanonickel(0) (Chapter 3.1.2).

3.1.2 Synthesis of 1,4-diisocyano-2,3,5,6-tetramethylbenzene

To enhance the solubility of the isonitriles, we decided to use the tetrametylated isonitrile, 1,4-diisocyano-2,3,5,6-tetramethylbenzene, that was prepared by a method similar to the one in previous subchapter (3.1.1).

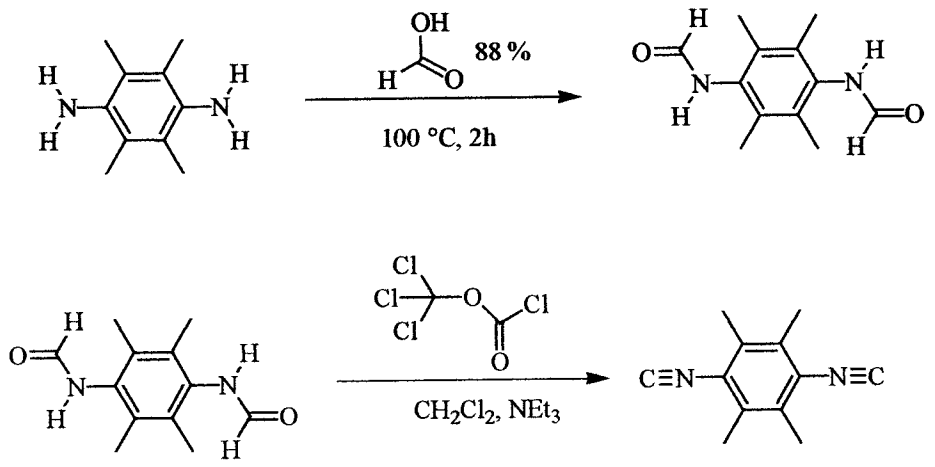

Equation 3.1.2 Synthesis of 1,4-diisocyano-2,3,5,6-tetramethyl benzene.

In the first step of its formation, the commercially available 2,3,5,6-tetramethyl phenylenediamine was reacted under reflux in a condensation reaction with formic acid and the product was precipitated with water to give 1,4-bis(N,N'-formylamido)-2,3,5,6-tetramethylbenzene as an air stable white powder in 82% yield. The compound proved to be insoluble in organic solvents and its NMR spectra were not recorded.

To obtain the isonitrile, the formamide was dehydrated with diphosgene as described for the methoxy derivative (3.1.1). Initial attempts to purify the compound by

column chromatography and by crystallization by the layering of a methylene chloride solution with hexanes produced fairly clean material, but the workup was not very efficient. Sublimation proved to be the method of choice and, in this way, the compound was produced as a white crystalline material in a 34% yield. The solid is stable in air at room temperature, however, a solution of the compound should be kept under nitrogen to avoid decomposition. Over longer periods of time, the solid should be stored under nitrogen at 4 °C to avoid decomposition.

In the ^{13}C NMR, a signal is observed at 168.870 ppm attributable to the carbonyl carbon atoms. The signal at 131.550 ppm is due to the carbon atoms of the phenyl ring that have a methyl substituent. A signal is observed at 126.724 ppm which is due to the phenyl carbon atoms attached to the isonitrile group. The signal of the methyl carbon atoms is observed at 16.366 ppm. In the ^{1}H NMR, a signal from the methyl protons is observed at 2.357 ppm. In the IR spectrum, a vibration is observed at 2115 cm^{-1} attributable to the stretching vibration of the isonitrile group. The melting point of the compound was observed at 112 °C.

3.1.3 X-Ray structural analysis of 1,4-diisocyano-2,3,5,6-tetramethylbenzene

In the course of this work, we had been able to isolate X-ray quality crystals of 1,4-diisocyano-2,3,5,6-tetramethylbenzene and, thus, we determined its solid state structure. It crystallizes in the space group C2/c with 4 molecules in the unit cell. The crystal data are summarized in Appendix 1.

The bisisocyanide is located on a crystallographical inversion centre with only half the molecule being crystallographically independent. Both crystallographically independent methyl groups show a disorder of the H atoms which have been refined as idealized disordered methyl groups with the two positions rotated from each other by 60°. The site distributions have been refined to be approximately 0.90/0.10 and 0.72/0.28 for the two types of methyls. Bond length and angles are in the expected range for aromatic isonitriles. (Figure 3.1) In particular, the most important distances are shown in Table 3.1.

Table 3.1 Selected bond lengths (Å) of 1,4-diisocyano-2,3,5,6-tetramethylbenzene.	
N1–C1 1.1628 (14)	C3–C4 1.4008 (13)
N1–C2 1.4045 (12)	C3–C2 1.4070 (13)

These distances are expected to vary upon coordination to a metal. In particular, it would be expected that coordination would lengthen N1-C1 and C3-C2 and shorten N1-C2 and C3-C4 due to metal ligand backbonding and the quinoidal character that it would induce to the isonitrile bridge.

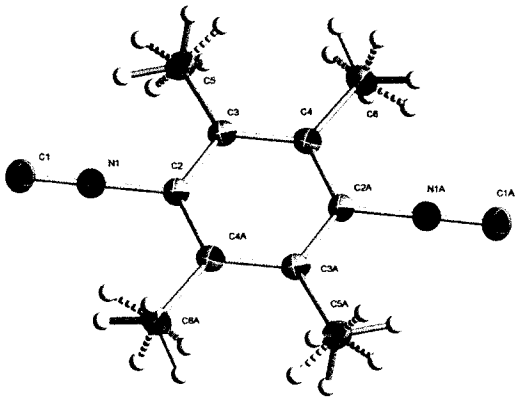

Figure 3.1 Molecular structure showing 30 % probability displacement ellipsoids. The disorder of the hydrohen atoms is shown.

3.1.4 Synthesis of para-nitroisocyanobenzene

In order to build a library of isonitrile ligands with different electronic and solubility properties, a nitro derivative was also prepared. *Para*-nitroisocyanobenzene was synthesized in a similar manor to the isonitriles described in the previous subchapters (3.1.1. and 3.1.2).

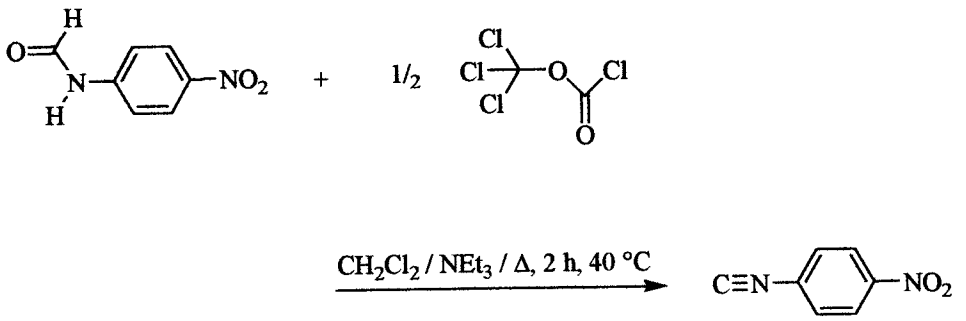

Equation 3.1.4 Synthesis of *para*-nitroisocyanobenzene.

The crude product was purified by sublimation to give a 21% yield of the isonitrile as a white solid. It was necessary to sublime the crude product several times for complete purity. Unlike its more volatile analogues in the previous subchapters, the compound in virtually odor free. The solid is air stable but solutions should be kept under nitrogen to avoid slow decomposition. In the ^{13}C NMR, a signal that is due to the isonitrile carbon atom is observed at 169.3 ppm. The phenyl carbon atom with the nitro substituent has a signal observed at 147.3 ppm. A signal from the phenyl carbon atom attached to the isonitrile is observed at 131.0 ppm that is a triplet with a ^{14}N coupling constant of 16.0 Hz. Two singlets are observed at 127.4 and 124.9 ppm attributable to the signals of the unsubstituted phenyl carbon atoms. In the ^{1}H NMR, two doublets are observed at 8.230 and 7.508 ppm with coupling constants of 2 × 9.0 Hz that are due to the proton signals of the phenyl ring. In the IR spectrum, two separate sets of signals are observed. The first set using CaF_2 had a strong vibration at 2121 cm^{-1} due to the isonitrile group. Two strong signals are also observed from the nitro group with an asymmetric and symmetric stretching frequency at 1520 and 1345 cm^{-1} repectively. Using a KBr pellet, a broad absorption is observed at 2130 cm^{-1} attributable to the isontrile. Two signals are due to the asymmetric and symmetric stretching frequencies of the nitro group respectively at 1541 and 1349 cm^{-1}. The melting point of the compound was observed to be 81 °C.

At this point, a few comments concerning the synthesis and workup of the isonitriles should be made. To begin with, the synthesis and isolation of the crude

products were all very similar but the workup of the three isonitriles varied slightly. The thermal sensitivity of the methoxy derivative made it necessary to obtain a clean product by crystallization while the nitro derivative had to be sublimed several times for complete purity. The tetramethyldiisonitrile seemed to be the easiest to purify by either crystallization or sublimation. Sublimation will be used as the purification method in all subsequent reactions due to the time consuming procedure involved in the crystallization technique. The tetramethyldiisonitrile was prepared to enhance the solubility of our complexes and because it can bridge two metal centers and was selected as the main isonitrile used in our work.

3.2 Phosphines

3.2.1 Synthesis of tris(p-anisyl)phosphine

The two most common types of phosphines are alkyl and aryl substituted ones. In general, alkyl phosphines and their complexes are very soluble and more electron donating, and, thus, for many applications they would be the ligands of choice. On the other hand, they are typically very sensitive towards oxidation and are generally not easy to handle. Aryl phosphines are much less air sensitive, however, most lack the solubility of their alkyl counterparts and their complexes, especially the larger oligomers, will not be soluble enough for easy chemical manipulation. To overcome this disadvantage while keeping their enhanced stability, we introduced alkyl or ether substituents on the aryl rings. Depending on the type of substituent on the aryl ligands, their net ability to transfer electron density to the aryl moiety was varied as well. Thus, a small library of aryl phosphines with different electronic as well as solubility properties was established.

The first member of this library is a phosphine of the PR_3 type which has the ability to be incorporated into metal complexes containing central atoms in low oxidation states. The stability of the PR_3 complexes results from the combination of soft-donor/soft-acceptor ligands with the soft acceptor nature of metals in low oxidation states. In the context of this research, the phosphine will be used to synthesize a dinitrogen complex of the type $M(N_2)_2(PR_3)_4$ which will be the starting materials for the synthesis of the organometallic oligomers.

Tris(*p*-anisyl)phosphine was prepared using a procedure similar to the literature method described by Kubas et al.[2]

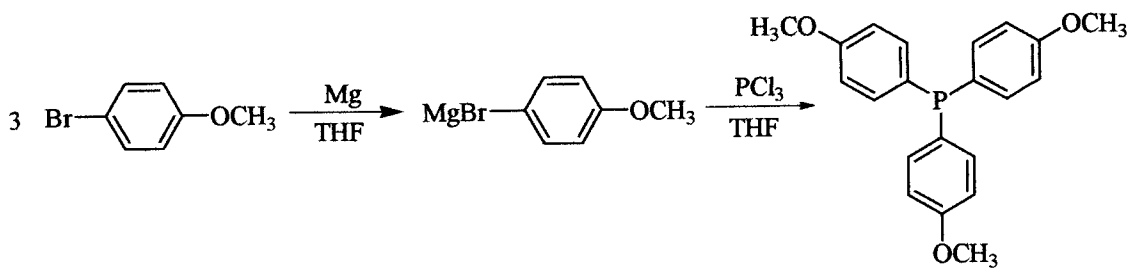

Equation 3.2.1 Synthesis of tris(*p*-anisyl)phosphine.

The first step in the synthesis is the formation of the Grignard reagent by the addition of *p*-bromoanisole to an iodine activated magnesium suspension. The Grignard reagent was then reacted with phosphorus trichloride in a nucleophilic substitution reaction and hydrolyzed with a 10% aqueous NH_4Cl solution to remove the unreacted Grignard reagent. After workup, crystallization from diethylether produced a 39% yield of the product as white needles. The solid is stable in air at room temperature but solutions of the ligand should be kept under nitrogen to avoid decomposition. In the ^{13}C NMR, a signal is observed at 159.780 ppm attributable to the phenyl carbon atoms with the methoxy substituent. Three doublets are observed at 134.740, 114.009, and 113.895 ppm that are due to the other three phenyl carbon atoms with ^{31}P coupling constants of 20.51, and 2 × 7.64, respectively. A singlet is observed at 55.196 ppm due to the methyl carbon atoms. In the ^{1}H NMR, a doublet of a doublet is observed from the phenyl protons at 7.220 ppm with ^{1}H and ^{31}P coupling constants of 8.70 and 7.40 Hz respectively. A signal from the remaining phenyl protons is observed at 6.870 ppm with a coupling constant of 8.70 Hz. The singlet at 3.795 ppm is due to the methyl proton signal. The ^{31}P NMR also has a signal observed at -10.83 ppm.

3.2.2 Synthesis of 1,2-Bis(di(p-anisyl)phosphino)ethane

In a related study, chealating phosphines that are *para* substituted dppe derivatives were used because they were expected to give more soluble complexes than does the parent dppe ligand. The bidentate ligands generally give complexes that are more stable than their monodentate analogues because both phosphorus atoms coordinate to the metal acid on entropic barriers to their simultaneous release being present. A library of chelating phosphines was established to allow a wide range of net electron transfer abilities to the metal center as discussed in the previous subchapter (3.2.1).

1,2-Bis(di(*p*-anisyl)phosphino)ethane was prepared according to the procedure in the previous subchapter (3.2.1).

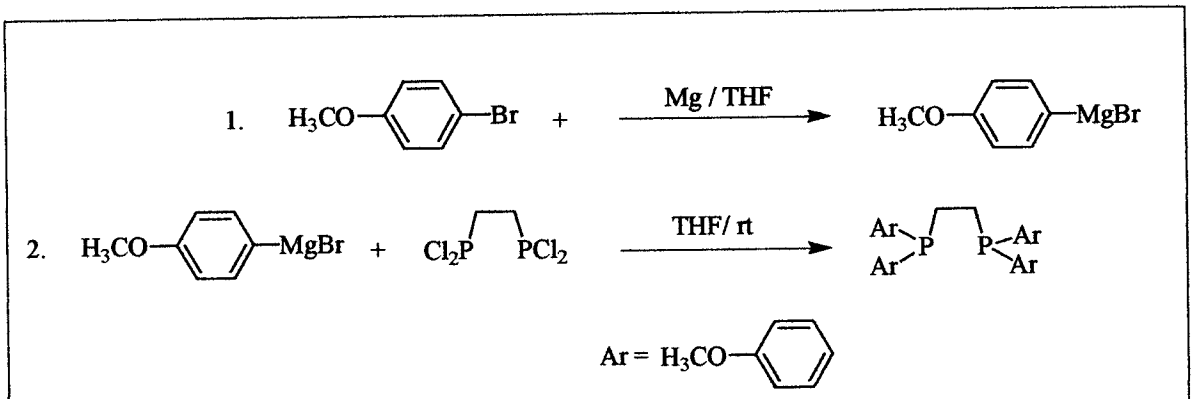

Equation 3.2.2 Synthesis of 1,2-bis(di(*p*-anisyl)phosphino)ethane.

A Grignard reagent was prepared by combining *p*-bromoanisole with iodine activated magnesium in a THF solution. The Grignard reagent was then reacted with bis(dichlorophosphino)ethane in a nucleophilic substitution reaction and the mixture was hydrolyzed with a 10 % aqueous NH_4Cl solution to remove the unreacted Grignard reagent. After workup, the phosphine was isolated by crystallization from toluene in 40% yield as a white crystalline powder. In the ^1H NMR, a multiplet is observed between 7.280 and 7.241 ppm assigned to the signals of the phenyl protons. A doublet is observed at 6.84 ppm with a coupling constant of 8.80 Hz that is due to the signal of the remaining phenyl protons. A pseudo triplet is observed at 2.000 ppm which is due to the

signal of the CH_2 protons. A singlet is observed at 3.788 ppm attributable to the signal of the methyl protons. The ^{31}P NMR has a signal observed at -16.621 ppm.

3.2.3 Synthesis of 1,2-Bis[di(p-ethylphenyl)phosphino]ethane

The next member in the library of chealating phosphines is an ethyl substituted dppe derivative. This dppe derivative should have solubility properties similar to its anisyl analogue but the ethyl substituent being σ-electron donating while the methoxy group has σ-electron withdrawing and π-electron donating effects. The electronic properties of the two derivatives will be systematically different and should prove interesting.

1,2-Bis[di(*p*-ethylphenyl)phosphino]ethane was prepared using a procedure similar to the method described in the previous subchapters (3.2.1 and 3.2.2).

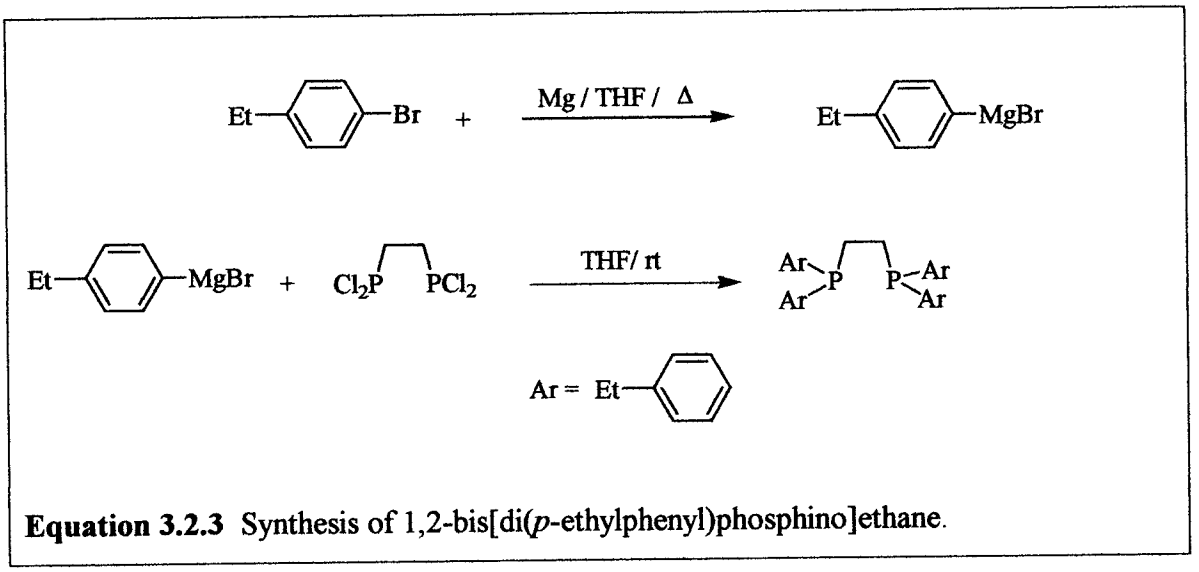

Equation 3.2.3 Synthesis of 1,2-bis[di(*p*-ethylphenyl)phosphino]ethane.

After workup, the solid was crystallized from a toluene / hexane solution to give an 82% yield of the product as a white crystalline solid. The solid is stable in air at room temperature but solutions of the compound should be kept under nitrogen to avoid decomposition. In the ^1H NMR, a multiplet between 7.271 and 7.233 ppm is observed that is due to the protons from the phenyl ring. The remaining proton signals are observed as a doublet at 7.146 ppm with a coupling constant of 8.80 Hz. A quartet at

2.626 ppm is attributable to the signal of the CH_2 protons with coupling constants of 7.60 and 15.20 Hz. At 2.062 ppm, a pseudo doublet with a ^{31}P coupling constant of 4.00 Hz. The signal of the methyl protons is observed at 1.218 ppm that is a triplet with a coupling constant of 8.00 Hz. The ^{31}P NMR has a signal observed at -14.774 ppm.

Since this reaction was completed, studies in our group have shown that the purity of the compound in Equation 3.2.3 could be significantly improved if the crystallization is initiatied with methanol instead of hexanes. Also, the reaction in Equation 3.2.3 was carried out using Aldrich 99.9% high purity magnesium and as a result gave a higher yield and a cleaner product in comparison to the reactions in Equations 3.2.1 and 3.2.2 that were completed in reagent grade magnesium and thus gave lower yields. The reagent grade magnesium apparently either did not allow complete reduction to occur on the surface of the metal, or it resulted in its partial decomposition due to the impurities as MgO or $Mg(OH)_2$. The high purity magnesium will be therefore be used in all subsequent reactions.

3.3 Dinitrogen complexes

3.3.1 Synthesis of trans-bis[bis{di(p-anisyl)phosphino}ethane]bis(dinitrogen) molybdenum(0)

The metal-diisonitrile building blocks needed for the generation of the nano-rod complexes were synthesized using Mo and W dinitrogen complexes as the precursors. The dinitrogen complexes were synthesized by two different synthetic methods. The first method utilizes liquid sodium amalgam[3] with the phosphine and $MoCl_5$ in THF. The mercury contained in the sodium amalgam mixture is not only highly toxic, but its disposal is also very tedious and expensive. The second method uses high purity (99.9 %) magnesium as discussed in the previous subchapter (3.2.3) in place of the sodium amalgam. Giving comparable yields, the latter method was determined to be the method of choice because the use of a toxic reagent is eliminated, as the clean up procedure is easier, and the disposal of the mercury is eliminated.

A series of dinitrogen complex with various substituted phosphine ligands will be discussed. The first member in this series, *trans*-bis[bis{di(*p*-anisole)

phosphino}ethane]bis(dinitrogen)molybdenum(0), was synthesized by the sodium amalgam method which is a method similar to that described by Kubas et al.[2]

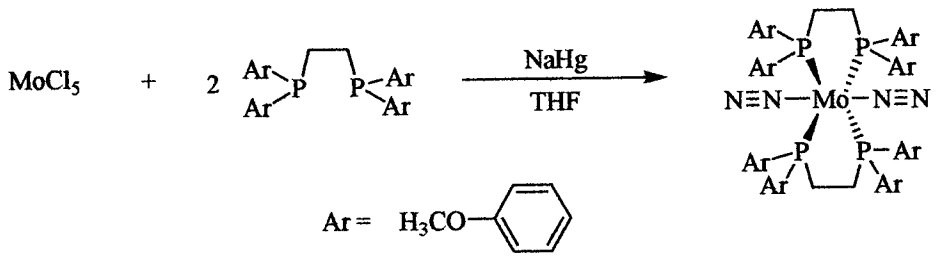

Equation 3.3.1 Synthesis of *trans*-bis[bis{di(*p*-anisyl)phosphino}ethane]bis(dinitrogen) molybdenum(0).

A THF solution of 1,2-bis(di(*p*-anisyl)phosphino)ethane was combined with NaHg and $MoCl_5$ was added to the suspension. The suspension was then stirred vigorously for 60 h under a constant pressure of nitrogen to ensure that a complete reaction occurs. After the removal of the NaHg by filtration, the solvent was removed *in vacuo* and the resulting solid was dissolved in toluene following which methanol was used to precipitate the product. A 39% yield of the product was produced as a yellow-orange powder. This powder was determined by NMR to contain approximately 20% tetrahydride (*e.g.*, $(C_{30}H_{16}O_4P_2)_2H_4Mo$) which formed as side product and could not be removed via crystallization. In the ^{13}C NMR, a signal is observed at 160.523 ppm that is due to the signal of the methoxy aryl carbon atoms. Three doublets are observed at 130.306, 134.513, and 114.558 ppm with ^{31}P coupling constants of 7.44, 11.46, and 21.12 Hz repectively. Two singlets are observed at 54.787 and 25.787 ppm that are due to the signals of the methyl and CH_2 carbon atoms. In the ^1H NMR, a multiplet is observed between 7.283 and 7.244 ppm attributable to the phenyl proton signals. A doublet is observed at 6.71 ppm with a coupling constant of 8.80 Hz that is due to the signal of the remaining phenyl protons. A singlet at 3.234 is observed for the signal of the methyl protons and the signal of the CH_2 protons with a ^{31}P coupling constant of 4.00 Hz is observed at 2.323 ppm. The ^{31}P NMR has a signal observed at 39.347 ppm. In the IR

spectrum, an asymmetric and symmetric vibration was observed at 2359 and 2336 cm^{-1} due to the dinitrogen group. The melting point was observed to be 74°C. The tetrahydride can be recognized by its characteristic quintet at ~ -5 ppm that is due to the proton signals of the hydrides.

3.3.2 Attempted Synthesis of trans-bis[bis{di(p-ethylphenyl)phosphino} ethane]bis(dinitrogen) molybdenum(0)[2]

The second dinitrogen complex in this series, *trans*-bis[bis{di(*p*-ethylphenyl) phosphino}ethane]bis(dinitrogen)molybdenum(0), was prepared by a method similar to the one in the previous subchapter (3.3.1) using the magnesium method.

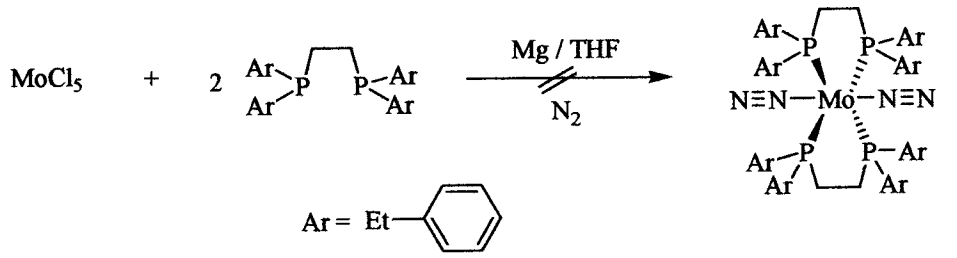

Equation 3.3.2 Synthesis of *trans*-bis[bis{di(*p*-ethylphenyl)phosphino}ethane] bis(dinitrogen)molybdenum(0).

High purity magnesium was combined with 1,2-bis(di(*p*-ethylphenyl) phosphino)ethane in THF and $MoCl_5$ was added to the suspension. The suspension was stirred for 48 h and then after workup, it was crystallized from a toluene / methanol mixture which produced a yellow solid that was determined by ^1H NMR to be the starting material 1,2-bis(di(*p*-ethylphenyl)phosphino)ethane. The reaction was repeated using new reagents and freshly degassed solvents and similar results were achieved. Since this reaction was completed, studies in our group have shown that using pure phosphine crystallized from methanol usually gave the desired product.

In summary, as stated in subchapter 3.3.1, the high purity magnesium method is the method of choice to synthesize the dinitrogen complexes due to the comparable yields

and the elimination of hazardous materials. It has also been determined by other members of our group that using pure phosphine crystallized from methanol is necessary to prepare the ethyl substituted dinitrogen complex. Furthermore, the methoxy substituted dinitrogen complex was found to be very soluble in solution, impeding its purification, but looking well for the usability of its eventual oligomer products.

In addition to the properties of the complexes already discussed, an explanation of the origins of their color should be given. The low intensity color (yellow-orange) of a dinitrogen complex can be attributed to the d-d transitions in the complex which are Laporte forbidden due to its center of inversion. The Laporte selection rule can be by passed by distortion of the complex from its precise octahedral symmetry with an asymmetrical vibration. Such a distortion can allow a Laporte forbidden d-d transition to occur which would promote an electron into an *e* orbital to create an environment in which two electrons have opposite spins. The electronic transition allows the absorbtion of light to occur resulting in a rather intense Laporte-forbidden d-d band to be detected.

3.4 Ferrocene chemistry

3.4.1 Synthesis of o-benzylhydroxylamine

The central intermediate for the synthesis of ferrocenyl isocyanide is ferrocenyl amine. As explained in the introduction, several different approaches for its synthesis have been reported in the literature. The method of Knox et al.[4] describes the synthesis of ferrocenylamine using O-benzylhydroxylamine as the precursor. O-benzylhydroxylamine hydrochloride is the starting material in the synthesis of O-benzylhydroxylamine. A literature method[4] describes the synthesis of O-benzylhydroxylamine hydrochloride using O-benzylacetoxime as the precursor. The method involves the hydrolysis of O-benzylacetoxime with concentrated hydrochloric acid to produce the product, O-benzylhydroxylamine hydrochloride. O-benzylhydroxylamine hydrochloride is commercially available and was used in this procedure to avoid the multiple step synthesis of the desired starting material.

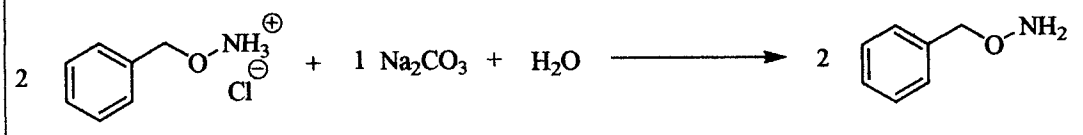

Equation 3.4.1 Synthesis of *o*-benzylhydroxylamine.

O-benzylhydroxylamine hydrochloride was deprotonated with Na_2CO_3 in an aqueous solution. After workup, the light yellow oil produced was purified by distillation to give an 83% yield of the product as a light yellow oil. A solution of the compound should be kept under nitrogen to avoid decomposition. Impurities are observed in the ^{1}HNMR which were removed by distillation. In the ^{13}C NMR, a signal is observed at 136.941 ppm that is due to the signal of the carbon atom with the CH_2 substituent. The signals at 127.700, 127.647, and 127.146 ppm are attributable to the remaining phenyl carbon atoms, while a signal at 177.088 ppm is observed for the carbon atom of the CH_2 group. In the ^{1}H NMR, a multiplet is observed between 7.45 and 7.28 ppm that is due to the signals of the phenyl carbon atoms. The amine proton signals are observed at 5.390 ppm and the signal from the CH_2 protons is observed at 4.676 ppm.

The synthesis of ferrocenylamine as described by Knox et al.[4] combines *o*-benzylhydroxylamine with lithiated ferrocene. The mixture is acidified followed by a basic extraction. The method gives only a 12-13% yield as reported in the literature. The synthesis of ferrocenylamine using *o*-benzylhydroxylamine as the starting material was attempted and a no yield was obtained.

3.4.2 Synthesis of ferrocenylamine

The alternative method described by Knox et al.[4] was the most convenient method found to synthesize ferrocenylamine until a new method described by Leusen et al.[5] using α-azidostyrene[6] as the starting material proved to be more successful.

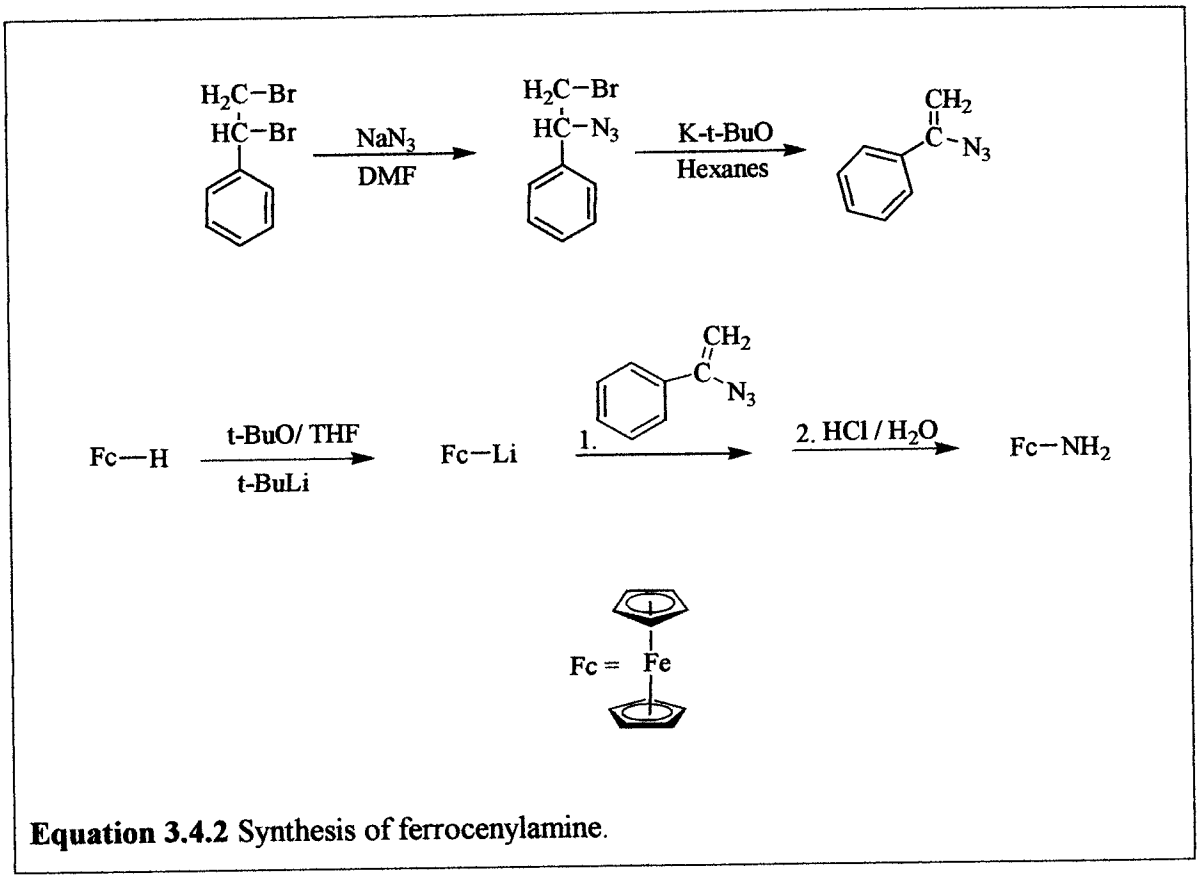

Equation 3.4.2 Synthesis of ferrocenylamine.

Changes to the procedure in our hands included the use of toluene in place of benzene to avoid the use of this carcinogen. In the first step, 1,2-dibromo-1-phenyl ethane and sodium azide were reacted in dimethylformamide. Extraction with hexanes followed by the addition of toluene and potassium *tert*-butoxide produced α-azidostyrene as a crude product. Purification by column chromatography produced a 74% yield of the vinyl azide product as a yellow solid. In the ^{1}H NMR, a multiplet is observed between 8.90 and 7.20 ppm attributable to the proton signals of the phenyl ring. Two CH_2 proton signals are observed at 5.553 and 5.076 ppm.

In the synthesis of ferrocenylamine using the method described by Leusen et al.[5], lithiated ferrocene was reacted with α-azidostyrene. Acidification of the mixture with HCl followed by hydrolysis and the precipitation with a base afforded a red oil which was purified by sublimation to give a 9% yield (0.780 g, 0.386 mmol) of the product as a dark red oil. The literature describes the compound as a red solid. The compound could not be purified by sublimation. Further purification techniques were not attempted due to the low yield. Column chromatography could possibly be used in future reactions to remove the impurities in the compound. In the ^{1}H NMR, a mixture of the *cis* and *trans* isomers are present. The signals observed at 4.150, 3.983, 3.915, 3.831, and 3.740 ppm are attributable to the proton signals of the Cp ring. Two signals are observed at 2.216 and 2.331 ppm that are due to the protons of the amine group.

3.4.3 Synthesis of ferrocenylamine (Gabriel method)

The most reliable route for the synthesis of ferrocenylamine (Equation 3.4.3) was the Gabriel synthesis as described by Bildstein et al.[7]

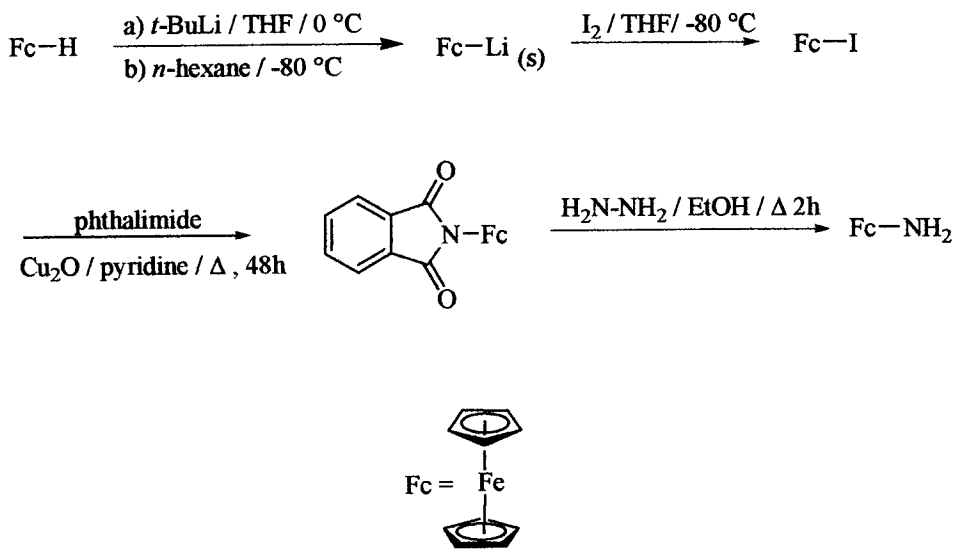

Equation 3.4.3 Synthesis of ferrocenylamine.

In the first step, ferrocene was metallated with tert-butyllithium in THF. The main advantage of this procedure is the selective monometalation of the ferrocene. A 92% yield of the product was produced as a yellowish pyrophoric powder. Due to the pyrophoric nature of the material, no spectroscopic data were recorded.

Lithioferrocene is a very sensitive material and was thus never stored but was always directly converted into iodoferrocene by reaction with iodine in THF. The iodo product was isolated as orange-brown oil in 70% yield. The oil solidified upon standing at 4 °C. In the ^{1}H NMR, a singlet is observed at 4.192 ppm attributable to the signal of the hydrogen atoms at the unsubstituted Cp ring. The substituted Cp ring exhibits two doublets of doublets with coupling constants of 2.40 and 1.60 Hz at 4.412 and 4.154 ppm, respectively.

Starting from iodoferrocene, N-ferrocenylphthalimide was then synthesized by a copper (I) oxide catalyzed coupling reaction with phthalimide in refluxing pyridine. After workup, the product was isolated as dark red crystals in a 28% yield. In the ^{13}C NMR spectrum of N-ferrocenyl phthalimide a peak is observed at 166.806 ppm attributable to the carbonyl carbon atoms. Two singlets are observed at 134.016 and 123.079 ppm which

are due to two phenyl carbon atoms. The signals observed at 88.570, 69.508, 65.537, and 62.935 ppm are attributable to the Cp carbon atoms. The ^{1}H NMR of the N-ferrocenyl phthalimide exhibits two multiplets at 7.897 and 7.760 ppm caused by the phenyl protons. Three proton signals are observed for the Cp rings. One of the signals at 4.226 ppm is a singlet that is due to the protons of the unsubstituted Cp ring. The other two proton signals are observed as doublets of doublets at 5.009 and 4.208 ppm and are due to the protons of the substituted Cp ring with coupling constants of 2 × 2.00 Hz.

Finally, ferrocenylamine was synthesized by treatment of N-ferrocenyl phthalimide with hydrazine in a Gabriel type reaction. The product was isolated in a 97 % yield as a yellow solid. The product was stable in air for short periods of time, but solutions should be kept under nitrogen to avoid decomposition. The ^{1}H NMR of ferrocenylamine exhibits a singlet at 4.099 ppm due to the proton signal of the unsubstituted Cp ring. The signals observed at 3.994 and 3.842 ppm are due to the proton signals of the substituted Cp ring. The amine hydrogen atoms cause the singlet at 2.588 ppm. The overall yield of ferrocenylamine is very high and consistant at approximately 90 % as compared to the 9 % yield obtained from the azide reaction.

3.4.4 X-Ray structural analysis of ferrocenylamine

Despite the general interest ferrocenylamine has attracted as a versatile starting material for a manifold of organometallic compounds, its solid-state structure has not been reported previously. Thus, attempts were made to grow single crystals of this important organometallic building block. By slowly cooling a saturated etheral solution down to 4 °C, X-ray quality crystals were produced and the structure was determined by single crystal X-ray structural analysis at 90 K. It was found to crystallize in the tetragonal space group $I4_1/a$ with a = 23.5540(15), b = 5.8964(8) Å and Z = 16. A molecular representation of the structure is shown in Figure 3.2.

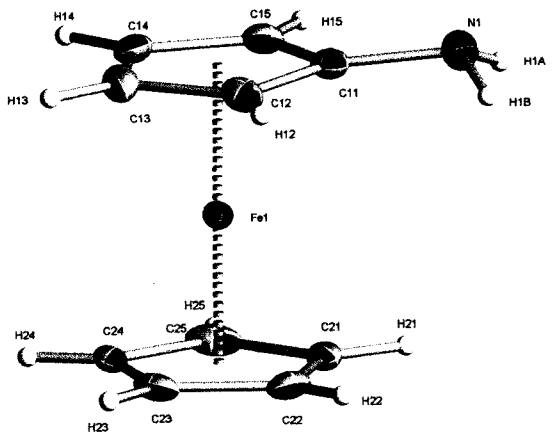

Figure 3.2 ORTEP representation of ferrocenylamine. Ellipsoids are drawn at 50% probability.

The ferrocenyl part of the molecule is unexceptional displaying the expected sandwich structure. Thus, the η^5-cyclopentadienyl rings show no significant deviation from planarity, conventional iron to ring centroid distances of 1.6564(11) and 1.6564(11) Å are observed, and the two cyclopentadienyl rings deviate by only 10.5(2.9)° from an ideal staggered conformation.

The average angle around the nitrogen atom is 112(2)° making the geometry slightly distorted from the ideal sp^3 geometry with the amine hydrogen atoms pointing below the plane of the cyclopentadienyl ring. Thus, the lone pair on the nitrogen atom is in an orientation to allow interaction with the π-electron density of the adjacent aromatic ring. Consequently, an influence on the C-C bond distances due to delocalization of the free electron pair into the π* orbital might be expected. However, the average C-C bond distances of the two cyclopentadienyl rings, which are 1.415(3) Å for the amine substituted and 1.423(4) Å for the unsubstituted rings, do not differ significantly.

One of the two amine hydrogen atoms is hydrogen bonded to the nitrogen atom of a neighboring molecule, forming a N-H···N hydrogen bridge. The hydrogen acceptor

amine group then itself acts as a hydrogen bond donor, thus extending the hydrogen bridges to give infinite chains. (Figure 3.3)

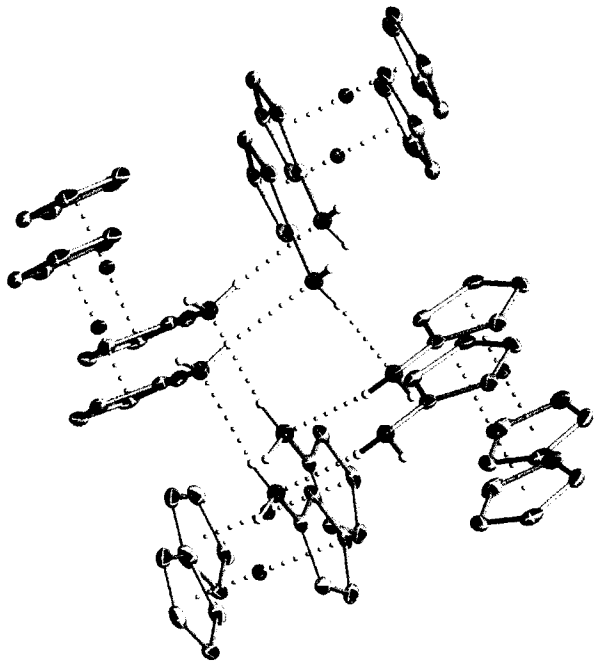

Figure 3.3 Representation of the helical chain formed by the hydrogen bridges. The ferrocenyl hydrogen atoms are omitted for clarity.

Due to the uncertainty of the hydrogen positions, the values for the N-H and H···N distances, which are 0.85(3) and 2.414(35) Å, respectively, will not be discussed in detail. The more reliable N(donor)-N(acceptor) distance of 3.249(3) Å is consistent with a weak to moderate interaction.[8] Thus, the bond energy associated with the N-H···N can be roughly estimated to be less than 5 kcal mol^{-1}. As expected for hydrogen bonds, the H-bonding interactions in ferrocenyl amine are directionally significant. Thus, the angle of the two hydrogen bonds originating at each nitrogen atom is near to 90° and by cooperation of the individual hydrogen bonds a helical chain with four-fold symmetry results. A hydrogen-bonded spiral is propagating along the crystallographic four fold screw axis in the direction of the c-axis of the unit cell.

Only four other cyclopentadienyl amine compounds have been structurally characterized to date,[9] and, of those, only 1,1'-bisferrocenylamine exhibits N-H···N hydrogen bridges. This molecule is electronically and sterically very similar to ferrocenyl amine, but both of its amine groups can act as donors for hydrogen bonding and the two ferrocenylamine rings can be rotated with regard to each other. A multitude of different N-H···N interactions thus becomes possible and no cooperation of the individual hydrogen bonds to form a regular network such as is observed for ferrocenyl amine might be expected. Instead, 1,1'-bisferrocenylamine forms a complicated irregular network of hydrogen bonds ranging from 2.325 up to 2.619 Å in length. Two independent molecules are found in its unit cell and the amine groups seem to be oriented in such a way as to allow for the maximum number of hydrogen bonds possible in the solid state. The carbon atoms in the Cp rings of both molecules are basically eclipsed. The amine groups in one of the molecules are located on eclipsed carbon atoms, those in the other molecules are rotated by one fifths of the Cp ring. The hydrogen atoms of three of the four amine groups are pointing below the planes of the cyclopentadienyl rings, while those of the forth one are located atop the Cp ring. All of the crystal data are summarized in Appendix 2.

3.4.5 Synthesis of Isocyanoferrocene

Several synthetic methods have been reported for the synthesis of isocyanides as discussed in the introduction. The method for the synthesis of isocyanoferrocene is similar to the method described in Chapter 3.1

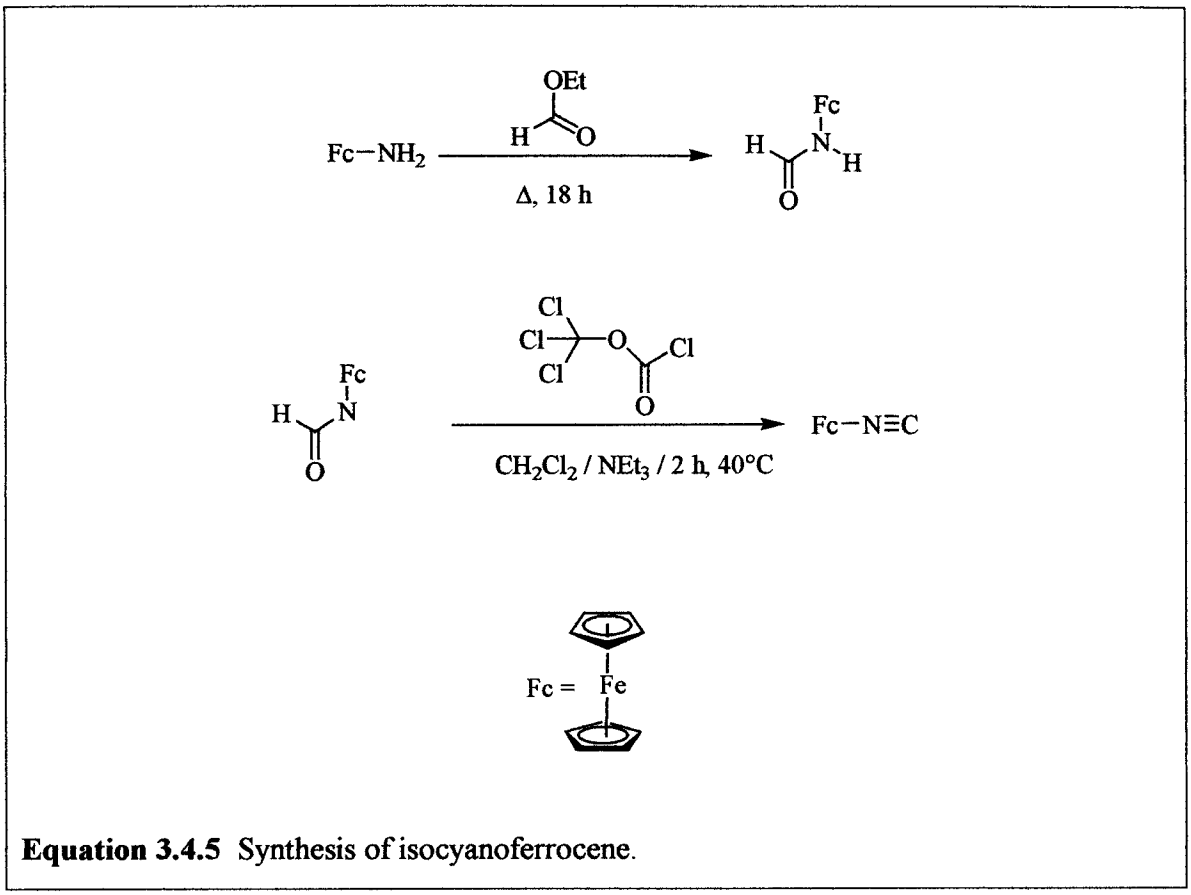

Equation 3.4.5 Synthesis of isocyanoferrocene.

In the first step, the condensation reaction of ferrocenylamine with ethyl formate produced a 76% yield of ferrocenylformamide as a dark orange solid. The solid is stable in air and solution. As discussed in the introduction, due to the *cis-trans* isomerism and a monomer-dimer equilibrium three isomers are present in toluene solutions of formylferrocenylamine. In the ^{1}H NMR, only two singlets of equal intensity are observed in the aldehyde and N-H region at 8.309 and 7.817 ppm, respectively. Thus, it has to be assumed that some of the signals are broadened out by exchange processes. In the Cp-H region three sets of proton signals are observed with an intensity ratio of approximately 1: 0.9: 2. The Cp-H proton signals with an intensity ratio of 1 consist of a singlet at 4.061 ppm and two doublets of doublets at 4.575 and 3.789 ppm with coupling constants of 4.00 Hz, are attributable to the unsubstituted and substituted Cp rings, respectively. The set with an intensity ratio of 0.9 shows one singlet at 4.002 ppm for the unsubstituted Cp ring and two doublets of doublets at 3.906 and 3.695 ppm for the substituted rings with coupling constants of 4.00 Hz, respectively. The final set with the intensity ratio of 2

exhibits a singlet at 3.985 ppm which is due to the unsubstituted Cp-H proton signal. Two doublets of doublets from the substituted Cp ring are found at 3.731 and 3.712 ppm with coupling constants of 3.60 Hz. The literature values reported by Knox et al.[4] differ slightly from those observed here. This can be attributed to the use of different solvents and different concentrations which would be expected to affect the equilibria between the three isomers.

Some impurities observable in the NMR spectra could not be removed by recrystallization. The melting point of the compound was observed at 62 °C which is about 10 °C degrees lower than that reported in the literature. The temperature difference seen between the literature value and the experimental value is consistent with the impurities that are seen in the NMR spectra.

The formamide was then converted into the isocyanide as shown in Equation 3.4.5. The crude solid was purified by sublimation to give a 77% yield of the product as a dark orange solid. The product was stable in air for short periods of time but solutions should be kept under nitrogen to avoid decomposition. In the ^{13}C NMR, a triplet is observed at 167.04 and 7.95 ppm with ^{14}N coupling constants of 5.23 and 15.29 Hz, respectively. Additional singlets are observed at 70.938, 70.764 and 66.860 ppm attributable to Cp carbon atoms. In the ^{1}H NMR, two doublets of a doublet are observed at 4.089 and 3.545 ppm, with coupling constants of 2 × 2.00 Hz. A singlet is observed at 3.900 ppm, is due to the proton signal of the unsubstituted Cp ring. In the IR spectrum, a vibration was observed at 2122 cm^{-1} due to the isonitrile group. The melting point of the compound was observed to be 48 °C which is in agreement with the value reported by Knox et al.[10]

3.4.6 Synthesis of para-ferrocenylaniline

Para-nitrophenylferrocene is the starting material for the synthesis of *para*-ferrocenylaniline. The synthesis is similar to a method described by Hu et al.[11]

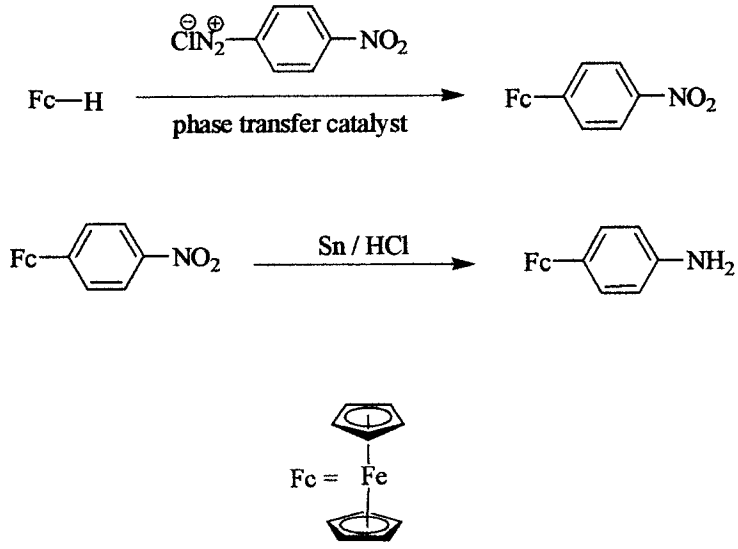

Equation 3.4.6 Synthesis of *para*-ferrocenylaniline.

In the first step of the reaction, ferrocene was arylated with the appropriate diazonium salt under phase transfer conditions. After workup, crystallization from hexanes, and then further purification by sublimation, a 55% yield of the nitro complex was produced as dark purple crystals. This solid is stable in air and solution. In the ^{1}H NMR spectrum of *para*-nitrophenylferrocene, two doublets are observed at 8.513 and 7.668 ppm attributable to the phenyl proton signals. The observed coupling constant is 8.80 Hz. The substituted Cp ring exhibits two signals, which are doublets of doublets at 4.472 and 4.475 ppm with coupling constants of 2 × 5.20 and 2 × 4.40 Hz, respectively. The proton signal of the unsubstituted Cp ring appears as a singlet at 4.068 ppm.

In the second step of the reaction, *para*-nitrophenylferrocene was reduced to the amine with tin under acidic conditions. A solution of NaOH was then added to the suspension to give a pH of 14. After workup, a 93% yield of the product was produced as a dark orange solid. The solid is stable in air and solution. The ^{1}H NMR spectrum of

para-nitrophenylferrocene reveals the phenyl proton signals as doublets at 7.303 and 6.651 ppm with a coupling constant of 8.40 Hz. Two multiplets are observed at 4.552 and 4.249 ppm that are due to the signals of the substituted Cp ring. The unsubstituted ring exhibits a singlet at 4.405 ppm. The amine signal is observed at as a broad singlet at 3.620 ppm.

3.4.7 Synthesis of para-isocyanoferrocenylbenzene

The *para*-ferrocenylaniline was then converted into the isocyanide by the same method described in subchapter 3.4.5.

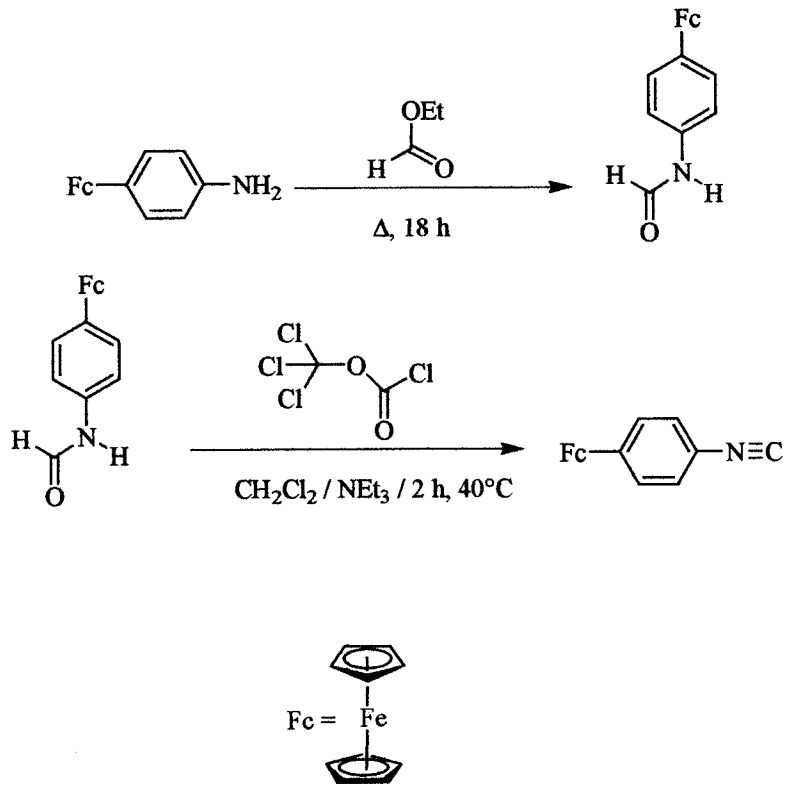

Equation 3.4.7 Synthesis of *para*-isocyanoferrocenylbenzene.

The final *para*-isocyanoferrocenylbenzene product was isolated as a dark orange solid in a 28 % yield from *n*-formylferrocenylaniline. The solid is air stable at room

temperature for short periods of time, however, the product should be kept under nitrogen in solution to avoid decomposition. In the ^{1}H NMR spectrum, two doublets are found at 6.939 and 6.806 ppm, that are due to the phenyl proton signals with coupling constants of 8.40 Hz. The substituted Cp ring results in two proton signals at 4.282 and 4.085 ppm that are doublets of doublets with coupling constants of 2 × 2.00 and 2 × 1.60 Hz, respectively. A singlet is observed at 3.801 ppm that is due to the proton signals of the unsubstituted Cp ring. In the IR spectrum, a vibration is observed at 2120 cm^{-1} due to the isonitrile stretching mode. The melting point was observed at 84 °C.

3.5 Nickel complexes

3.5.1 Synthesis of tetrakis(para-methoxyisocyanobenzene)nickel(0)

Ni(0) complexes are important for our project because they are expected to have tetrahedral geometries. We decided to use substituded isonitrile ligands for our research for the reasons discussed in the introduction. This will allow a library of the nickel(0) complexes to be made with a range of properties.

The first complex in this library is tetrakis(*para*-methoxyisocyanobenzene) nickel(0) which was synthesized by a method similar to that reported by Ittell et al.[12]

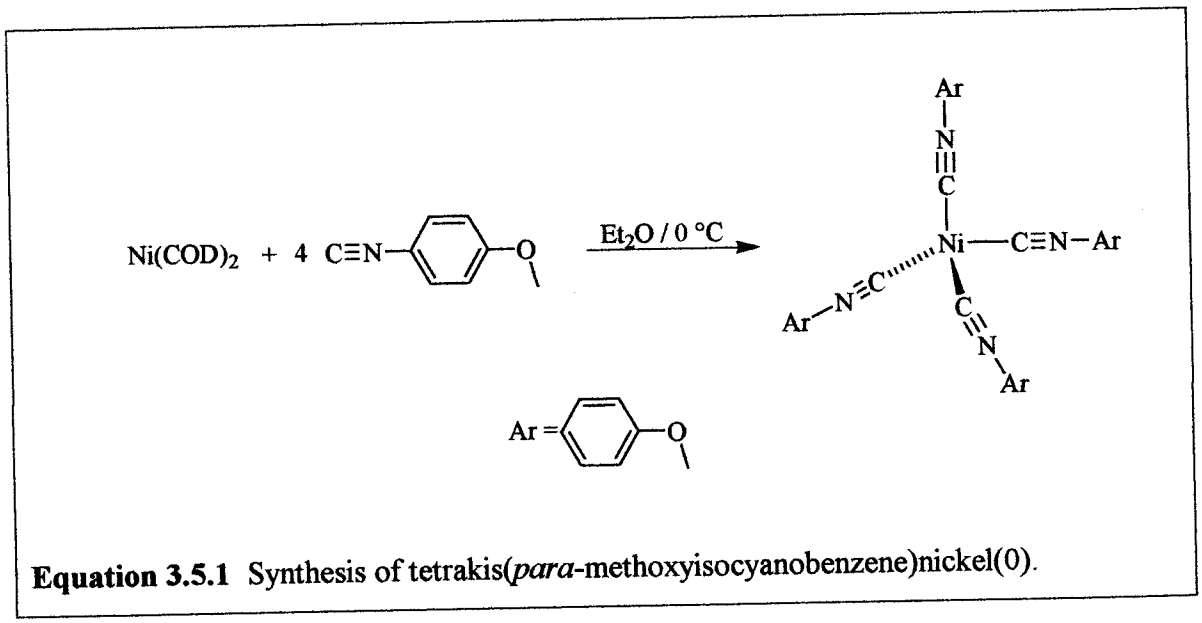

Equation 3.5.1 Synthesis of tetrakis(*para*-methoxyisocyanobenzene)nickel(0).

Bis(1,5-cyclooctadiene)nickel(0) was combined with *para*-methoxyisocyanobenzene in an ether solution and the mixture was stirred for 2 h. An 87% yield of the product was collected by filtration as a crude yellow solid and purified by crystallization from THF.

In the ^{13}C NMR, a signal is observed at 165.373 ppm which is due to the isonitrile carbons with a ^{14}N coupling constant of 4.73 Hz. The signals at 157.770, 126.653, 123.371, and 114.146 ppm are attributable to the carbon atoms of the phenyl rings. A signal is also observed at 55.473 ppm which is due to the carbon atoms of the methyl groups. In the ^{1}H NMR, two doublets are observed at 6.982 and 6.337 ppm with coupling constants of 8.40 Hz. A singlet is observed at 3.034 ppm that is due to the protons of the methyl groups. In the IR spectrum, a vibration was observed at 2017 cm^{-1} due to the isonitrile group. The melting point of the compound was observed to be 98 °C.

3.5.2 X-Ray structure analysis of Tetrakis(para-methoxyisocyanobenzene)nickel(0)

In the course of this work, the first tetrahedral nickel (0) complex isoelectronic to NiO_4 was structurally characterized. The complex crystallizes in the orthorhombic space group $P2_12_12_1$ with 4 molecules in the unit cell. The aromatic hydrogen atoms were taken from a difference Fourier calculation and the methyl hydrogen atoms were placed at calculated positions. All hydrogen atoms were isotropically refined. The crystal data are summarized in Appendix 3. What is interesting about this complex is that the environment around the nickel center varies from the standard tetrahedral angles of 109.5° (Figure 3.4). Table 3.2 lists the angles which are of immense interest in the complex.

Table 3.2 Selected bond lengths (Å) and angles (°) of tetrakis(*para*-methoxy isocyanobenzene)nickel(0).
C41–Ni1–C31 103.28 (10)
C41–Ni1–C11 114.3728 (10)
C31–Ni1–C11 109.66 (9)
C41–Ni1–C21 114.25 (10)
C31–Ni1–C21 112.24 (10)
C11–Ni1–C21 103.26 (10)
Ni1-C_x 1.846 (2) (Avg.)
C_x-N_x 1.174 (3) (Avg.)
N_x-$C_{(aryl)}$ 1.394 (3) (Avg.)

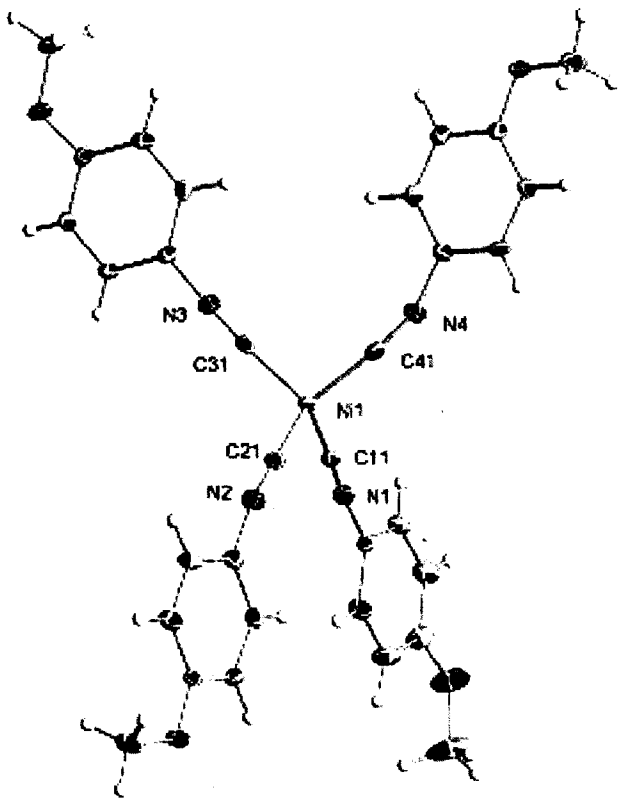

Figure 3.4 ORTEP plot of tetrakis(*para*-methoxyisocyanobenzene)nickel(0).

3.5.3 Synthesis of tetrakis(isocyanoferrocene)nickel(0)

The next two complexes in this library contain ferrocene units that were linked to the nickel center. The synthesis of tetrakis(isocyanoferrocene)nickel(0) was attempted by a method similar to that described in the previous subchapter (3.5.1).

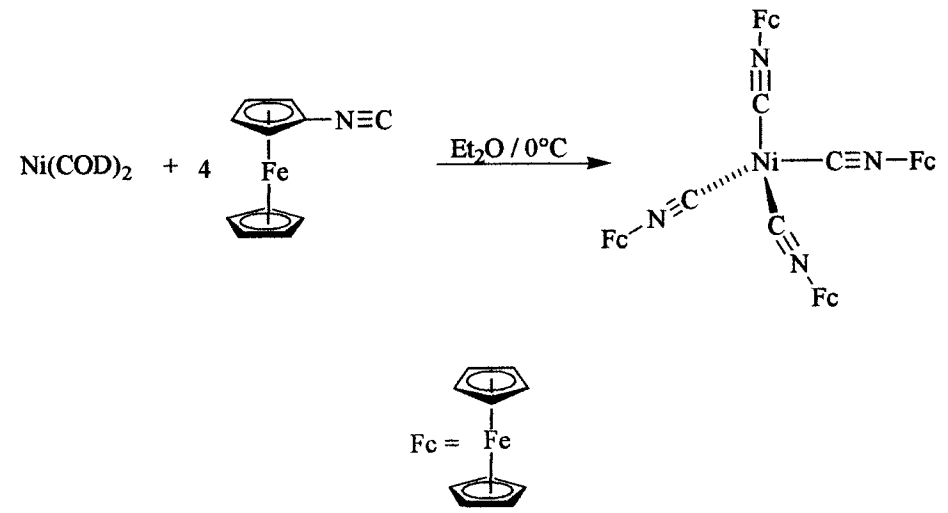

Equation 3.5.3 Synthesis of tetrakis(isocyanoferrocene)nickel(0).

An 81% yield of the penta metallic product was produced as a crude dark orange powder. Attempts to recrystallize the solid from a CH_2Cl_2 / hexanes solution at -19 °C proved to be unsuccessful. A dark blue solution resulted when the product was stored at -19 °C for approximately 24 h. It is presumed that oxidation of the product occurred by O_2 when it was dissolved in CH_2Cl_2; CH_2Cl_2 was the only solvent that would dissolve the product. Attempts to dissolve the product in other organic solvents (*e.g.*, THF and toluene) were unsuccessful. The product has not been isolated at this time. Further attempts to recrystallize the product are under way. In the IR spectra of the crude product, a vibration was observed at 2122 cm^{-1}, attributable to the stretching vibration of the isonitrile group.

3.5.4 Synthesis of tetrakis(para-isocyanoferrocenylbenzene)nickel(0)

This specific compound was prepared to increase the solubility of the previous nickel complex (subchapter 3.5.2) in organic solvents via the addition of the phenyl ring. Tetrakis(*para*-isocyanoferrocenylbenzene)nickel(0) was prepared by the same method as the other nickel complexes described in Chapter 3.5.

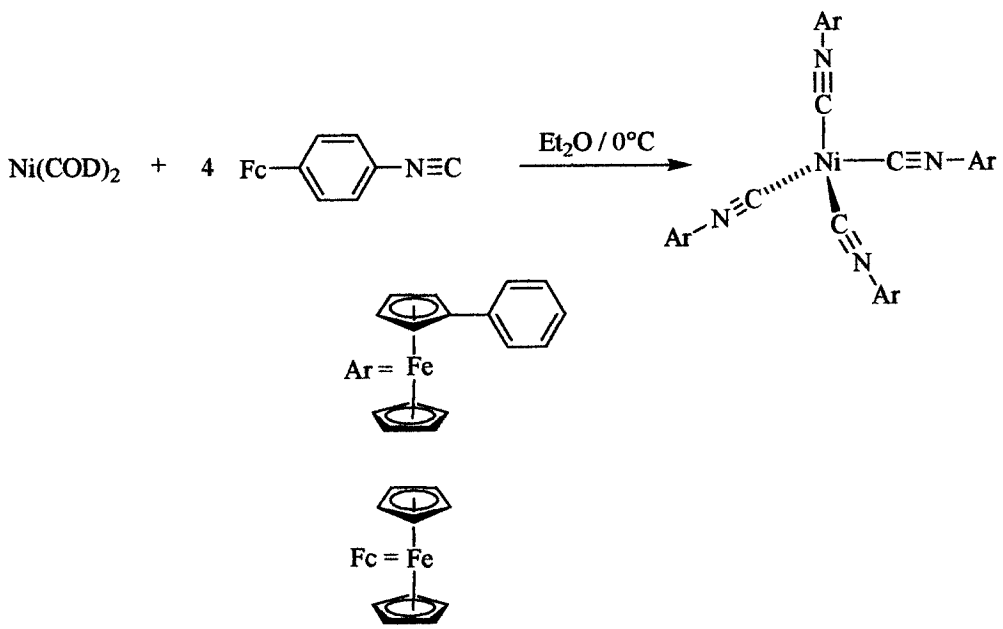

Equation 3.5.4 Synthesis of tetrakis(*para*-isocyanoferrocenylbenzene)nickel(0).

The product did not precipitate out of solution. Therefore, the dark orange solution was concentrated *in vacuo*, layered with hexanes, and was placed at -19 °C for crystallization. The product has not been isolated at this time. Recrystallization with other organic solvents are currently under way.

3.5.5 Synthesis of tetrakis(para-nitro-isocyanobenzene)nickel(0)

To add to the various nickel complexes used in this series, an attempt was made to synthesize tetrakis(*para*-nitro-isocyanobenzene)nickel(0). The synthetic method was thus duplicated from Chapter 3.5.

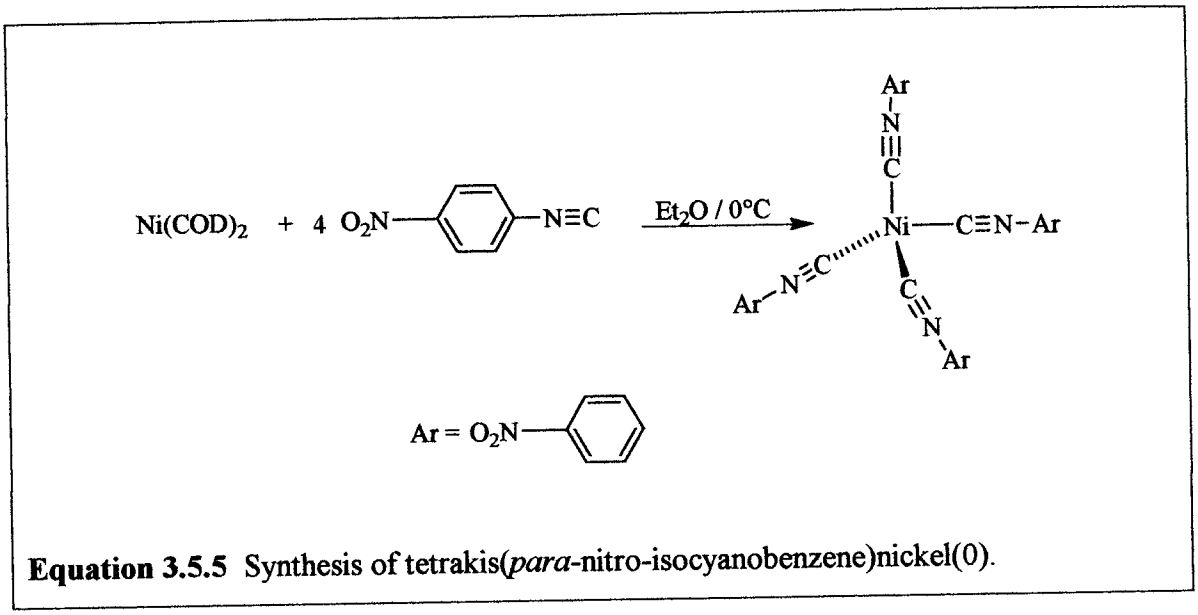

Equation 3.5.5 Synthesis of tetrakis(*para*-nitro-isocyanobenzene)nickel(0).

Attempts to crystallize the crude dark red solid from a THF / hexanes solution at -19 °C were not successful. Recrystallization attempts are currently under way with other organic solvents.

In reference to the nickel complexes, the crystallization of the methoxy derivative proved to be the most successful. Recrystallization attempts of the remaining compounds are currently in progress in varied solvents. It is hoped that the correct solvent mixtures will thus be established.

3.6 Nanorod building blocks

3.6.1 Synthesis of bis[bis{di(p-ethylphenyl)phosphino}benzene]bis(ferrocenyl-isocyanide)molybdenum(0)

A molybdenum dinitrogen complex[13] combined with two equivalents of isocyanoferrocene gave the first complex in the library of capped nanorod building blocks. The reaction scheme of bis[bis{di(*p*-ethylphenyl)phosphino}benzene]bis (isocyanoferrocene)molybdenum is shown in Equation 3.6.1.

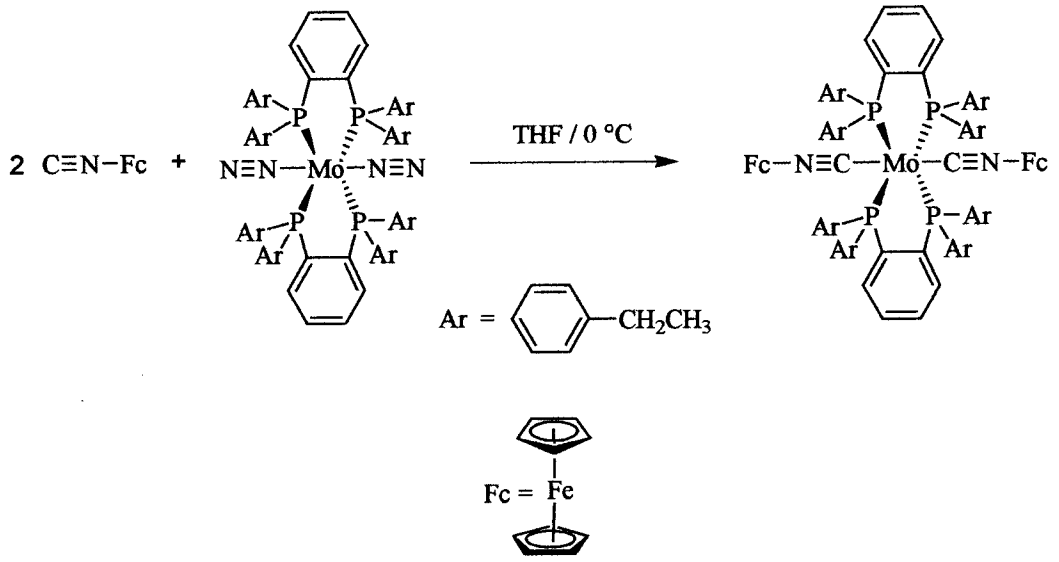

Equation 3.6.1 Synthesis of bis[bis{di(*p*-ethylbenzene)phosphino}benzene]bis (isocyanoferrocene)molybdenum(0).

Two equivalents of isocyanoferrocene were combined with the dinitrogen complex in a THF solution and the suspension was stirred for 30 minutes. The resulting solid was crystallized at -19°C from a THF / hexanes solution to give a crude dark orange solid. The dark orange solid was then recrystallized from a toluene / hexanes solution at -19°C to produce a 20% yield of the trimetallic product as dark orange fibrous crystals. The crystals are fairly stable in air at room temperature.

In the ^{1}H NMR, a broad signal is observed at 7.799 which is due to the eight protons of the phenyl rings bridging the phosphorus atoms. The signals at 7.304 and 6.987 with coupling constants of 7.20 and 8.00 Hz are attributable to the protons from the remaining phenyl rings. Two broad signals are observed at 4.065 and 3.774 ppm that are due to the protons from the substituted Cp ring. The broad signal observed at 3.921 ppm is due to the protons from the unsubstituted Cp ring. A quartet is observed due to the protons of the CH_2 groups at 2.500 ppm with coupling constants of 7.60 and 15.00 Hz. A signal is observed at 1.154 ppm that is a triplet with a coupling constant of 7.60 Hz attributable to the protons of the methyl group. In the IR spectrum, a vibration was observed at 2122 cm^{-1} due to the isonitrile group. The melting point of the compound was observed to be 104 °C. An X-ray structure of the product was not successful due to the fibrous morphology of the crystal.

3.6.2 Synthesis of Bis[bis{di(p-ethylphenyl)phosphino}benzene]bis(isocyano-ferrocenylbenzene)molybdenum(0)

Bis[bis{di(*p*-ethylphenyl)phosphino}benzene]bis(isocyanoferrocenylbenzene) molybdenum(0) was prepared as a benzene derivative of the complex in the previous subchapter 3.6.1. The reaction scheme is thus shown below (Equation 4.6.2)

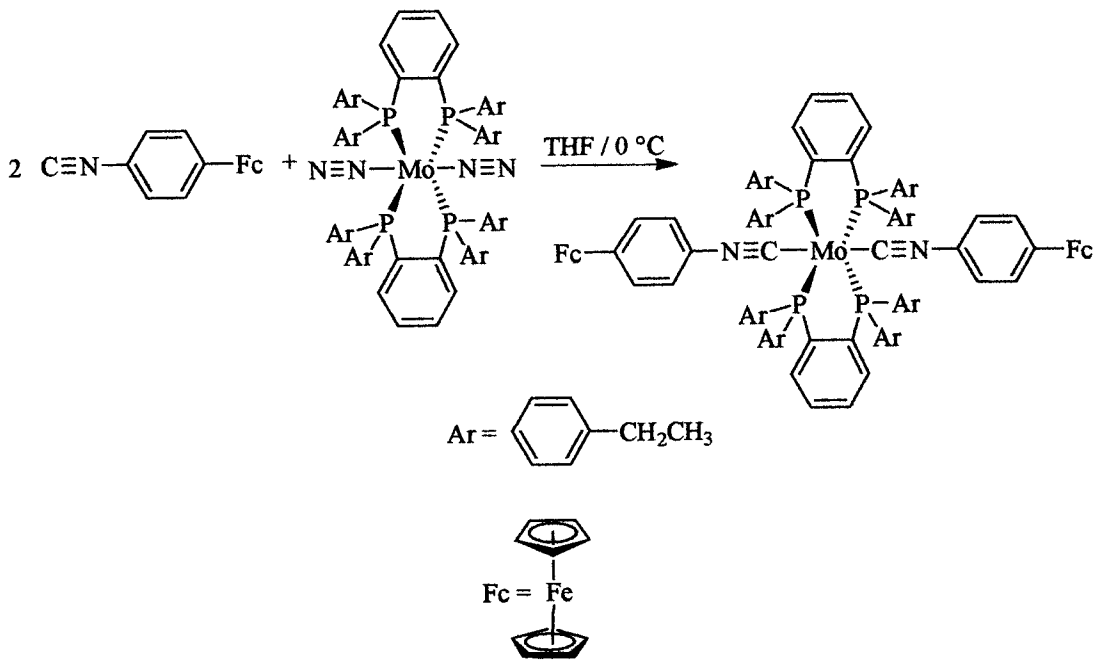

Equation 3.6.2 Synthesis of bis[bis{di(*p*-ethylphenyl)phosphino}benzene]bis (isocyanoferrocenylbenzene)molybdenum(0).

Recrystallization from a toluene / hexane mixture at -19°C produced an 81% yield of the product as a dark purple crystalline material. The solid seems stable in air at room temperature for short periods of time.

In the ^{1}H NMR, a broad signal is observed at 7.802 ppm that is due to eight protons of the phenyl ring bridging the phosphorus atoms. The remaining phenyl rings attached to the phosphorous atoms have signals observed at 7.371, and 6.881 ppm which are doublets with couplings constants of 7.60 Hz, and 8.00 Hz respectively. The phenyl ring attached to the ferrocene has a broad signal at 6.079 ppm. A broad signal is observed for the protons of the unsubstituted Cp ring at 4.078 ppm. The substituted Cp rings have two broad proton signals at 4.405 and 3.905 ppm. A quartet is observed for the protons of the CH_2 group at 2.446 ppm with coupling constants of 7.60 and 15.20 Hz. The methyl group has a signal at 1.093 which is a triplet with a coupling constant of 7.20 Hz. In the IR spectrum, a vibration was observed at 1877cm^{-1} due to the isonitrile group.

The melting point of the compound was observed to be 225 °C. An X-ray structure of the product was not successful due to the thin crystal morphology.

These complexes (Chapter 4.6) not only possess the Laporte forbidden d-d transitions as discussed in Chapter 3.3, but also a metal-to-ligand charge-transfer transition (MLCT transition) where an electron makes a transition from a *d* orbital of the central metal atom (*e.g.*, Mo) into a π^* orbital of the isonitrile ligand. The MLCT transitions occur with ligands that have low lying π^* orbitals, including aromatic ligands, and are responsible for color changes in these type of complexes.

References

1. M. Hanack, S. Kamenzin, C. Kamenzin, L. R. Subramonian, *Synthetic Metals* **2000**, *110*, 93-103.
2. G. J. Kubas, C. J. Burns, J. Eckert, S. W. Johnson, A. C. Larson, P. J. Vergamini, C. J. Unkefer, G. R. K. Khalsa, S. A. Jackson, O. Eisenstein, *J. Am. Chem. Soc.* **1993**, *115*, 569-581.
3. ADH Chemistry Experiment Papers: Hunter, A. D.: "Solid Sodium Amalgam," in *Inorganic Experiments, 2nd Edition*, J. D. Woollins Ed., VCH: New York, 2003; pp 211.
4. G. R. Knox, P. L. Pauson, D. Willison, *Organometallics* **1990**, *9*, 301-306.
5. D. Van Leusen, B. Hessen, *Organometallics* **2001**, *20*, 224-226.
6. G. Smolinsky, *J. Am. Chem. Soc.* **1962**, *27*, 3557.
7. B. Bildstein, M. Malaun, H. Kopacka, K. Wurst, M. Mitterbock, K. H. Ongania, G. Opromolla, P. Zanello, *Organometallics* **1999**, *18*, 4323-4336.
8. G. A. Jeffrey *An Introduction to Hydrogen Bonding*, Oxford University Press: Oxford, 1997.
9. a) Y. Takaki,; Y. Sasada, *J. Nitta Phys. Soc. Jpn* **1959**, *14*, 771. b) R. D. Rogers, R Shakir, J. L. Atwood, D. W. Macomber, Y.-P. Wang, M. D. Rausch, *J. Chrystallogr. Spectrosc. Res.* **1988**, *18*, 767. c) K. Sunkel, U. Birk, S. Soheili, C. Stramm, R. J. Teuber, *Organomet. Chem.* **2000**, *599*, 247. d) A. Shafir, M. P. Power, G. D. Whitener, J. Arnold, *Organometallics* **2000**, *19*, 3978.
10. G. R. Knox, P. L. Pauson, D. Willison, *Organometallics* **1990**, *9*, 301-306.
11. P. Hu, K. Quing Zhao, H. Bo Xu, *Molecules* **2001**, *6*, M249.
12. S. D. Ittel, "Complexes of Nickel (0)," in *Inorg. Synth.*, R.J. Angelici, Ed., Wiley: New York, 1990; Vol 28, pp 98-99.
13. J. B. Updegraff III, The Synthesis of Organometallic Nanorods from Molybdenum and Tungsten Diisonitrile Complexes and a New Method to Synthesize Air Stable Sodium Cyclopentadienide, Master of Science, Youngstown State University, August 2004.

Chapter Four-Tricarbonyl Chromium Complexes

Section One

Introduction

The chemistry of η^6-benzenechromiumtricarbonyl, $(\eta^6\text{-}C_6H_6)Cr(CO)_3$, and its derivatives continues to be of immense interest. In our research, we are trying to synthesize low molecular weight complexes with structures similar to repeating units of organometallic polymers.[1] A series of complexes were prepared with varied substituents, *e.g.* $(\eta^6\text{-}C_5H_5)Fe(CO)_2$, Fp, groups σ-bonded to arene rings, and $Cr(CO)_3$ centers π-bonded to these rings.[1a,2] The structural, spectroscopic, and electrochemical data of these complexes will be compared to the conventional $(\eta^6\text{-arene})Cr(CO)_3$ complexes with main group substituents. The properties of the $(\eta^6\text{-}C_6H_6)Cr(CO)_3$ complex will be measured and used as a standard for the substituted arenes.

The structural and electrochemical data of the standard $(\eta^6\text{-}C_6H_6)Cr(CO)_3$ complex was studied and the results were thus reported. Through X-ray characterization, it was established that the benzene ring is planar and the chromium tricarbonyl center is π-bonded to the benzene ring to give a 3-D tripod.[3]

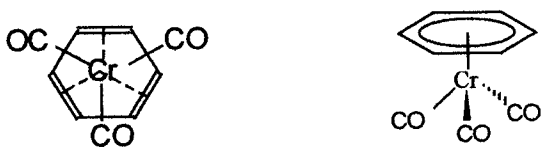

Figure 4.1.1 Three-dimensional tripod of $(\eta^6\text{-}C_6H_6)Cr(CO)_3$.

It has been reported that the chromium atom in the center of the complex contains a partial positive charge because of the carbonyl groups electron withdrawing effect.
It has also been determined that the standard complex has a dipole moment from the benzene ring to the tripod.[4] In the substituted arene complexes, the significance of π-

symmetry interactions has been proven to provide diverse alterations in the reactivity[5], spectroscopic properties[6], bonding[7], and structures[8] of these species that can be utilized to identify and enumerate these interactions.[3c]

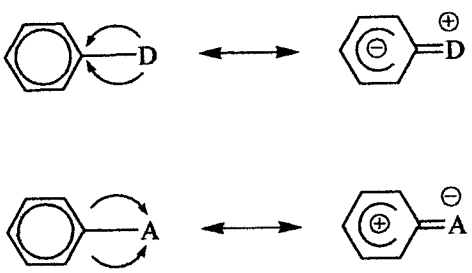

Figure 4.1.2 π-Symmetry interactions of substituted (η^6-arene)$Cr(CO)_3$ complexes (where D = a π-donor substituent, *e.g.* NMe, and A = a π acceptor substituent, *e.g.* NO_2).

The interaction between an arene and a substituent has been a vital subject matter in physical organic chemistry. As an example, it has been observed that an arene in a substituted (η^6-arene)$Cr(CO)_3$ complex, *e.g.* (η^6-1,3,5-$C_6H_3Fp_3$)$Cr(CO)_3$, Fp = (η^6-C_5H_5)$Fe(CO)_2$[9], is very nonplanar. The arene was also found to exhibit a crown like geometry where the Fp groups and the carbon atoms to which they are attached being bent significantly away from the $Cr(CO)_3$ fragment.[9,1a,2a] The geometry of the chromium complex was first thought to be due to the Fe-Cr interaction, but was later determined to be an expression of the π-donor character of the Fe-aryl bond.[1a,1b,1c,1d,2a,2b,9,10] In order to have a more complete understanding of the communication between the substituents and the rest of the molecule, the electrochemical data of the complex was evaluated.

It has been determined via cyclic voltammety that the addition of a Fp group to the benzene ring of a standard $Cr(CO)_3$ complex increases its electron richness. It was observed that the incremental effects of the electron richness were dependent upon the character of other substiuents on the benzene ring and, the relative positions of the substituents with respect to the Fp group.[2b,9] It was determined that the more electron rich the initial complex the smaller the incremental effect of each additional Fp group upon the oxidation potential. It was established that the addition of the first Fp group to the

chromium complex caused a 230-mV decrease in $E^{o'}$ and the third caused a 170-mV decrease in $E^{o'}$.[2b] A model was thus developed to test this hypothesis.

A universal model was prepared to test the electronic communications between the substituents on the arene rings and the $Cr(CO)_3$ center.[14] The model was established to "predict and explain the electron richness of the chromium centers in these substituted (η^6-arene)$Cr(CO)_3$ complexes as a function of the π-donor and / or π-acceptor character of the substituents."[3c] The predicted structure of the π-donor substituent was first recognized.

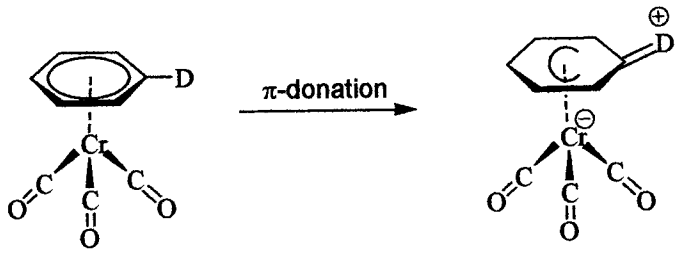

Figure 4.1.3 π-Donor interactions, D = a π-donor, *e.g.* NMe_2, OMe, or F.

In Figure 4.3, π-donation contributes to the electronic structure of the complex via a resonance form having an exocyclic double bond, a positive charge localized on D, and a negative charge localized on the $Cr(CO)_3$. The $Cr(CO)_3$ center in the charge separated zwitterionic ion has an 18–electron configuration and is anticipated to repel the electron density of the exocyclic double bond. The π-donor substituent is therefore predicted to bend away from the $Cr(CO)_3$ center. The consequence of this action is the loss of arene planarity and the complete nonbonding of D is expected in extreme cases.[11] Similar studies were completed on complexes with π-acceptor substituents.

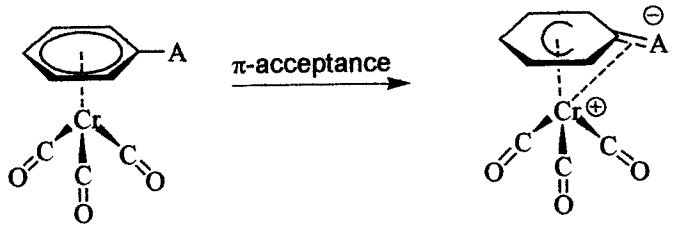

Figure 4.1.4 π-Acceptor interactions, A = a π-acceptor, *e.g.* CO_2Me, C(O)Me, or CF_3.

The π-acceptor substituents are also expected to have π-symmetry interactions. First, the exocyclic double bond is predicted to bend toward, and bond with, the 16-electron cationic $Cr(CO)_3$ to complete its 18 valence electron count. The total electronic contribution from the resulting resonance form to the overall bonding of the complex is anticipated to be comparatively small compared to the π-donor case due to both steric reasons and also because this contribution would result in a decreased electron density on the electron deficient $Cr(CO)_3$ center. Very little structural distortion of the complex is anticipated under these conditions for π-acceptors.[3b,3c]

The characterization by X-ray crystallography of substituted (η^6-arene)$Cr(CO)_3$ complexes such as tricarbonyl(η^6-trifluoromethylbenzene)chromium(0)[12] and tricarbonyl(η^6fluorobenzene) chromium(0)[13] have been completed. The structural data are compared with that of related (η6-arene)$Cr(CO)^3$complexes reported in the literature.

Section Two
Experimental

4.2.1 Tricarbonyl(η^6-fluorobenzene)chromium(0)

Comment

The compound crystallizes in the monoclinic space group $P2_1/c$, with Z = 4 (Fig. 4.2.1 and Table 4.2.1a). The fluoro functional group is displaced out of the least-squares plane defined by the atoms C1, C2, C3, C4, C5, and C6. The F atom and its *ipso* C atom, C1 are bent by 0.0082 (17) and 0.0100 (8) Å, respectively, away from the Cr atom. This distortion is consistent with the earlier structure-property relationship study of (η^6-arene)chromium(tricarbonyl)complexes[3c], which revealed that π-donor groups on the arene bend away from the chromium fragments. The degree of bending was shown to be strongly correlated with the π-donor / π-acceptor strength of the substituents.[3b] It is therefore not surprising that the observed structural distortion for this F substituent is similar to that reported for the OMe group, another moderately strong π-donor[3b], in (anisole)$Cr(CO)_3$.[3c] The title compound was prepared from chromium(0) hexacarbonyl and fluorobenzene in a tetrahydrofuran/dibutyl ether mixture.[14] Pale-yellow crystals were grown by the slow diffusion of a layer of hexane into a methylene chloride solution.

Table 4.2.1a Crystal data	**Table 4.2.1b Data collection**
$Cr(C_6H_5F)(CO)_3$	Bruker *P*4 diffractometer
Mr = 232.13	diffractometer
Monoclinic, $P2_1/c$	ω scans
a = 6.4048 (8) Å	Absorption correction: multi-scan(*SADABS*
b = 11.0668 (5) Å	in *SAINT-Plus*; Bruker, 1997-1999)
c = 12.7124 (16) Å	T_{min} = 0.542, T_{max} = 0.743
β = 102.940 (2) °	8984 measured reflections
V = 878.18 (19) Å ^{3}	2190 independent reflections
Z = 4	2067 reflections with I > 2σ(I)
D_x = 1.756 Mg m^{-3}	R_{int} = 0.023
Mo K_α radiation	θ_{max} = 28.3°
Cell parameters from 7097 reflections	h = -8 → 8
θ = 2.5±28.3°	k = -14 → 14
μ = 1.29 mm^{-1}	l = -16 → 16
T = 100 (2) K	
Block, yellow	
0.46 × 0.28 × 0.23 mm	

Table 4.2.1c Refinement	**Figure 4.2.1** ORTEP plot of title compound. Ellipsoids are at the 50% probability level.
Refinement on F^2 $R[F^2 > 2\sigma(F^2)] = 0.025$ $wR(F^2) = 0.070$ $S = 1.08$ 2190 reflections 147 parameters All H-atom parameters refined $w = 1/[\sigma^2(F_o^2) + (0.042P)^2 + 0.2388P]$ where P = $(F_o^2 + 2F_c^2)/3$ $(\Delta/\sigma)_{max} = < 0.001$ $\Delta\rho_{max} = 0.43$ e×Å^{-3} $\Delta\rho_{min} = -0.32$ e×Å^{-3}	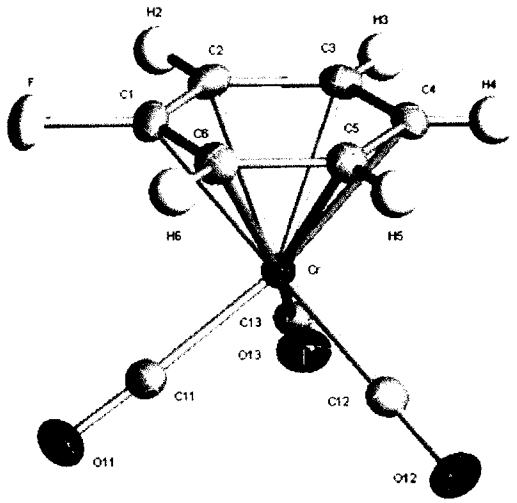

Table 4.2.1d
Selected geometric parameters (Å, °).

Cr–C11 1.8441 (12)	O11–C11 1.1495 (15)
Cr–C12 1.8442 (12)	O12–C12 1.1534 (15)
Cr–C13 1.8493 (12)	O13–C13 1.1521 (15)
Cr–C1 2.2151 (12)	C1–C2 1.3908 (18)
Cr–C6–2.2221 (12)	C1–C6 1.406 (2)
Cr–C4–2.2292 (12)	C2–C3 1.4191 (17)
Cr–C2–2.2343 (12)	C3–C4 1.4015 (17)
F–Cl 1.3442 (14)	C4–C5 1.4154 (16)
C11–Cr–C12 90.44 (6)	C5–C6 1.4047 (17)
C11–Cr–C13 88.44 (5)	C4–C3–C2 120.69 (11)
C12–Cr–C13 87.51 (6)	C3–C4–C5 119.73 (10)
F–Cl–C2 118.55 (11)	C6–C5–C4 120.42 (11)
F–Cl–C6 118.51 (11)	C5–C6–C1 118.24 (10)
C2–Cl–C6 122.92 (11)	O11–C11–Cr 177.82 (12)
C1–C2–C3 117.97 (11)	O12–C12–Cr 179.12 (11)
	O13–C13–Cr 179.07 (10)

4.2.2 Tricarbonyl(η^6-trifluoromethylbenzene)chromium(0)

Comment

The title compound crystallizes in the monoclinic space group $P2_1/c$ with Z = 4 (Fig 4.2.2 and Table 4.2.2a). The trifluoromethyl functional group is tilted out of the least squares plane defined by the atoms C1/C2/C3/C4/C5/C6. The trifluoromethyl atom C7 is bent by 0.024 (4) Å towards the Cr atom. This distortion is consistent with an earlier structure-property relationship study of (η^6-arene)tricarbonylchromium(0) complexes[3c] which revealed that π-accepting groups on the arene remain in the plane of the arene or are slightly towards the tricarbonylchromium fragments. The degree of bending was shown to be strongly correlated with the π-donor / π-acceptor strength of the substituents.[3b] It is therefore not surprising that the observed structural distortion for this CF_3 derivative is similar to that observed for other moderately strong π-accepting substituents, *e.g.* $SiMe_3$, C(O)Me, and CO_2Me.[3c] The title compound was prepared from hexacarbonyl chromium(0) and trifluoromethylbenzene in dibutyl ether.[14] Pale-yellow crystals were grown by the slow diffusion of a layer of hexane into a methylene chloride solution.

Table 4.2.2a Crystal data	**Table 4.2.2b Data collection**
$Cr(C_6H_5F)(CO)_3$	Bruker *P*4 diffractometer
Mr = 232.13	diffractometer
Monoclinic, $P2_1/c$	ω scans
a = 6.4048 (8) Å	Absorption correction: multi-scan(*SADABS*
b = 11.0668 (5) Å	in *SAINT-Plus*; Bruker, 1997-1999)
c = 12.7124 (16) Å	T_{min} = 0.542, T_{max} = 0.743
β = 102.940 (2) °	8984 measured reflections
V = 878.18 (19) Å ^{3}	2190 independent reflections
Z = 4	2067 reflections with I > 2σ(I)
D_x = 1.756 Mg m^{-3}	R_{int} = 0.023
Mo K_α radiation	θ_{max} = 28.3°
Cell parameters from 7097 reflections	h = -8 → 8
θ = 2.5±28.3°	k = -14 → 14
μ = 1.29 mm^{-1}	l = -16 → 16
T = 100 (2) K	
Block, yellow	
0.46 × 0.28 × 0.23 mm	

Table 4.2.2c Refinement	**Figure 4.2.2** ORTEP plot of title compound. Ellipsoids are at the 50% probability level.
Refinement on F^2 $R[F^2 > 2\sigma(F^2)] = 0.025$ $wR(F^2) = 0.070$ $S = 1.08$ 2190 reflections 147 parameters All H-atom parameters refined $w = 1/[\sigma^2(F_o^2) + (0.042P)^2 + 0.2388P]$ where P = $(F_o^2 + 2F_c^2)/3$ $(\Delta/\sigma)_{max} = < 0.001$ $\Delta\rho_{max} = 0.43$ e×Å^{-3} $\Delta\rho_{min} = -0.32$ e×Å^{-3}	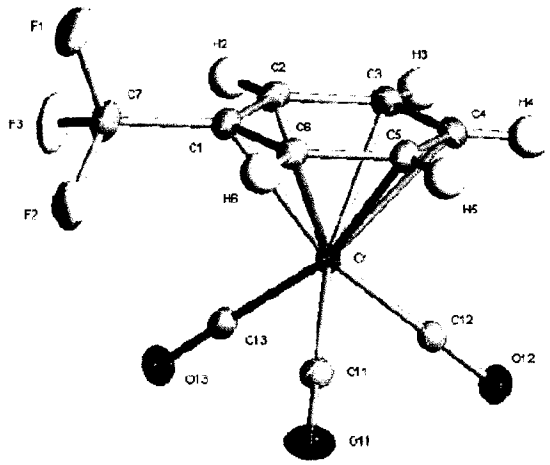

Table 4.2.2d
Selected geometric parameters (Å, °).

Cr–C11 1.8441 (12)	O11–C11 1.1495 (15)
Cr–C12 1.8442 (12)	O12–C12 1.1534 (15)
Cr–C13 1.8493 (12)	O13–C13 1.1521 (15)
Cr–C1 2.2151 (12)	C1–C2 1.3908 (18)
Cr–C6–2.2221 (12)	C1–C6 1.406 (2)
Cr–C4–2.2292 (12)	C2–C3 1.4191 (17)
Cr–C2–2.2343 (12)	C3–C4 1.4015 (17)
F–Cl 1.3442 (14)	C4–C5 1.4154 (16)
C11–Cr–C12 90.44 (6)	C5–C6 1.4047 (17)
C11–Cr–C13 88.44 (5)	C4–C3–C2 120.69 (11)
C12–Cr–C13 87.51 (6)	C3–C4–C5 119.73 (10)
F–Cl–C2 118.55 (11)	C6–C5–C4 120.42 (11)
F–Cl–C6 118.51 (11)	C5–C6–C1 118.24 (10)
C2–Cl–C6 122.92 (11)	O11–C11–Cr 177.82 (12)
C1–C2–C3 117.97 (11)	O12–C12–Cr 179.12 (11)
	O13–C13–Cr 179.07 (10)

References

1. (a) A. D. Hunter, *Organometallics* **1989**, *8*, 1118-1120. (b) A. D. Hunter, A. B. Szigety, *Organometallics* **1989**, *8*, 2670-2679. (c) R. Chukwu, A. D. Hunter, B. D. Santarsiero, *Organometallics* **1991**, *10*, 2141- 2152. (d) R. Chukwu, A. D. Hunter, B. D. Santarsiero, S. G. Bott, J. L. Atwood, J. Chassaignac, *Organometallics* **1992**, *11*, 589-596. (e) R. Mcdonald, K. C. Sturge, A. D. Hunter, L. Shilliday, *Organometallics* **1992**, *11*, 893-899.
2. (a) A. D. Hunter, J. L. McLernon, *Organometallics* **1989**, *8*, 2679-2688. (b) G. B. Richter-Addo, A. D. Hunter, *Inorg. Chem.* **1989**, *28*, 4063-4065. (c) G. B. Richter-Addo, A. D. Hunter, D. Ristic-Petrovic, J. L. McLernon, *Organometallics* **1992**, *11*, 864-870.
3. (a) A. Solladie-Cavallo, *Polyhedron* **1985**, *4*, 901-927. (b) A. D. Hunter, V. Mozol, S. D. Tsai, *Organometallics* **1992**, *11*, 2251-2262. (c) A. D. Hunter, L. Shilladay, W. S. Furey, M. J. Zaworotko, *Organometallics* **1992**, *11*, 1550-1560. (d) E. L. Muetterties, J. R. Bleeke, E. J. Wucherer, T. Albright, *Chem. Rev.* **1982**, *82 (5)*, 499-525.
4. (a) C. M. Lukehart, *Fundamental Transition Organometallic Chemistry*; Brooks / Cole: Monterey, 1985, pp 1-140. (b) H. Lumbroso, C. Segard, B. Roques, *Journal of Organometallic Chemistry* **1973**, *61*, 249-260. (c) R. W. Neuse, *Journal of Organometallic Chemistry* **1975**, *99*, 287-295.
5. (a) J. March, *Advanced Organic Chemistry, Reactions, Mechanisms, and Structure,* 3rd ed.; Wiley and sons: New York, 1985, pp 453-462. (b) F. A. Carey, R. J. Sundberg, *Advanced Organic Chemistry, Part A: Structure and Mechanisms*, 3rd ed.; Plenum: New York, 1990, pp 196-209.
6. G. C. Levy, R. L. Lichter, G. L. Nelson, *Carbon –13 Nuclear Magnetic Resonance Spectroscopy*; Wiley and Sons: New York, 1980. (b) J. B. Stothers, *Carbon –13 NMR Spectroscopy*; Academic:New York, 1972. (c) J. D. Memory, N. K. Wilson, NMR of Aromatic Compounds; Wiley and Sons: New York, 1982. (d) G. L. Nelson, G. C. Levy, J. D. Cargioli, *J. Am. Chem. Soc.* **1972**, *94*, 3089-3094. (e) D.

F. Ewing, *Org. Magn. Reson.* **1979**, *12*, 499-524. (f) A. R. Katritzky, R. D. Topsom, *Angew. Chem., Int. Ed. Engl.* **1970**, *9*, 87-100. (g) G. L. Nelson, E. A. Williams, *Prog. Phys. Org. Chem.* **1976**, *12*, 229-342. (h) J. Bromilow, R. T. C. Brownlee, D. J. Craik, M Sadek, R. W. Taft, *J. Org. Chem.* **1980**, *45*, 2429-2440. (i) H. M. Hugel, D. P. Kelly, R. J. Spear, J. Bromilow, R. T. C. Brownlee, D. J. Craik, *Aust. J. Chem.* **1979**, *32*, 1511-1519. (j) R. T. C. Brownlee, M. Sadek, *Aust. J. Chem.* **1981**, 34, 1593-1602. (k) J. Bromilow, R. T. C. Brownlee, R. D. Topsom, R. W. Taft, *J. Am. Chem. Soc.* **1976**, *98*, 2020-2022. (l) G. E. Maciel, J. J. Natterstad, *J. Chem. Phys.* **1965**, *42*, 2427-2435.

7. (a) G. W. Dillow, P. Kebarle, J. Am. Chem. Soc. 1989, 111, 5592-5596. (b) S. Chowdhury, H. Kishi, G. W. Dillow, P. Kebarle, *Can. J. Chem*, **1989**, *67*, 603-610. (c) I. R. Gould, D. Ege, J. E. Moser, S. Farid, *J. Am. Chem. Soc.* **1990**, *112*, 4290-4301. (d) G. Ferguson J. M. Robertson, *Adv. Phys. Org. Chem.* **1963**, *1*, 203-281. (e) W. J. Hehre, R. W. Taft, R. D. Topsom, *Prog. Phys. Org. Chem.* **1966**, *4*, 31-71. (g) K. Jug, A. M. Koster, *J. Am. Chem. Soc.* **1990**, *112*, 6772-6777.
8. F. H. Allen, O. Kennard, R. Taylor, *Acc. Chem. Res.* **1983**, *16*, 146-153. (b) A. Domenicano, A. Vaciago, C. A. Coulson, *Acta Crystallogr., Sect. B* **1975**, *31*, 221-234. (c) A. Skancke, In *Flouroine-Containing Molecules*; J. F. Liebman A. Greenberg, W. R. Dolbier Jr., Eds.; VCH Publishers: New York, 1988, pp 43-64.
9. G. B. Richter-Addo, A. D. Hunter, N. Wichrowska, *Can. J. Chem.* **1989**, *68*, 41-48.
10. (a) J. Li, A. D. Hunter, B. D. Santarsiero, S. G. Bott, J. L. Atwood, Unpublished observations. (b) R. P. Stewart, P. M. Treichel, *J. Am. Chem. Soc.* **1970**, *92*, 2710-2718.
11. M. Lacoste, H. Rabao, D. Astruc, N. Ardion, E. Varet, J. Y. Saillard, A. Le Beuze, *J. Am. Chem. Soc.* **1990**, *112*, 9548-9557. (b) L. S. Crocker, B. M. Mattson, D. M. Heinekey, *Organometallics* **1990**, *9*, 1011-1016. (c) L. S. Crocker, D. M. Heinekey, *J. Am. Chem. Soc.* **1989**, *111*, 405-406. (d) A. Ceccon, A. Gambaro, A. Venzo, *J. Chem. Soc., Chem. Commun.* **1985**, 540-542. (e) A. Ceccon, A. Gambaro, A. Venzo, *J. Organomet. Chem.* **1984**, *275*, 209-222. (f) A. Ceccon, A.

Gambaro, A. M. RomaninA. Venzo, *J. Organomet. Chem.* **1983**, *254*, 199-205. (g) M. Lacoste, F. Varret, L. Toupet, D. Astruc. *J. Chem . Soc.* **1987**, *109*, 6504-6506. (h) R. D. Rieke, W. P. Henry, J. S. Arney, *Inorg. Chem.* **1987**, *26*, 420-427. (i) S. N. Milligan, R. D. Rieke, *Organometallics* **1983**, *2*, 171-173.

12. M. Zeller, A. D. Hunter, C. L. Perrine, J. Payton , *Acta Crystallogr., Sect. E* **2004,** *60*, 668-669.
13. M. Zeller, A. D. Hunter, C. L. Perrine, J. Payton , *Acta Crystallogr. Sect. E* **2004,** *60*, 650-651.
14. A. D. Hunter, L. Shilliday, W. S. Furey, M. Zaworotko, *J. Chem. Educ.* **1998,** *75*, 891-893.

Chapter 5
Conclusion

The tetramethyl bisisonitrile was selected as the main isonitrile used in our work because it can enhance the solubility of our complexes and bridge two metal centers. The synthesis of isocyanoferrocene and *para*-isocyanoferrocenylbenzene were successful, but the yields need to be improved. In the synthesis of isocyanoferrocene, a procedure using ferrocenylphthalimide as the precursor proved to be most successful. Using this method, ferrocene was first monolithated and reacted with iodine. Iodoferrocene was then converted into N-ferrocenylpthalimide and the amine was liberated using the Gabriel method. Ferrocenylformamide and N-formylferrocenylaniline, used as the precursor in the synthesis of isocyanoferrocene and *para*-isocyanoferrocenylbenzene, respectively, were both synthesized by a formylation reaction of the respective amine with ethyl formate. In future projects, using cyclic voltammetry, the oxidation potentials of the molybdenum or nickel centers having isocyanoferrocene or *para*-isocyanoferrocenylbenzene ends will be determined depending on other substituents on the molecules. The work completed in this thesis is very valuable and will contribute to the success of polymer synthesis in our group.

Appendix 1: Crystallographic Data Tables for 1,4-Diisocyano-2,3,5,6-tetramethylbenzene

Table 1.1 Crystal data	**Table 1.2 Data collection**
$C_5H_{12}N_2$	Bruker SMART CCD area-detector
Mr = 184.24	diffractometer
Monoclinic, C2/c	ω scans
a = 17.1518 (17) Å	Absorption correction: none
b = 5.1324 (5) Å	4935 measured reflections
c = 12.3670 (12) Å	1257 independent reflections
β = 112.010 (2) °	1181 reflections with $I > 2\sigma(I)$
V = 100.32.02 (17) Å^3	R_{int} = 0.080
Z = 4	θ_{max} = 28.3°
D_x = 1.221 Mg m^{-3}	h = -22 → 21
Mo K_α radiation	k = -6 → 6
Cell parameters from 4202 reflections	l = -16 → 16
θ = 2.6±28.3°	
μ = 0.07 mm^{-1}	
T = 100 (2) K	
Block, colorless	
0.50 × 0.35 × 0.35 mm	

Table 1.3 Refinement	**Figure 1.1** ORTEP plot of title compound. Ellipsoids are at the 50% probability level.
Refinement on F^2 $R[F^2 > 2\sigma(F^2)] = 0.046$ $wR(F^2) = 0.131$ $S = 1.05$ 1257 reflections 69 parameters H-atom parameters constrained $w = 1/[\sigma^2(F_o^2) + (0.0698P)^2 + 0.449P]$ where $P = (F_o^2 + 2F_c^2)/3$ $(\Delta/\sigma)_{max} = 0.016$ $\Delta\rho_{max} = 0.32$ e×Å^{-3} $\Delta\rho_{min} = -0.27$ e×Å^{-3}	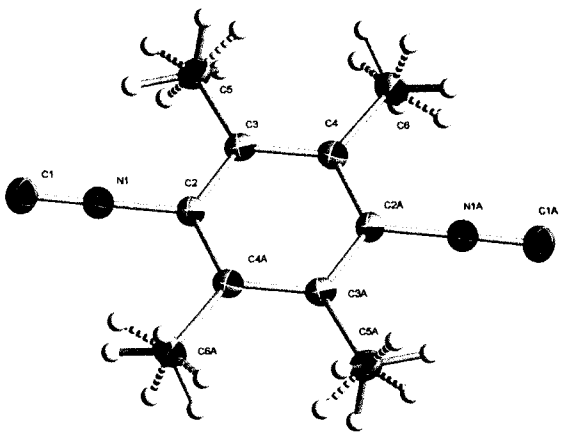

Table 1.4

Selected geometric parameters (Å, °).

N1–C1 1.1628 (14)	C3–C5 1.5106 (13)
N1–C2 1.4045 (12)	C4–C6 1.5105 (13)
C3–C4 1.4008 (13)	C2–C4 1.4065 (13)
C3–C2 1.4070 (13)	C3–C4–C6 121.39 (8)
C1–N1–C2 178.30 (10)	C2^i–C4–C6 120.69 (9)
C4–C3–C2 117.65 (9)	N1–C2–C4^i 117.59 (8)
C4–C3–C5 121.14 (8)	N1–C2–C3 117.99 (8)
C2–C3–C5 121.20 (9)	C4^i–C2–C3 124.42 (9)
C3–C4–C2 117.92 (9)	

Appendix 2: Crystallographic Data Tables for Ferrocenylamine

Table 2.1 Crystal data	**Table 2.2 Data collection**
$C_{10}H_{11}N_2Fe_1$	Bruker SMART CCD area-detector
Mr = 201.05	diffractometer
tetragonal, $I4_1/a$	ω scans
$a = b = 23.5540$ (15) Å	Absorption correction: semiempiracle from
$c = 5.8964$ (8) Å	multi scans
$V = 3271.3$ (5) Å ^{3}	15654 measured reflections
$Z = 16$	2037 independent reflections
$D_x = 1.633$ .g cm^3	2001 reflections with I > 2σ(I)
Mo K_α radiation	$R_{int} = 0.0240$
Cell parameters from 5819 reflections	$\theta_{max} = 28.29°$
$\theta = 1.73 \pm 28.29°$	h = -31 → 31
$\mu = 0.07$ mm^{-1}	k = -31 → 31
$T = 90$ (2) K	l = -7 → 7
needle, yellow-orange	
0.60 × 0.11 × 0.06 mm	

Table 2.3 Refinement	**Figure 2.1** ORTEP plot of title compound. Ellipsoids are at the 50% probability level.
Refinement on F^2 $R[F^2 > 2\sigma(F^2)] = 2001$ $wR(F^2) = 0.0822$ $S = 1.343$ 2037 reflections 153 parameters H atoms treated by a mixture of independent and constrained refinement $w = 1/[\sigma^2(F_o^2) + (0.0698P)^2 + 0.6662P]$ where P = $(F_o^2 + 2F_c^2)/3$ $(\Delta/\sigma)_{max} = 0.001$ $\Delta\rho_{max} = 0.493$ e×Å^{-3} $\Delta\rho_{min} = -0.254$ e×Å^{-3}	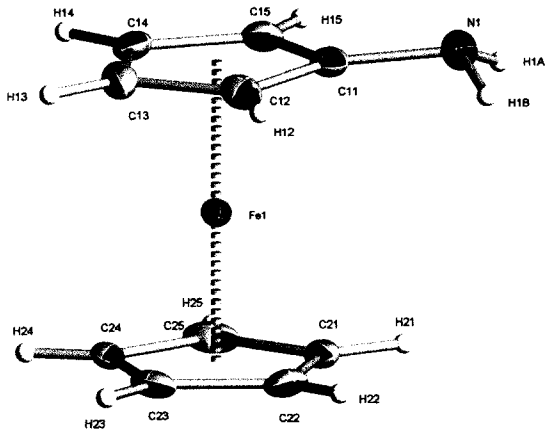

Figure 2.2 Representation of the helical chain formed by the hydrogen bridges. The ferrocenyl hydrogen atoms are omitted for clarity.

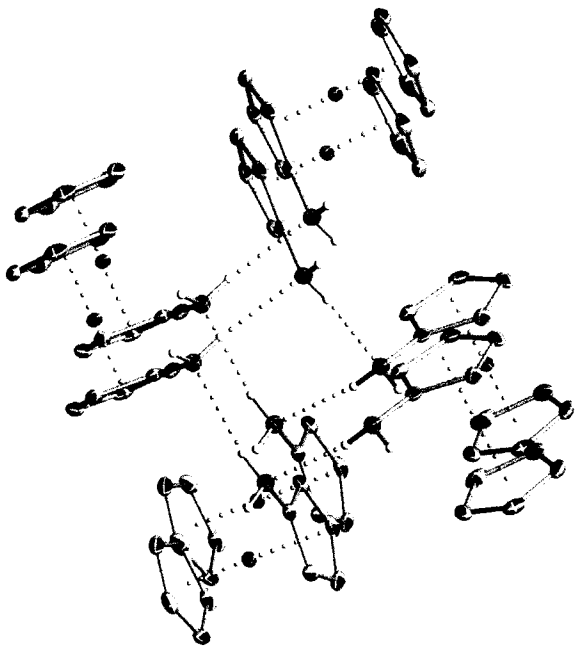

Table 2.4

Selected geometric parameters (Å, °).

Fe1–C13 2.025 (2)	C11–N1–H1B 112 (2)
Fe1–C14 2.031 (2)	C11–N1–H1A 113 (2)
Fe1–C24 2.042 (2)	H1B–N1–H1A 111 (3)
Fe1–C25 2.044 (2)	N1–C11–C15 125.2 (2)
Fe1–C23 2.046 (2)	N1–C11–C12 125.6 (2)
Fe1–C12 2.050 (2)	C11–C15–C14 108.0 (2)
Fe1–C22 2.051 (2)	C23–C24–C25 107.8 (2)
Fe1–C21 2.055 (2)	C22–C21–C25 107.6 (2)
Fe1–C11 2.097 (2)	C21–C25–C24 108.4 (2)
C15–C11 1.420 (3)	C14–C13–C12 108.1 (2)
C15–C14 1.427 (3)	C13–C14–C15 107.9 (2)
N1–C11 1.406 (3)	C21–C22–C23 108.0 (2)
N1–H1B 0.85 (4)	C15–C11–C12 108.1 (2)
N1–H1A 0.85 (3)	C24–C23–C22 108.2 (2)
C24–C23 1.408 (4)	C11–C12–C13 107.8 (2)
C24–C25 1.416 (4)	
C21–C22 1.414 (4)	
C21–C25 1.416 (4)	
C13–C14 1.418 (4)	
C13–C12 1.428 (4)	
C22–C23 1.420 (4)	
C11–C12 1.422 (4)	

Appendix 3: Crystallographic Data Tables for Tetrakis (*para*-methoxyisocyanobenzene)nickel(0)

Table 3.1 Crystal data	**Table 3.2 Data collection**
$C_{32}H_{28}N_4NiO_4$	Bruker SMART CCD area-detector
Mr = 591.21	diffractometer
Orthorhombic, $P2_12_12_1$	ω scans
a = 9.6709 (8) Å	Absorption correction: multi-scan
b = 15.2324 (13) Å	(SADABS in SAINT+; Bruker,1997-1999)
c = 19.0955 (16) Å	Tmin = 0.74297, Tmax = 0.86
V = 2813.0 (4) Å ^{3}	28954 measured reflections
Z = 4	6979 independent reflections
D_x = 1.396 Mg m^{-3}	6048 reflections with I > 2σ(I)
Mo K_α radiation	R_{int} = 0.0474
λ = 0.71073 Å	θ_{max} = 28.28°
Cell parameters from 7213 reflections	h = -12 → 21
θ = 2.3605-28.2675°	k = -20 → 20
μ = 0.734 mm^{-1}	l = -24 → 25
T = 100 (2) K	
Block, yellow	
0.4 × 0.4 × 0.2 mm	

Table 3.3 Refinement	**Figure 3.1** ORTEP plot of title compound. Ellipsoids are at the 50% probability level.
Refinement on F^2 $R[F^2 > 2\sigma(F^2)]$ = 0.0382 $wR(F^2) = 0.0824$ $S = 1.049$ 6979 reflections 374 parameters H-atom parameters constrained $w = 1/[\sigma^2(F_o^2) +$ $(0.0418P)^2 + 0.000P]$ where P = $(F_o^2 +$ $2F_c^2)/3$ $(\Delta/\sigma)_{max} = 0.001$ $\Delta\rho_{max} = 0.733$ e×Å^{-3} $\Delta\rho_{min} = -0.236$ e×Å^{-3}	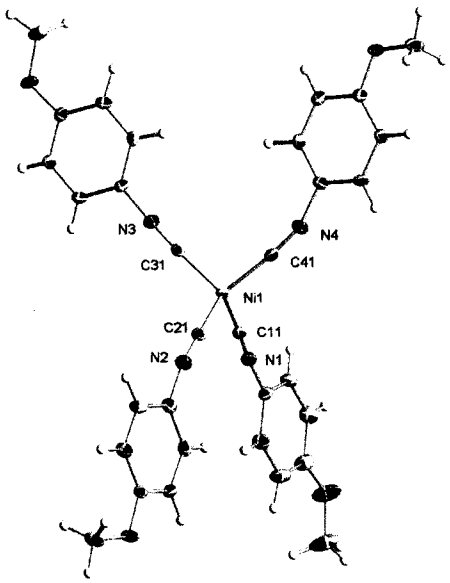

Table 3.4

Selected geometric parameters (Å, °).

Ni1–C41 1.840 (2)	C24–C23–H23 119.8
Ni1–C31 1.846 (2)	C22–C23–H23 119.8
Ni1–C11 1.847 (2)	C45–C46–C47 119.3 (2)
Ni1–C21 1.852 (2)	C45–C46–H46 120.4
C31–N3 1.171 (3)	C47–C46–H46 120.4
N3–C32 1.392 (3)	C15–O1–C18 117.5 (2)
O2–C25 1.367 (3)	C47–C42–C43 120.0 (2)
O2–C28 1.427 (3)	C47–C42–N4 121.3 (2)
C11–N1 1.169 (3)	C43–C42–N4 118.7 (2)
C41–N4 1.181 (3)	C36–C37–C32 120.4 (2)
C21–N2 1.173 (3)	C36–C37–H37 119.8
N2–C22 1.395 (3)	C32–C37–H37 119.8
N4–C42 1.398 (3)	C37–C36–C35 119.6 (2)
O4–C45 1.374 (3)	C37–C36–H36 120.2
O4–C48 1.425 (3)	C35–C36–H36 120.2
N1–C12 1.392 (3)	C44–C43–C42 120.1 (2)
O3–C35 1.362 (3)	C44–C43–H43 120.0
O3–C38 1.435 (3)	C42–C43–H43 120.0
C23–C24 1.377 (3)	O4–C45–C44 114.9 (2)
C23–C22 1.390 (3)	O4–C45–C46 124.5 (2)
C23–H23 0.9500	C44–C45–C46 120.6 (2)
C46–C45 1.389 (3)	C27–C22–C23 119.8 (2)
C46–C47 1.394 (3)	C27–C22–N2 121.0 (2)
C46–H46 0.9500	C23–C22–N2 119.1 (2)
O1–C15 1.373 (3)	C23–C24–C25 119.9 (2)
O1–C18 1.429 (3)	C23–C24–H24 120.0

C42–C47 1.386 (3)
C42–C43 1.398 (3)
C37–C36 1.380 (3)
C37–C32 1.389 (3)
C37–H37 0.9500
C36–C35 1.392 (3)
C36–H36 0.9500
C43–C44 1.371 (3)
C43–C43 0.9500
C45–C44 1.388 (3)
C22–C27 1.386 (3)
C24–C25 1.399 (3)
C24–H24 0.9500
C28–H28A 0.9800
C28–H28B 0.9800
C28–H28C 0.9800
C44–H44 0.9500
C12–C17 1.391 (3)
C12–C13 1.396 (3)
C32–C33 1.395 (3)
C27–C26 1.392 (3)
C27–H27 0.9500
C33–C34 1.383 (3)
C33–H33 0.9500
C35–C34 1.397 (3)
C14–C13 1.379 (3)
C14–C15 1.389 (3)
C14–H14 0.9500
C34–H34 0.9500
C16–C17 1.374 (3)
C16–C15 1.394 (3)

C25–C24–H24 120.0
O2–C28–H28A 109.5
O2–C28–H28B 109.5
H28A–C28–H28B 109.5
O2–C28–H28C 109.5
H28A–C28–H28C 109.5
H28B–C28–H28C 109.5
C43–C44–C45 120.0 (2)
C43–C44–H44 120.0
C45–C44–H44 120.0
C17–C12–N1 120.3 (2)
C17–C12–C13 120.0 (2)
N1–C12–C13 119.7 (2)
C37–C32–N3 120.0 (2)
C37–C32–C33 120.3 (2)
N3–C32–C33 119.6 (2)
C22–C27–C26 120.3 (2)
C22–C27–H27 119.9
C26–C27–H26 119.9
C34–C33–C32 119.3 (2)
C34–C33–H33 120.3
C32–C33–H33 120.3
O3–C35–C36 124.8 (2)
O3–C35–C34 115.0 (2)
C36–C35–C34 120.1 (2)
C13–C14–C15 119.7 (2)
C13–C14–H14 120.2
C15–C14–H14 120.2
C33–C34–C35 120.2 (2)
C33–C34–C34 119.9
C35–C34–H34 119.9

C16–H16 0.9500	C17–C16–C15 120.1 (2)
C48–H48A 0.9800	C17–C16–H16 120.0
C48–H48B 0.9800	C15–C16–C16 120.0
C48–H48C 0.9800	O4–C48–H48A 109.5
C47–H47 0.9500	O4–C48–H48B 109.5
C17–H17 0.9500	H48A–C48–H48B 109.5
C26–C25 1.391 (3)	O4–C48–H48C 109.5
C26–H26 0.9500	H48A–C48–H48C 109.5
C38–H38A 0.9800	H48B–C48–H48C 109.5
C38–H38B 0.9800	C42–C47–C46 120.0 (0)
C38–H38C 0.9800	C42–C47–H47 120.0
C13–H13 0.9500	C46–C47–H47 120.0
C18–H18A 0.9800	C16–C17–C12 119.9 (2)
C18–H18B 0.9800	C16–C17–H17 120.1
C18–H18C 0.9800	C12–C17–H17 120.1
C41–Ni1–C31 103.28 (10)	C25–C26–C27 119.6 (2)
C41–Ni1–C11 114.3728 (10)	C25–C26–H26 120.2
C31–Ni1–C11 109.66 (9)	C27–C26–H26 120.2
C41–Ni1–C21 114.25 (10)	O2–C25–C26 124.9 (2)
C31–Ni1–C21 112.24 (10)	O2–C25–C24 115.2 (2)
C11–Ni1–C21 103.26 (10)	C26–C25–C24 119.9 (2)
N3–C31–Ni1 176.41(19)	O3–C38–H38A 109.5
C31–Ni3–C32 176.9 (2)	O3–C38–H38B 109.5
C25–O2–C28 117.31 (17)	H38A–C38–H38B 109.5
N1–C11–Ni1 177.7 (17)	O3–C38–H38C 109.5
N4–C41–Ni1 173.6 (2)	H38A–C38–H38C 109.5
N2–C21–Ni1 174.3 (2)	H38B–C38–H38C 109.5
C21–N2–C22 163.4 (2)	O1–C15–C14 124.5 (2)
C41–N4–C42 160.0 (2)	O1–C15–C16 115.2 (2)
C45–O4–C48 117.36 (18)	C14–C15–C16 120.2 (2)
C11–N1–C12 170.0 (2)	C14–C13–C12 120.0 (2)

C35–O3–C38 116.63 (19)	C14–C13–H13 120.0
C24–C23–C22 120.4 (2)	C12–C13–H13 120.0
C24–C23–H23 119.8	O1–C18–H18A 109.5
C22–C23–H23 119.8	O1–C18–H18B 109.5
C45–C46–C47 119.3 (2)	H18–C18–H18B 109.5
C11–N1–C12 170.0 (2)	O1–C18–H18C 109.5
C35–O3–C38 116.63 (19)	H18A–C18–H18C 109.5
C24–C23–C22 120.4 (2)	H18B–C18–H18C 109.5